A Thesis

entitled

Nonlinear Modeling of Beam-Column Joints using Artificial Neural Networks

by

Nirmala Suwal

Submitted to the Graduate Faculty as partial fulfillment of the requirements for the

Master of Science Degree in

Civil Engineering

_____

Dr. Serhan Guner, Committee Chair

_____

Dr. Douglas Karl Nims, Committee Member

_____

Dr. Luis Alexander Mata, Committee Member

_____

Dr. Scott C. Molitor, Acting Dean
College of Graduate Studies

The University of Toledo

August 2023

An Abstract of

Nonlinear Modeling of Beam-Column Joints using Artificial Neural Networks

by

Nirmala Suwal

Submitted to the Graduate Faculty as partial fulfillment of the requirements for the
Master of Science Degree in
Civil Engineering

The University of Toledo
August 2023

Beam-column joints play a critical role in transferring forces between beam and column elements and maintaining structural integrity during severe loading. While the nonlinear behaviors of beams and columns are commonly modelled in global frame analyses through the use of plastic hinges, the behavior of joints through the use of rigid end offsets is often omitted. The objective of this study is to develop an artificial neural network and derive the plastic hinge curves required for modeling beam-column joints in global frame analyses. As the first step, a feed-forward artificial neural network (FFNN) is developed to predict the shear strengths of beam-column joints. A comprehensive dataset of 598 experimental joint specimens is compiled from 153 previously published research studies. The 555 data points which passed the exploratory data analysis are used to train, test, and validate the proposed network for applicability to a wide range of input variables and joint configurations. The accuracy and reliability of the proposed FFNN were evaluated using a comprehensive set of evaluation metrics in comparison with three

existing networks from the literature. The network predicted shear strength is used to derive shear stress-strain and moment-rotation curves for joint hinges. A spreadsheet tool is developed to execute the network formulations, calculate joint shear strength, and derive joint hinge curves for practical use by engineers and researchers.

Acknowledgments

First and foremost, I express my deepest gratitude to God for giving me the strength and courage to reach this point in my life. Without His grace, I wouldn't have come this far.

I thank my family members, Ram Pd. Suwal, Nani Chhori Suwal, Laxmi Pd. Suwal, Sarmila Suwal, and my loved ones who have been unwavering emotional and mental support throughout this academic journey. Your boundless love, care, and encouragement have played a crucial role in helping me overcome obstacles.

I thank Dr. Serhan Guner for being an excellent mentor. His profound knowledge and guidance in structural engineering have greatly enhanced my engineering skills. I consider it a great privilege to have had the opportunity to work under his supervision.

Lastly, I would like to acknowledge the Department of Civil Engineering at The University of Toledo for granting me a graduate assistantship throughout my graduate studies. This invaluable support has allowed me to dedicate myself to my research and studies. In special, I would like to thank Dr. Defne Apul, Dr. Douglas Nims, and Dr. Alex Spivak for all the support and invaluable advice, which are greatly appreciated.

I am incredibly grateful for this opportunity, and it has truly been a privilege to be a part of such a supportive and dynamic academic community.

Table of Contents

List of Tables

List of Figures

List of Abbreviations

ACI ……..…….American Concrete Institute
Adam ……...…… Adaptive Moment Estimation
AI ……. …….. Artificial Intelligence
ALF ……..Axial Load Factor
ANN ……Artificial Neural Network

B ……. Bond Slip Failure

CSI ……...….....Computers and Structures, Inc.
CV ……...…… Coefficient of Variation

DSFM ……..Disturbed Stress Field Model

EC……..…Eurocode
EDA ……..…Exploratory Data Analysis
ELM ……..…Extreme Learning Machine

FFNN ……..……..Feed-Forward Neural Network

JT …….Joint Type

KNN ……K-Nearest Neighbor

MAE ……Mean Absolute Error
MARS ……..Multi Adaptive Regression Splines
MCFT ……..Modified Compression Field Theory
ML ……....Machine Learning
MSE …… Mean Squared Error

RMSE ……..Root Mean Square Error

S …….. Joint Shear Failure
S-F ……... Combined Joint Shear and Interface Flexure Failure
SVM ……Support Vector Machine

List of Symbols

α ……..Joint type constant
β …… ……. Stochastic moment function constant
ε.……Root mean square function constant
γ ……... Shear strain
φ_b……..Beam longitudinal reinforcement diameter
v_{crack}……... Shear stress value for cracking
v_{bond} ……...……... Bond strength
v_{max} ……..Maximum shear stress
v_{resid} ……..Shear stress value for residual point
v_{yield} ……..Shear stress value for yielding point
θ ……. …… Rotation
ρ_b …… Beam longitudinal reinforcement ratio
ρ_c ……..…… Column longitudinal reinforcement ratio
ρ_{jt} ……..... Joint transverse reinforcement ratio
σ_a ……Axial stress in the column
τ ……... Shear strength
τ_{exp} ……Experimental shear strength
τ_{pred}. ……..Predicted shear strength

A_g ……...……... Column gross area
A_j ……. Area of joint core
b …….. Biases
b_b ……. Beam width
b_c……...……..... Column width
cc …….....Concrete cover
D_i …….Cook's distance
f'_c ……. Concrete compressive strength
f_u …….. Ultimate strength of reinforcement
f_y …….. Yield strength of reinforcement
f_{yb} ……. Beam longitudinal reinforcement yield strength
f_{yc} ……. Column longitudinal reinforcement yield strength
f_{yjt} ……. Joint transverse reinforcement yield strength
h_b…….. Beam depth
h_{be} …… Effective depth of beam (to the centroid of reinforcement)

h_c ……. Column depth
I_t ……... Threshold limit
j ……....Constant
k ……...Learning rate
L_b …….Length of beam between two points of contraflexure
L_c ……. Column length between two points of contraflexure
l_s ……...Embedment length
M_{bond} …… Equivalent moment capacity for bond strength
M_{crack}…… Equivalent moment capacity for cracking strength
M_{max} …….Equivalent moment capacity for shear strength
M_{resid}. ……....Moment value for residual
M_{yield} …… Moment value for yielding
n……Total number of data points
P ……... Axial load
p ……...Total number of weights and biases
P_{exp} ……...Experimental load
P_p ……..Predicted load
p_t ……... Principal tensile stress
R ……... Correlation coefficient
R^2……. Determination coefficient
S_d ……...Root mean square propagation term
T ……... Tension force in the beam longitudinal reinforcement
u ……... Net input
V_b …… Shear force in beam
V_c …… Shear force in column
V_d …… Stochastic momentum for gradient descent
w ……...……Joints with transverse reinforcement
w/o ……...Joints without transverse reinforcement
x …….. Input value
y ……...Output value

Chapter 1

Introduction and Objectives

Beam-column joints are a critical component of reinforced concrete frame structures. They are responsible for transferring forces between adjoining beams and columns while limiting story drifts and maintaining structural integrity. One important, and often omitted, aspect of global frame analyses is the modeling of beam-column joints. A beam-column joint (also called a joint core) is where a beam and column intersect in a building frame. While the nonlinear behaviors associated with beams and columns are commonly accounted for in global frame analyses, the behavior of joints through the use of rigid end offsets or other techniques that suppress joint deformations is often neglected [1]. The failure modes associated with joints include joint shear and bond-slip failures. Joint failures may also take place in combination with the beam and column failure modes that may include flexural and shear failure modes.

This study includes two parts. The first part of this study provides a comparative literature review of existing beam-column joint models and presents a practical joint modelling approach for integration into commonly used global frame analysis software [1]. The second part presents a development of a feed-forward neural network (FFNN) model

to predict beam-column joint shear strength with high accuracy and derivation of the plastic hinge curves required for modeling beam-column joints in global frame analysis. This thesis is written in a manuscript format, which means that each chapter is either published or submitted in journal papers. Table 1.1 summarizes each paper contained in this thesis, which research objective it addresses, and its main contributions.

Table 1.1: Summary of each paper contained in this thesis and their main contributions

Paper	**Chapter**	**Objective**	**Main Contributions**
Journal Paper I	Chapter 2	1	• Existing beam-column joint models are comprehensively reviewed. • A modeling approach of beam-column joints in global frame analysis software is proposed. • Application and validation of proposed modelling approach is assessed. • A spreadsheet tool that executes the derivation of joint hinges is shared as freeware.
Journal Paper II	Chapter 3	2	• A Feed-Forward Neural Network (FFNN) is proposed to predict shear strength of beam-column joint. • The accuracy of the proposed model is evaluated and compared with other networks. • Plastic hinge curves of beam-column joints are derived integrating proposed network predicted shear strength. • A spreadsheet tool that executes prediction of shear strength and derivation of joint hinge is shared as freeware.

This thesis is organized as follows. Chapter 2 presents the first part, Nonlinear modeling of beam-column joints in forensic analysis of concrete buildings and includes the journal paper published in *Concrete and Computers.* Chapter 3 presents the second part, Plastic Hinge Modeling of Reinforced Concrete Beam-Column Joints using Artificial Neural Network and includes a journal paper's manuscript submitted in *Engineering Structures.* Chapter 4 summarizes the global conclusions from Chapter 2 and Chapter 3. Chapter 4 is followed by References and Appendix.

Chapter 2

Journal Paper I – Nonlinear Modeling of Beam-Column Joints in Forensic Analysis of Concrete Buildings[1]

2.1 Abstract

Beam-column joints are a critical component of reinforced concrete frame structures. They are responsible for transferring forces between adjoining beams and columns while limiting story drifts and maintaining structural integrity. During severe loading, beam-column joints deform significantly, affecting, and sometimes governing, the overall response of frame structures. While most failure modes for beam and column elements are commonly considered in plastic-hinge-based global frame analyses, the beam-column joint failure modes, such as concrete shear and reinforcement bond slip, are frequently omitted. One reason for this is the dearth of published guidance on what type of hinges to use, how to derive the joint hinge properties, and where to place these hinges.

[1] Reprinted from Computers and Concrete, Vol. 31, No. 5, Nirmala Suwal & Serhan Guner, Nonlinear modeling of beam-column joints in forensic analysis of concrete buildings, © 2023, with permission from Techno-Press. For the published version, please refer to https://doi.org/10.12989/cac.2023.31.5.419 and https://www.utoledo.edu/engineering/faculty/serhan-guner/publications.html

Many beam-column joint models are available in literature but their adoption by practicing structural engineers has been limited due to their complex nature and lack of practical application tools. The objective of this study is to provide a comparative review of the available beam-column joint models and present a practical joint modeling approach for integration into commonly used global frame analysis software. The presented modeling approach uses rotational spring models and is capable of modeling both interior and exterior joints with or without transverse reinforcement. A spreadsheet tool is also developed to execute the mathematical calculations and derive the shear stress-strain and moment-rotation curves ready for inputting into the global frame analysis. An experimental validation study is also undertaken, which demonstrates that the modeling approach provides accurate response simulations. Important modeling considerations are also presented to assist practitioners in properly modeling beam-column joints in frame analyses.

2.2 Introduction

Forensic structural engineering studies structural systems with the objective of identifying the causes of structural failures. A plastic-hinge-based global frame analysis is commonly used in these studies to model the deformations, cracking, and failure modes in reinforced concrete buildings [1,2]. One important, and often omitted, aspect of global frame analyses is the modeling of beam-column joints. A beam-column joint (also called a joint core) is where a beam and column intersect in a building frame. While most beam and column failure modes are commonly considered in global frame analyses, the joint

failure modes, including concrete shear (see Figure 2-1a) and reinforcement bond slip (see Figure 2-1b), are frequently omitted. Experimental studies and post-earthquake inspections have demonstrated that beam-column joints may undergo severe deformation leading to local damage, or, in extreme cases, failures affecting the entire frame structure [3-5]. It is, therefore, imperative to model beam-column joints in a global frame analysis, especially for older structures with non-ductile joint designs.

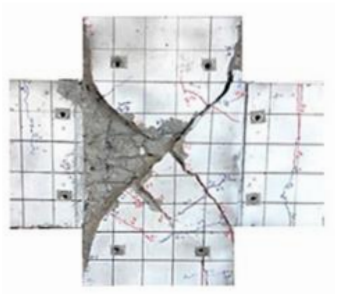

Gombosuren and Maki [6]

Pantelides et al. [7]

(a) Shear failure mode **(b)** Bond-slip failure

Figure 2-1: Beam-column joint primary failure modes

Modeling of beam-column joints can be undertaken using several theoretical approaches with varying degrees of complexity. They range from simple rotational spring models to more elaborate component or finite element models. More recently, machine-learning based models are also proposed. The main phenomena considered in all these joint models are the shear deformation in the joint core due to applied shear force from columns and beams and the bond slippage of the main reinforcing bars of beams passing through the joint core.

The objective of this study is to provide a comparative review of the available beam-column joint models and present a practical beam-column joint modeling approach for integration into commonly used global frame analysis software. The presented

modeling approach uses rotational spring formulations to model both interior and exterior joints with or without transverse reinforcement. The modeling approach is sought to be numerically efficient, readily implementable into global frame analysis tools, and sufficiently accurate. The developed spreadsheet tool is intended to assist engineers in deriving the joint hinge properties easily.

2.3 Review of Existing Beam-Column Joint Models

A significant amount of research has been conducted on the nonlinear modeling of beam-column joints. These can be categorized under five distinct types from simple to sophisticated: rigid-joint models, rotational spring models, component models, finite element models, and machine learning-based models (see Figure 2-2). The main objective of these models is to capture the shear deformation in the joint core and the bond slip of the reinforcing bars.

Subjected to lateral cyclic loading, joint cores experience high shear forces from the adjacent columns and beams. A bending moment applied from each side is carried by a force couple that is formed with tension in the tensile reinforcing bar, compression in the concrete, and the compressive reinforcing bar passing through the joint core. The shear force in the joint core results in shear deformations and the bending moment results in high bond stress between the reinforcement and surrounding concrete. The joint response due to shear and bond slip actions may significantly affect the overall stiffness and strength of a frame structure. Most available joint models are, therefore, formulated to capture these two important mechanisms.

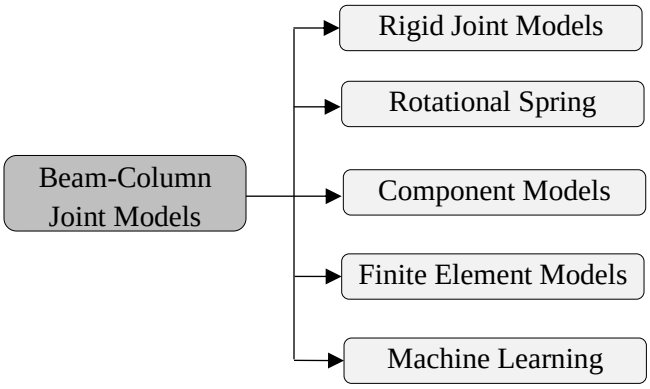

Figure 2-2: Classification of beam-column joint models

2.3.1 Rigid Joint Models

In the rigid-joint models, the beam-column joint core is assumed to be perfectly rigid with no explicit joint modeling undertaken. This model neglects the deformations in the joints and enforces the assumption that the beam and column members remain perpendicular even under significant deformations. Due to the stiffer properties of the joint cores, the nonlinear deformations are concentrated at the ends of the beams and columns, effectively neglecting the joint core behavior. According to Sharma et al. [8], analyzing 10 beam-column joints subassemblages without joint transverse reinforcement using a rigid joint model produces predictions of average ultimate strength that are 81% higher compared to those obtained using a rotational spring joint model. This suggests that the rigid joint model tends to overestimate strength and may lead to unsafe designs in terms of ultimate strength and displacement. This modeling approach may predict the global response of a frame reasonably accurately only if the joints are very well designed and the actual failure mode does not involve any beam-column joint cracking, damage, or nonlinear behavior [8]. For all other cases, this modeling approach is not recommended.

2.3.2 Rotational Spring Models

Rotational spring models have been used in numerous research studies due to their simplicity and reasonable accuracy. Most rotational spring models introduce rigid link elements and rotational springs in a joint core (see Figure 2-3). The rigid link elements simulate the higher strength and stiffness of the joint core (as compared to the adjoining beam and column elements) whereas the rotational spring hinges simulate the shear deformations in the joint core and bond slip behavior at the joint interfaces. The stress-strain or moment-rotation curves are derived, based on various formulations, to define the hinges in rotational spring models. These properties are developed from experimental data calibration based on the joint details and material properties.

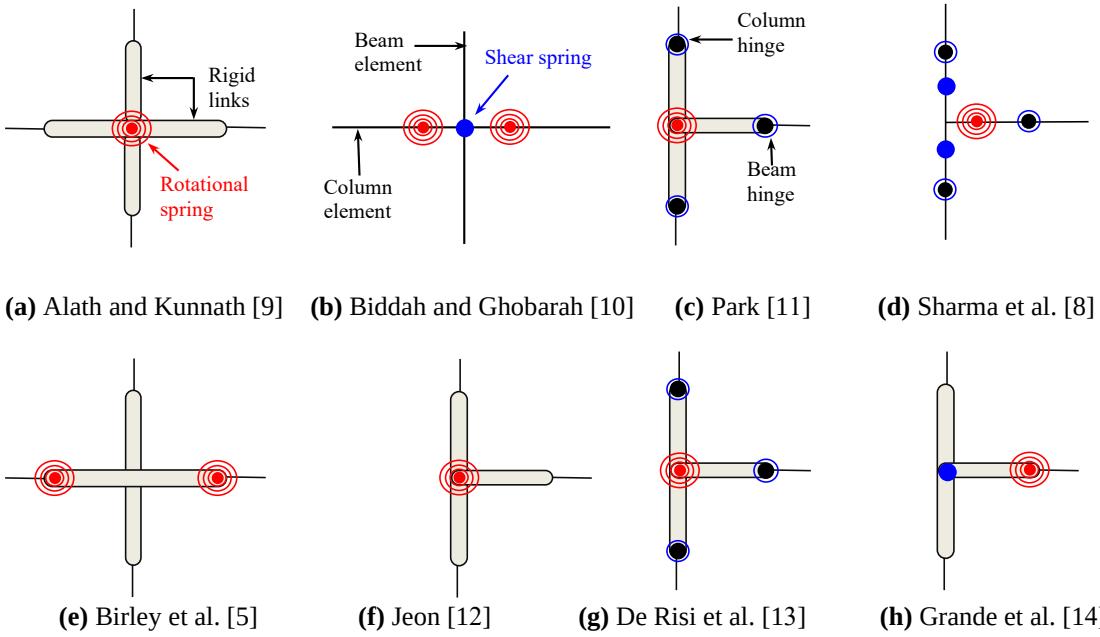

(a) Alath and Kunnath [9] **(b)** Biddah and Ghobarah [10] **(c)** Park [11] **(d)** Sharma et al. [8]

(e) Birley et al. [5] **(f)** Jeon [12] **(g)** De Risi et al. [13] **(h)** Grande et al. [14]

Figure 2-3: Mechanical representations of rotational spring models (selected samples)

Several rotational spring models are available in the literature. Alath and Kunnath [9] proposed a model, also known as the "scissor model," which models the joints with two components: rigid links and a zero-length rotational spring. The joint core geometry is

represented by rigid links while the rotational springs simulate the degrading shear behavior of the joint core. This model accounts only for the shear behavior while the bond slip mechanism is ignored. Biddah and Ghobarah [10] modified the Alath and Kunnath [9] model by introducing two separate nonlinear rotational springs in series, one for the joint shear deformation and the other for the bond slip behavior. The Modified Compression Field Theory (MCFT) [15] was used to calculate the shear-stress strain relationship. A bilinear idealization of the moment-rotation relationship was used to define the bond slip behavior, capturing critical points such as the cracking, yielding, and ultimate condition.

Park [11] proposed a semi empirical-analytical model reflecting two key parameters: joint aspect ratio and beam reinforcement index in developing a shear strength model for exterior joints with no transverse reinforcement (non-ductile joint). The shear stress-strain relationship is transformed into a moment-rotation relationship to represent the beam-column joint spring. Sharma et al. [8] proposed a model based on the limiting principal tensile stress theory. They assigned the shear springs to the column region and rotational springs to the beam region within the joint core. This model was developed for only exterior, non-ductile joints with no transverse reinforcement. Birley et al. [5] proposed a model for interior, ductile joints with transverse reinforcement. They used a modified dual-spring in series incorporated in the lumped plastic hinges of the beams. The first spring accounts for the beam response while the second spring captures the joint shear and bond slip responses. This study validated 10 experimental subassemblies of beam-column joints, with an average error of 8.6%.

To advance Park [11], Sharma et al. [8], and Birley et al. [5] models, Jeon [12] proposed a model that is applicable to the analysis of both exterior and interior joints with and without transverse reinforcement. Jeon [12] adopted the Alath and Kunnath [9] model by modifying the joint shear stress-strain curve based on the experimental data from Anderson et al. [16] and utilizing the bond model of Hassan [17]. In addition, Jeon [12] also proposed an empirical shear strength model to compute the shear strength capacity of joints. This study validated 28 experimental subassemblies of beam-column joints, with error ranging from 0.1% to 8.4%.

De Risi et al. [13] and Grande et al. [14] also adopted the "scissor model" of Alath and Kunnath [9] with modifications. De Risi et al. [13] calibrated the spring properties based on Celik and Ellingwood [18] and Jeon [12] whereas Grande et al. [14] developed a model to compute the shear strength capacity of joints using empirical formulations. Both the De Risi et al. [13] and Grande et al. [14] models are limited to exterior joints without transverse reinforcement.

These rotational spring models are categorized in Figure 2-4 according to the joint and ductility types. Ductile joints are typically those with sufficient amounts of transverse reinforcement in the joint core. Non-ductile joints may contain no shear reinforcement, insufficient amounts of shear reinforcement, and/or deficient design detailing. Non-ductile joints exhibit brittle and undesirable failure modes.

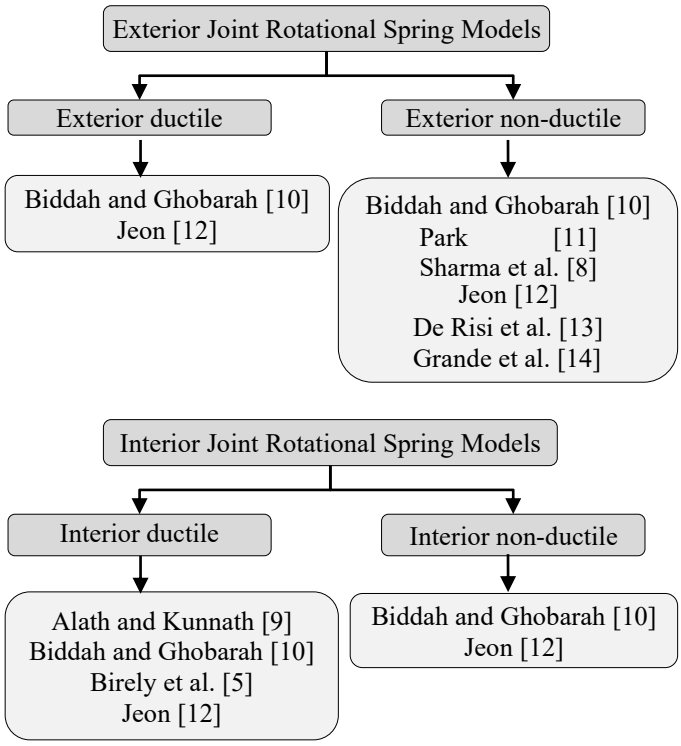

Figure 2-4: Rotational spring models (selected samples)

2.3.3 Component Models

Component models include sophisticated constitutive models that explicitly model joint core shear and bond slip behaviors. Several component models have been proposed in the literature (see Figure 2-5). Many such models use MCFT to determine the shear response of a joint core subjected to shear loads coupled with an axial load. Youssef and Ghobarah [19], Lowes and Altoontash [20], and Shin and Lafave [4] are examples of such models. These studies found that the MCFT underestimates the strength of beam-column joints with low amounts of transverse reinforcement while overestimating it for joints with high amounts of transverse reinforcement. To resolve this, Mitra and Lowes [21] modified the Lowes and Altoontash [20] model to broaden the range of applicability while improving the prediction accuracy. They modelled the shear load transfer within a joint core with a

diagonal compression strut rather than a shear stress field based on the MCFT. They also proposed a new bar-slip model to simulate the frictional resistance of bars combined with hysteretic strength loss.

These studies demonstrate that component models are highly versatile and accurate. However, they require the derivation of multiple constitutive models for the various springs used and are not readily implementable in global frame analysis tools using one-dimensional line elements. Therefore, their adoption by practicing structural engineers remains rather limited. In an attempt to make component models more applicable to frame analyses, Pan et al. [22] implemented the Mitra and Lowes [21] model into a nonlinear distributed-plasticity-based frame analysis procedure, VecTor5 [23], for the holistic modeling of frame buildings. They demonstrated practical modeling and successful simulation results based on an experimental validation study of nine specimens.

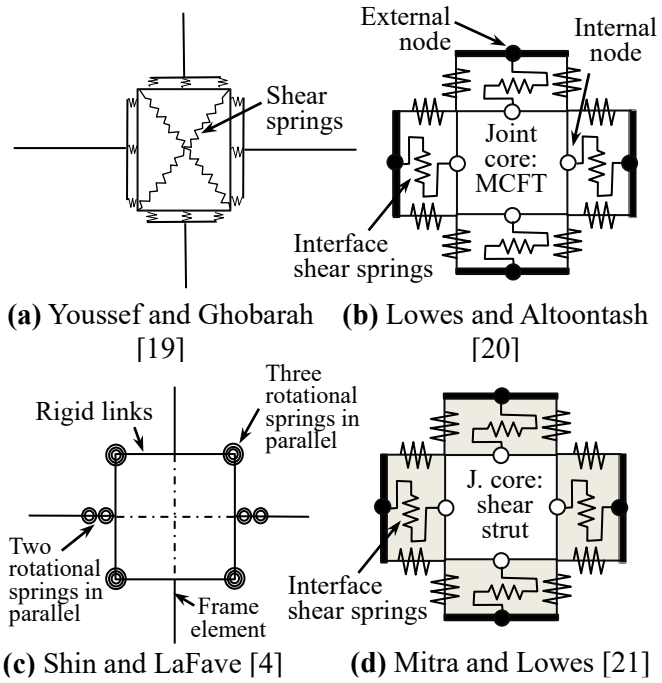

(a) Youssef and Ghobarah [19] **(b)** Lowes and Altoontash [20]

(c) Shin and LaFave [4] **(d)** Mitra and Lowes [21]

Figure 2-5: Mechanical representations of component models (selected samples)

2.3.4 Finite Element Models

Finite element modeling is useful for developing a more comprehensive understanding of the performance of the beam-column joints. Eligehausen et al. [24] utilized continuum finite elements based on microplane model for exterior joints. In this study, the concrete was modelled with an isotropic microplane material, reinforcement with a trilinear steel constitutive law, and the bond between reinforcement and concrete with discrete bond elements. Sharma et al. [25] simulated the behavior of exterior and interior joints using a similar finite element modeling approach. Sagbas et al. [26] modelled beam-column joints using a two-dimensional (2D) continuum element based on secant-stiffness solution algorithm employing a smeared rotating crack model of reinforced concrete [27]. The constitutive modeling of concrete and reinforcement employed the Disturbed Stress Field Model (DSFM) [28]. The bond slip of the longitudinal reinforcement was modelled using discrete truss bars elements. Guner and Vecchio [29] used a similar theoretical approach in the context of macro 1D elements as a part of a global frame analysis subjected to cyclic load reversals. In this study, beam and column behaviors are also simulated using a distributed inelasticity fiber-section approach. Sasmal and Nath [30] investigated the crack and failure patterns, shear strengths, cyclic load-displacement behaviors, and energy dissipation and ductility characteristics of several joint specimens using the finite element method. In this study, concrete and reinforcement were modelled as macro-elements – concrete with quadratic brick elements and reinforcement with discrete truss elements. Pan et al. [22] implemented a component joint model into a global nonlinear frame analysis method, VecTor5 [23]. In this study, both joint shear deformations and bond slip effects were simulated in addition to the nonlinearities in the beams and columns using DSFM

[28]. Abusafaqa et al. [31] employed the finite element method to study the effectiveness of ultra-high-performance concrete in beam-column joint strengthening. The concrete was defined with isometric eight node linear brick elements and reinforcement with two-node linear truss elements. The perfect bond was assumed between reinforcement and concrete, neglecting the bond slip behavior. The concrete damage plasticity model was used to simulate the behavior of concrete.

The analysis of beam-column joints using finite element modeling requires significant experience, computational resources, and time. Consequently, this approach is commonly used to simulate the behavior at the local level (i.e., isolated beam-column joints) as opposed to holistic modeling of building frames.

2.3.5 Machine Learning Models

Machine learning (ML) is a branch of artificial intelligence (AI) that trains computers to make predictions based on existing datasets and algorithms when fed new data. This approach provides a computational algorithm with the ability to learn and improve until it meets the desired performance rather than explicit coding [32]. ML models have been increasingly used for predicting the beam-column joint shear strength capacity and failure modes. By utilizing ML, Unal and Burak [33] created an empirical equation to predict the shear strength capacity of joints. Jeon et al. [34] proposed a joint shear strength model using a multi adaptive regression splines (MARS) algorithm. Kotsovou et al. [35] used an artificial neural network (ANN) to predict the shear strength capacity of the exterior joints. Mangalathu and Jeon [36] developed expressions to calculate the shear strength capacity and provided formulations to categorize the predicted failure modes. They used

the Lasso logistic regression algorithm [37]. To predict the shear strength capacity and failure mechanisms of exterior joints, Alwanas et al. [38] used an extreme learning machine (ELM) algorithm developed by Huang et al. [39]. Naderpour and Mirrashid [40] proposed two failure mode classifiers based on the decision tree method [41]. Gao and Lin [42] applied ten ML methods to predict the failure modes of beam-column joints. Alagundi and Palanisamy [43] employed ANNs to predict the shear strengths of exterior joints. Haido [44] also utilized ANNs to predict the shear strengths of interior and exterior joints and compared the prediction model with alternative approaches–contained in the existing building codes.

The analysis of beam-column joints using ML methods is a promising and evolving research field. The studies cited above indicated prediction accuracies as high as those obtained from the physics-based joint models discussed above. One important aspect of ML modeling is that the joint being modelled should be well represented by the dataset used for the development and training.

2.3.6 Discussion

Among the various types of beam-column joint models available, each model has its own strengths and weaknesses. No scientific consensus has been reached on an optimal model that applies to all cases [22]. Rotational spring models are simple, reasonably accurate, and suitable for practical implementation into global frame analysis software comprised of 1D line elements. Component and finite element models are shown to be more versatile and accurate for a wider range of conditions, but they are computationally demanding and require significant knowledge and effort from the engineer. Machine

learning models provide fast analysis times and promising results. The database selection and the similarity between the dataset and the joint being modelled plays a critical role in their prediction accuracy.

2.4 Proposed Beam-Column Joint Modeling Approach

As a part of this study, a beam-column joint modeling approach is proposed to aid practicing engineers in incorporating joint modeling into global frame analysis using 1D linear frame elements. The proposed approach integrates rotational spring models (due to their simplicity and reasonable accuracy) into commonly used lumped-plasticity-based frame analysis methods. Figure 2-6 shows the overview of the proposed approach.

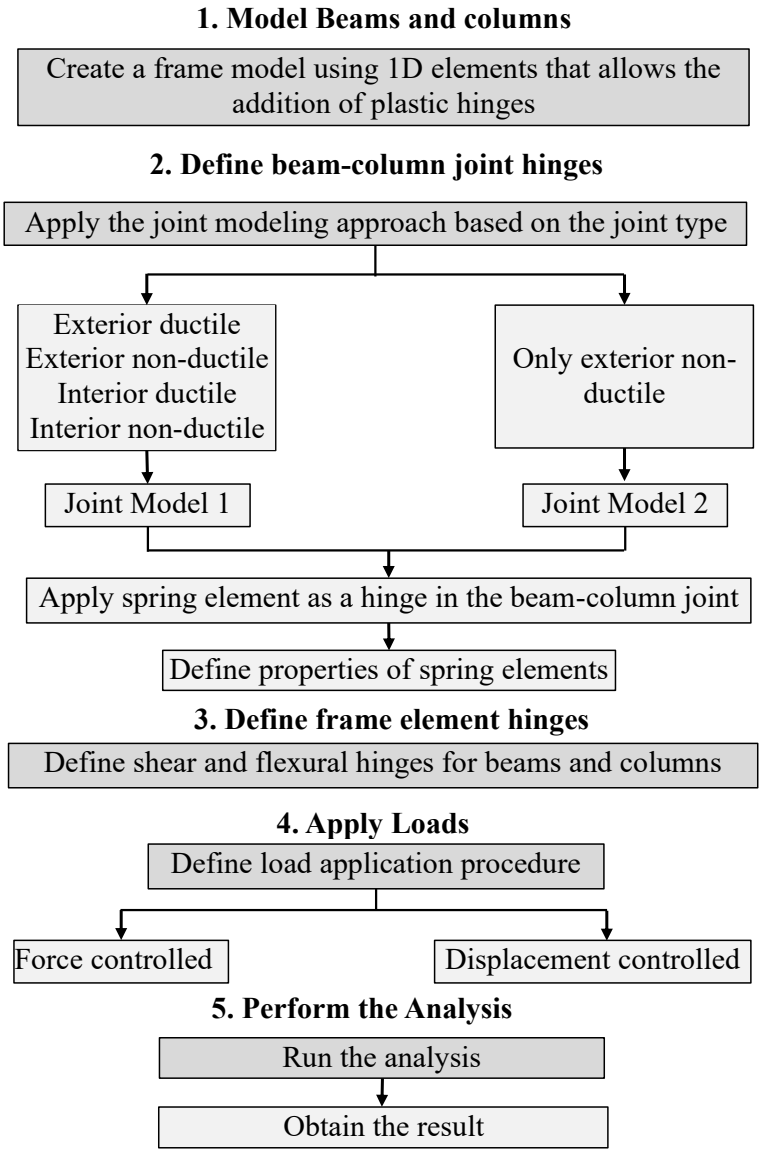

Figure 2-6: Flowchart of the proposed joint modeling approach

The first stage is common to any linear-elastic global frame analysis using 1D line elements with a center-line approach; therefore, it is not discussed further. The second stage is to define rotational spring elements as plastic hinges in beam-column joints. Figure 2-4 shows several rotational spring models based on the joint type. The analyst can select any of those models for the nonlinear modeling of the joints. The proposed approach uses two specific beam-column joint models as Model 1 and Model 2. Model 1 provides a wide

range of applicability to include exterior, interior, ductile, and non-ductile joints, and is based on Jeon [12]. Model 2 is exclusively for exterior non-ductile beam-column joints which are shown to sustain significant damage due to their brittleness and unbalanced nature [45] and is based on Sharma et al. [8].

To model a beam-column joint using Model 1, a rotational spring is introduced at the intersection of beam and column elements (see Figure 2-7). The joint core is represented by rigid end offsets due to the overlapping nature of the elements. The inserted rotational spring models the shear and bond slip effects.

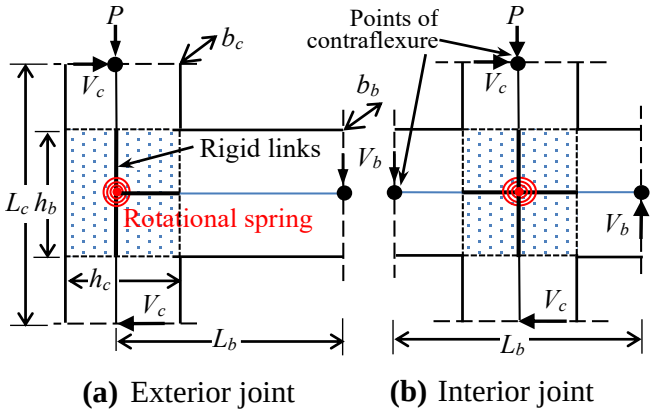

(a) Exterior joint **(b)** Interior joint

Figure 2-7: Location of rotational spring using Model 1

To define a rotational spring as a plastic hinge in a global frame analysis, the shear stress-strain curve should be developed. This curve can be constructed with four points: (1) cracking, (2) yielding, (3) maximum, and (4) residual, where each point is defined as a function of the shear strength (v_{max}). The input parameters required to compute v_{max} are the concrete compressive strength (f'_c), the cross-sectional dimensions of the beams and columns (b_b, b_c, h_b, h_c), the beam length (L_b), the axial load factor (ALF), and the reinforcement details. L_b is the length between two points of contraflexure or zero moment as shown in Figure 2-7. The ALF is defined as the ratio of the axial load (P) to the product

of three variables: column gross area (A_g), the in-plane geometry factor (1 for interior, 0.75 for exterior, and 0.5 for knee joint), and the transverse beam confinement factor (1 for joints with 0 or 1 transverse beam, and 1.2 for joints with 2 transverse beams). The input parameters related to the reinforcement include the beam longitudinal reinforcement ratio (ρ_b), the column longitudinal reinforcement ratio (ρ_c), the joint transverse reinforcement ratio (ρ_{jt}), the beam longitudinal reinforcement yield strength (f_{yb}), the column longitudinal reinforcement yield strength (f_{yc}), and the joint transverse reinforcement yield strength (f_{yjt}). V_b and V_c are the shear forces in the beams and columns, respectively. To facilitate the calculation process, a spreadsheet tool [46,47] is created for the calculation of v_{max} and shared as a freeware for the use of practicing engineers. The sheet employs the calculation process defined in Jeon [12].

Once v_{max} is computed, the shear stress-strain curve is defined as shown in Figure 2-8, where the yield and residual strengths are 95% and 20% of v_{max}, respectively. The cracking strength is defined as $0.48\sqrt{f'_c}$. Since there is a lack of analytical studies that compute the shear strain ordinates for cracking, yielding, maximum, and residual states, many studies have instead relied on experimental observations to propose shear strain ordinates. Anderson et al. [16] recommended the shear strain (γ) corresponding to the cracking and yielding strengths are 0.00043 and 0.006, based on experimental observation of 11 specimens but did not recommend any shear strains for maximum and residual states. To fill in these missing points on the backbone curve, Jeon [12] compiled a database of 44 exterior joints with transverse reinforcement, 28 exterior joints without transverse reinforcement, 47 interior joints with transverse reinforcement, and 35 interior joints without transverse reinforcement, and proposed mean shear strain at maximum and

residual points for each type based on experimental observations. The shear strains corresponding to the maximum and residual strengths respectively, 0.02 and 0.185 for exterior joints with transverse reinforcement, 0.016 and 0.077 for exterior joints without transverse reinforcement, 0.02 and 0.187 for interior joints with transverse reinforcement, and 0.019 and 0.117 for interior joints without transverse reinforcement. Figure 2-8 shows the shear stress-strain curves for exterior and interior joints with and without transverse reinforcement.

If the longitudinal reinforcement of a beam has insufficient straight embedment, a reduced shear stress-strain curve should be developed and used for that particular loading direction (e.g., upward in Figure 2-8) when defining the rotational spring. These curves are shown with red lines in Figure 2-8, where the bond strength (v_{bond}) is computed in terms of the shear strength proposed by Hassan [17]. The input parameters required to compute v_{bond} are the concrete compressive strength (f'_c), the reinforcement factor which is dependent on the beam longitudinal reinforcement diameter (φ_b) and concrete cover (cc), the axial load factor (ALF), the tension force in the beam longitudinal reinforcement (T), and the embedment length (l_s) of the beam reinforcement within joint. Once v_{bond} is computed, the shear stress-strain curve with bond slip is defined as shown in Figure 2-8 with red lines where the yield and residual strengths are 95% and 20% of v_{bond}, respectively. The developed spreadsheet [46] executes these calculations and provides the values required for the construction of the shear stress-strain curves.

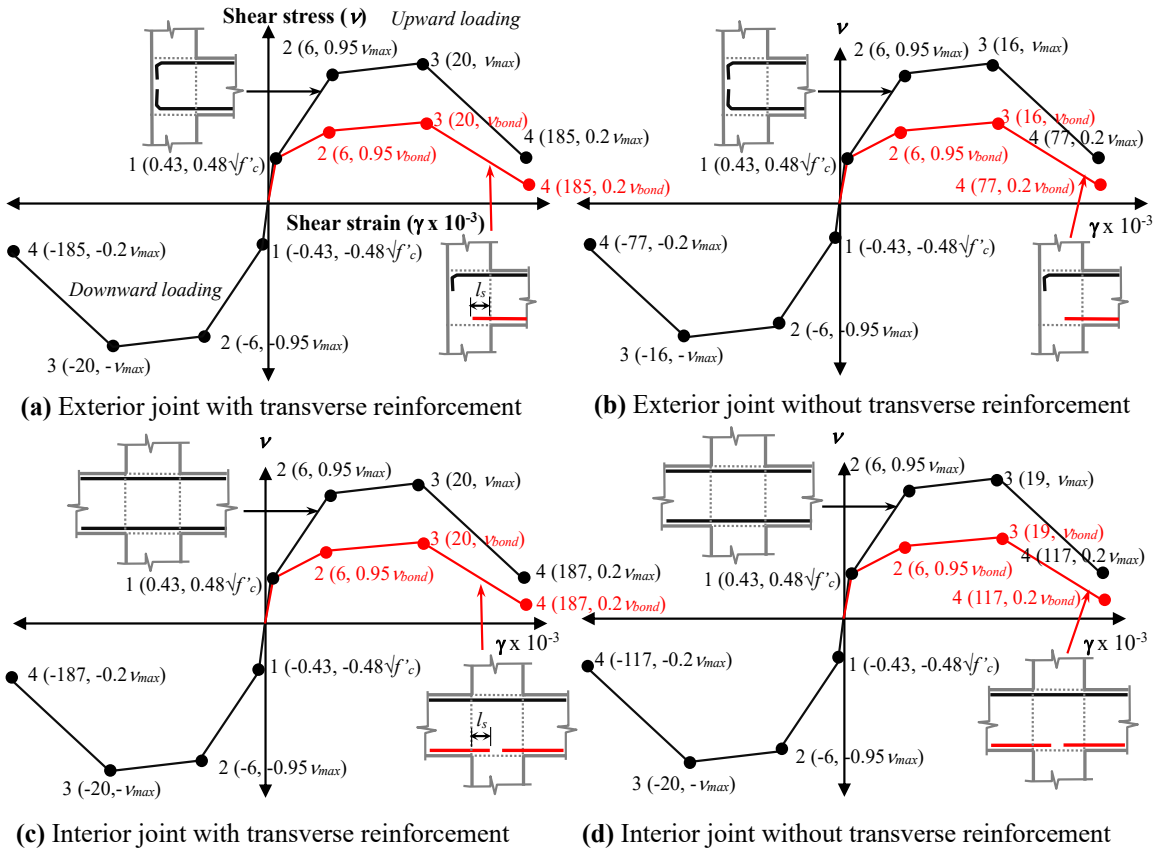

Figure 2-8: Shear stress-strain curve developed using Model 1 (adopted from [12])

To define a rotational spring in a global frame analysis, the calculated shear stress-strain points should be transformed into equivalent moment-rotation points. For this, the modeling approach uses the formulations proposed by Celik and Ellingwood [18] as shown below.

$$M_{\max} = v_{\max} A_j \frac{1}{\frac{1-h_c/L_b}{jh_{be}} - \frac{\alpha}{L_c}} \tag{1}$$

$$M_{bond} = v_{bond} A_j \frac{1}{\frac{1-h_c/L_b}{jh_{be}} - \frac{\alpha}{L_c}} \tag{2}$$

$$\theta = \gamma \tag{3}$$

M_{max} and M_{bond} are the equivalent moment capacities for shear and bond strengths, respectively, h_{be} is the effective depth of the beam (to the centroid of the reinforcement), A_j is the area of the joint core ($A_j = h_b \times h_c$), j is a constant taken as 0.875, and α is a constant equal to 2 for knee joints and 1 for all other joints. Since the joint rotation is the change in the angle between the two edges of the joint core, the rotation is equivalent to the shear strain as shown in Eq. (3). Using these equations, the equivalent moment-rotation curves for various joint and reinforcement anchorage conditions are shown in Figure 2-9. The developed spreadsheet [46] executes these calculations and provides the moment-rotation points for inputting into a global frame analysis when defining rotational hinges. The developed tool is validated against the maximum capacity of experimental testing of both exterior and interior joints with or without transverse reinforcement [47].

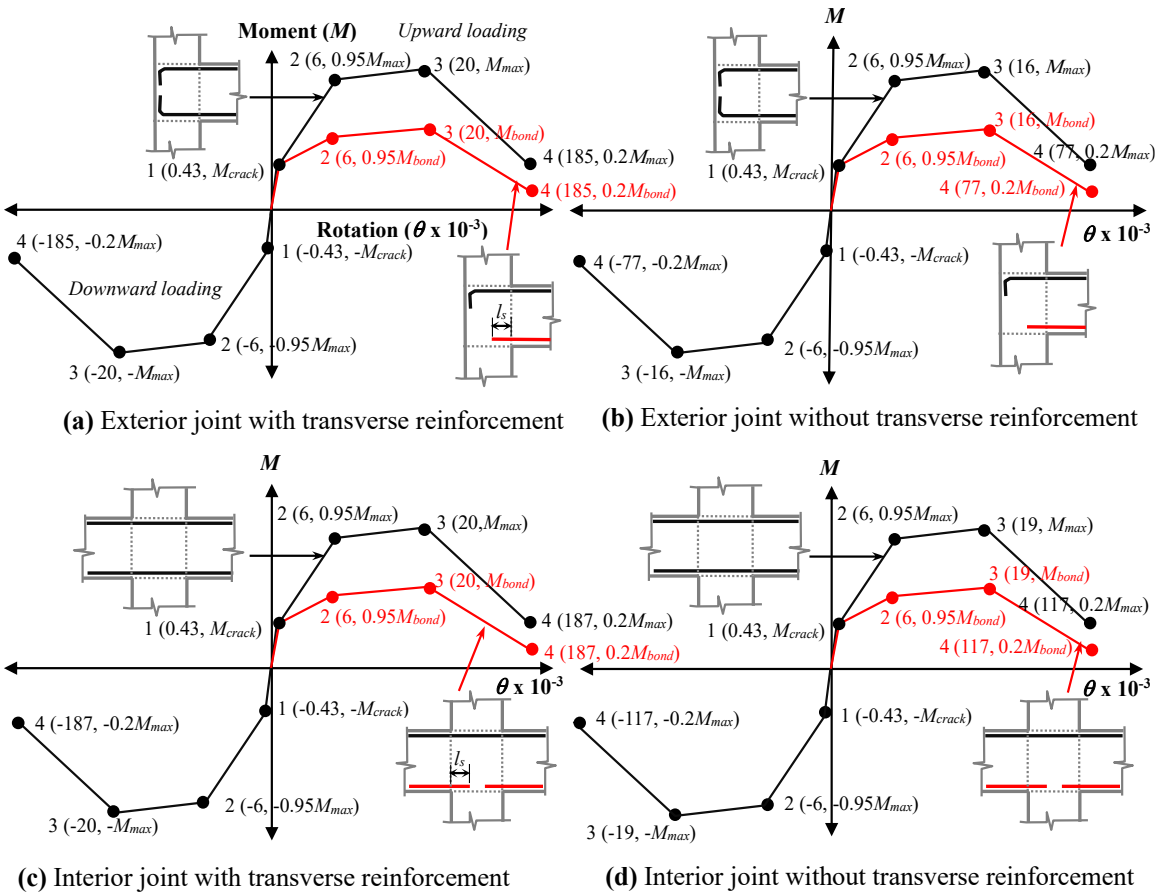

Figure 2-9: Moment-rotation curve developed using Model 1 (adopted from [12])

To model a beam-column joint using Model 2, two types of springs are defined as plastic hinges: a shear spring in the column region and a rotational spring in the beam region (see Figure 2-10). The shear spring models the shear deformations while the rotational spring models the bond slip behavior.

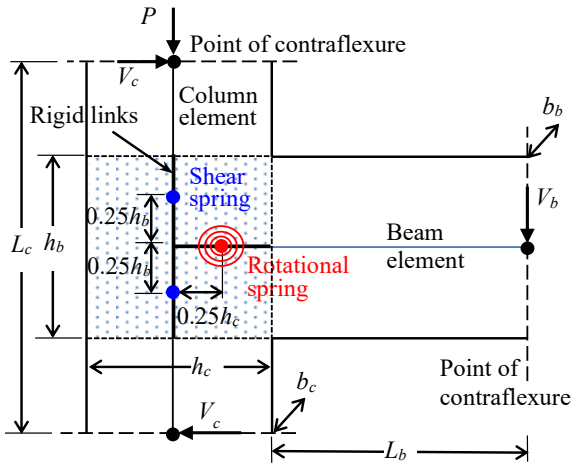

Figure 2-10: Location of spring elements in exterior joint using Model 2

Analogous to Model 1, four points should be defined to develop the shear stress-strain and moment-rotation curves required for the shear and rotation spring hinges, respectively. The input parameters required to define the shear strength and moment capacity are the concrete compressive strength (f'_c), the cross-sectional dimensions of the beams and columns (b_b, b_c, h_b, h_c,), the clear length of the beam from the face of the column to the point of contraflexure (L_b), the column length between two points of contraflexure (L_c), the axial stress in the column $\sigma_a = P / (h_c \text{ x } b_c)$, the principal tensile stress (p_t), and the tensile force in the beam longitudinal reinforcement (T). This model uses a failure criterion based on limiting principal tensile stresses in the joint core; therefore, the curves are developed by computing the shear and moment capacities at different principal tensile stress levels. For exterior joints with properly hooked reinforcing bars, the principal tensile stress for cracking is defined as $0.29\sqrt{f'_c}$, yielding and maximum as $0.42\sqrt{f'_c}$, and residual as $0.10\sqrt{f'_c}$, based on Priestley [48]. For exterior joints with insufficient straight embedment of beam longitudinal reinforcement, the principal tensile stress for cracking is defined as $0.13\sqrt{f'_c}$, both yielding and maximum as $0.19\sqrt{f'_c}$, and residual as $0.06\sqrt{f'_c}$, based on Murty

et al. [49]. Once the principal tensile stresses are defined, the shear stress and moments values corresponding to cracking, yielding, maximum, and residual are computed. In Figure 2-11, the shear stress and moment values for cracking are v_{crack} and M_{crack}, yielding are v_{yield} and M_{yield}, maximum are v_{max} and M_{max}, and residual are v_{resid} and M_{resid}, respectively. Similarly, the shear strains and rotations corresponding to cracking, yielding, maximum, and residual are defined as 0.0002, 0.002, 0.005, and 0.025, respectively for joints with properly hooked reinforcing bars, and 0.0002, 0.002, 0.005, and 0.015, respectively for joints with insufficient straight embedment of beam longitudinal reinforcement. The resulting shear stress-strain and moment-rotation curves are shown in Figure 2-11a and b, respectively. These values are used as input in a global frame analysis when defining the shear and rotational hinges. The developed spreadsheet [46] calculates both curves, as per the calculation process defined in Sharma et al. [8] and provides four pairs of data for copying and pasting into frame analysis software.

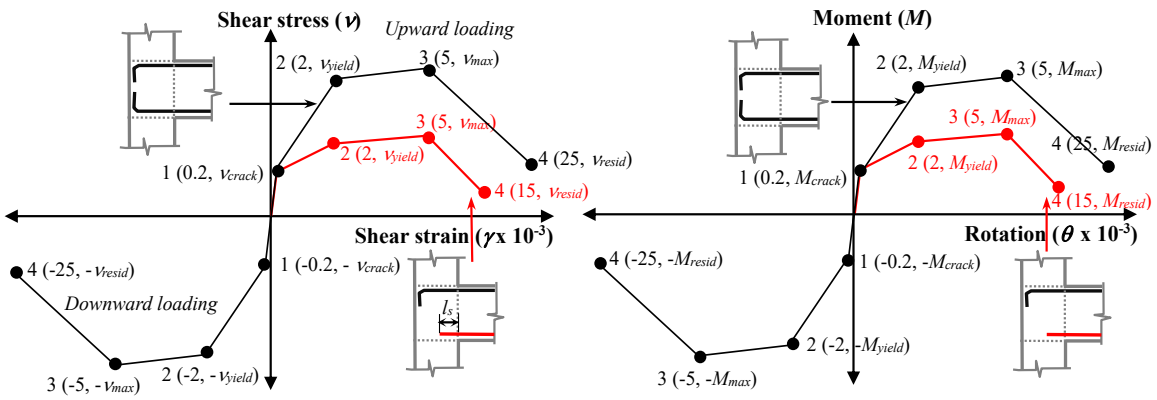

(a) Shear stress-strain curve

(b) Moment rotation-curve

Figure 2-11: Shear stress-strain and moment-rotation curve development using Model 2 (adopted from [8])

The third stage involves the derivation and placement of moment and shear hinges to model the inelastic behavior of beams and columns at the hinge locations. This is a common stage undertaken in plastic-hinge-based frame analysis and therefore only critical aspects are discussed. The moment hinge is assigned at the interface of the beams and columns (see Figure 2-10 and Figure 2-11) due to the peak values taking place at these points. The hinge length for the moment hinge is commonly taken as the cross-section depth (h_b) which is also recommended in CSI [50]. The shear hinge is defined $0.75h_b$ away from the interface with a depth of $1.5h_b$ [51]. A schematical overview of the hinge locations for beams, columns, and beam-column joints using either Models 1 or Model 2 is shown in Figure 2-12 and Figure 2-13 respectively.

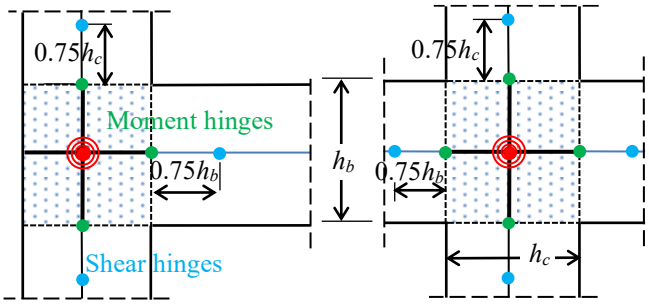

(a) Exterior joint **(b)** Interior joint

Figure 2-12: Beam, column, and joint modeling using Model 1

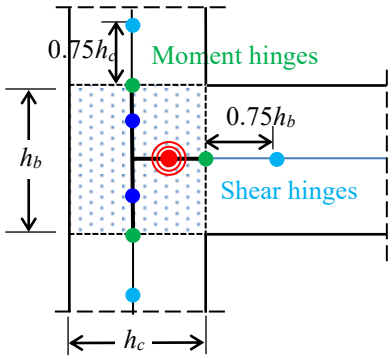

Figure 2-13: Beam, column, and joint modeling using Model 2

The fourth stage involves the application of the loads. This is common across various frame analysis methods. The loads could be applied in a force or displacement-controlled manner depending on the pushover analysis method used.

The final stage is to run the analysis and calculate the hinge conditions for each load stage. Common frame analysis software, such as SAP2000 [50], ETABS [52], RISA-3D [53], MIDAS Civil [54], PERFORM-3D [55] may be used. Some of the software provides color-coded hinge conditions which enables the identification of the hinge condition from Point 1 to 4 (see Figure 2-9 and Figure 2-11) to determine the governing behavior and failure mode.

2.5 Application and Experimental Validation of the Proposed Approach

The objective of this section is to demonstrate the application and experimental validation of the proposed modeling approach. It should be noted that the theoretical formulation of Model 1 was previously validated with the experimental tests of 28 interior and exterior joint specimens with errors up to 8.4% [12], and Model 2 with 12 exterior joint specimens with an average error of 8.6% [8]. For demonstration purposes, an exterior joint specimen from the literature is modelled with the proposed approach and the predicted responses are compared with the experimental results. The modelled experimental specimen is shown in Figure 2-14. The compressive strength of the concrete is 33.1 MPa. The column has 25M reinforcing bars with 10M hoops while the beam has 29M bars and 10M stirrups. The yield strength (f_y) and ultimate strength (f_u) of the reinforcement are 459 and 761 MPa for 29M bars, 470 and 742 MPa for 25M bars, and 427 and 654 MPa for 10M

bars, respectively. The top longitudinal reinforcement of the beam was bent into the joint, whereas the bottom reinforcement was extended straight 152 mm from the face of the column. The axial load applied to the column was 10% of the concrete compressive strength and the test setup used pin supports at the top and bottom of column. The beam and column have sufficient reinforcement (longitudinal and transverse) to prevent early beam and column damage while there is no transverse reinforcement in the joint to confine the core. Therefore, this is a well-suited specimen to validate beam-column joint modeling approaches.

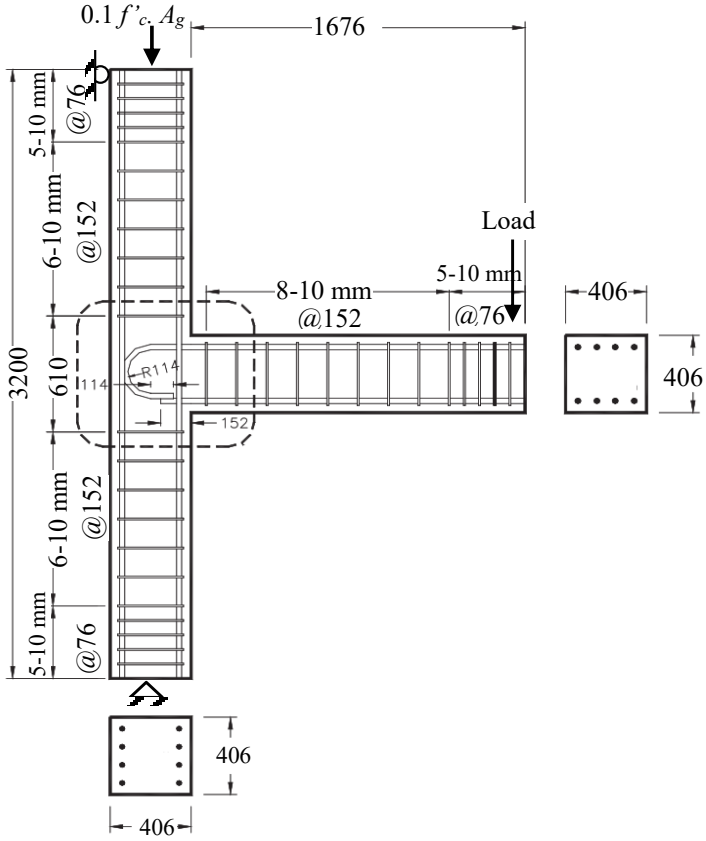

Figure 2-14: Experimental setup of the specimen modelled [56]

The proposed approach requires the use of either Model 1 or Model 2. However, for demonstration and validation purposes, both models are employed as presented below.

2.5.1 Using Joint Model 1

The procedure discussed in Section 2.4 is applied to this specimen. A rotational spring element is defined as the plastic hinge in the joint as shown in Figure 2-7. This rotational spring represents shear and bond slip behaviors. The joint shear stress-strain, and moment-rotation curves are derived with the help of the developed spreadsheet and presented in Figure 2-15. The shear strengths in the upward and downward loading directions are calculated as 2.90 MPa and -5.36 MPa, respectively, and the moment capacities in the upward and downward loading directions are calculated as 186 kNm and -345 kNm, respectively. These values are then used in the global frame analysis software to define the plastic hinges shown in Figure 2-16a.

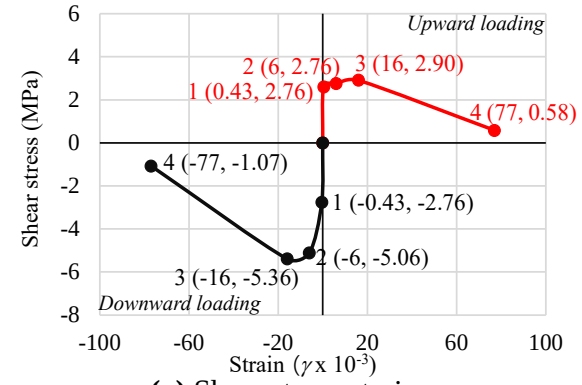

(a) Shear stress-strain curve

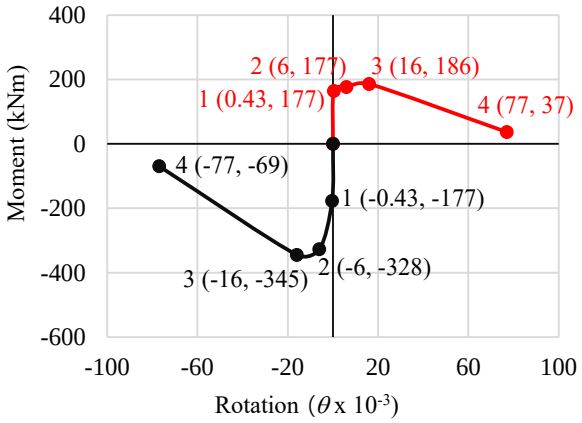

(b) Moment-rotation curve

Figure 2-15: Shear stress-strain and moment-rotation curves using Model 1

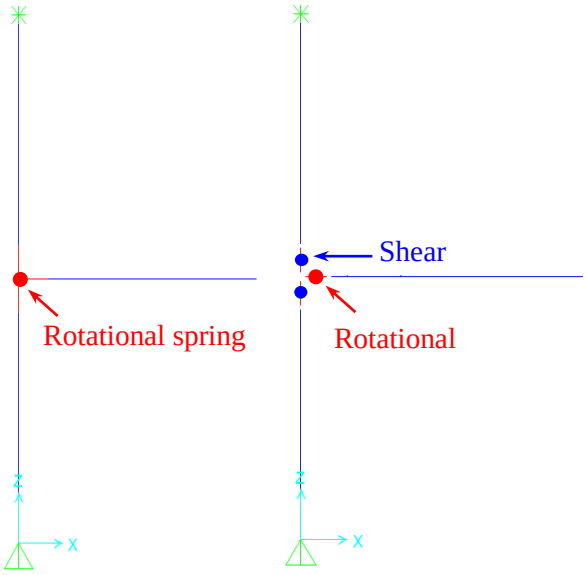

(a) Model 1 **(b)** Model 2

Figure 2-16: Frame models developed with joint

2.5.2 Using Joint Model 2

The procedure discussed in Section 2.4 is applied to this specimen. Two types of spring elements are required by this model. A shear spring hinge is used to model shear deformation while a moment spring hinge is used to model the bond slip effect as shown in Figure 2-10. The joint shear stress-strain, and moment-rotation curves are derived with the help of the developed spreadsheet and presented in Figure 2-17. The shear strengths in the upward and downward loading directions are computed as 0.40 MPa and -0.74 MPa, respectively, and the moment capacities in the upward and downward loading directions are computed as 194 kNm and -354 kNm, respectively. These values are used as the spring characteristics in the global frame analysis software to model the joint's behavior. These values are then used in the global frame analysis software to define the plastic hinges shown in Figure 2-16b.

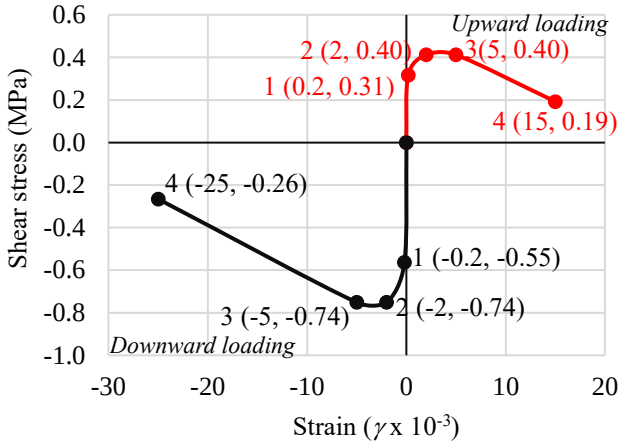

(a) Shear stress-strain curve for the shear spring

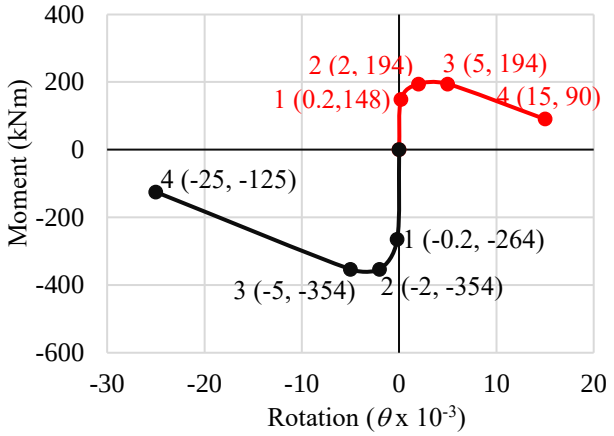

(b) Moment rotation curve for the rotational spring

Figure 2-17: Shear stress-strain and moment-rotation curves obtained using Model 2

2.5.3 Defining Beam and Column Hinges

In the third stage, plastic hinges for shear and moment are derived and placed at the critical location of the frame elements as discussed in Section 2.4. Figure 2-18a and b show the location of all plastic hinges (for both frame elements and joint) using both joint models. These are the final frame models used in this validation study.

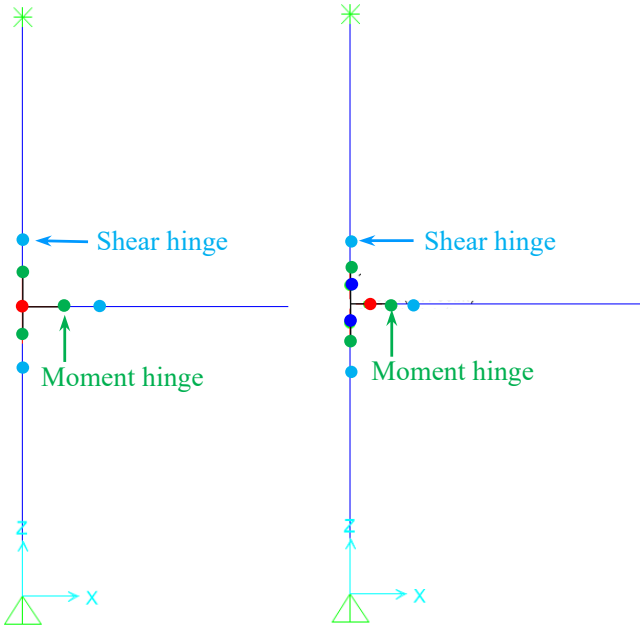

(a) Model 1 **(b)** Model 2

Figure 2-18: Frame models developed with all hinges

2.5.4 Applying the Loads and Performing the Analysis

In the fourth stage, a constant axial load of 542 kN is applied at the column. A displacement-controlled pushover analysis protocol is used for the load application at the tip of the cantilever beam. In the fifth stage, the analysis is run until the failure of the specimen.

2.5.5 Comparison of Predicted and Experimental Results

Figure 2-19 shows the progression of the joint damage under increased beam loading in the experimental study. Level I corresponds to the first yielding of the longitudinal reinforcement, Level II to the formation of the bond slip mechanism, Level III

to significant shear cracking in the joint core, Level IV to significant spalling of concrete at joint interface, and Level V is the loss of the load capacity.

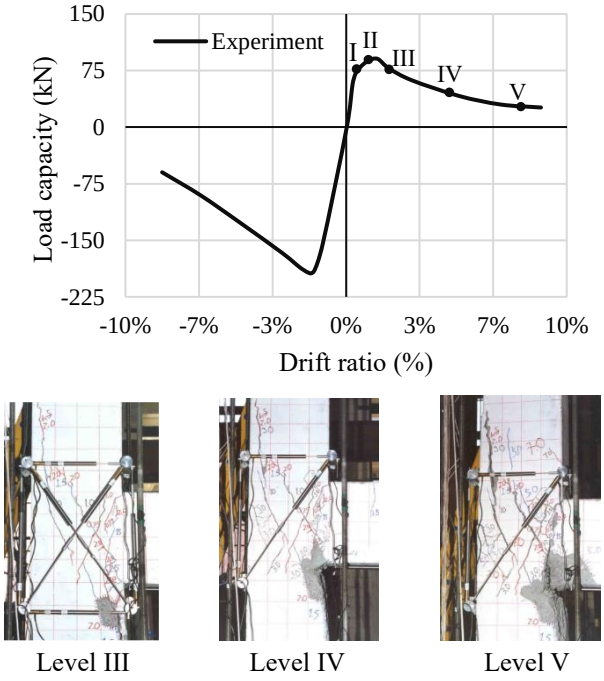

Figure 2-19: Joint damage progression [7]

Figure 2-20 shows the comparison of the analysis results (using the proposed modeling approach) with the experimental results. Both models performed numerically efficiently and provided accurate responses.

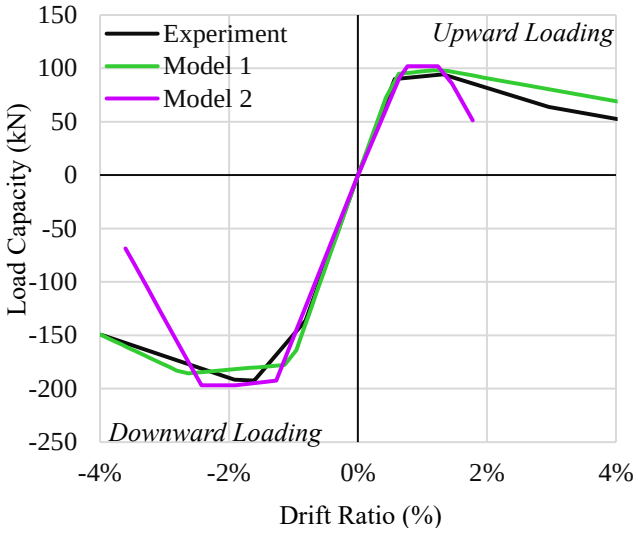

Figure 2-20: Comparison of the analysis results with the experimental result

Model 1 captured the experimental load capacity reasonably well. The ratio of the predicted load (P_p) to the experimental load (P_{exp}) is 0.96 and 1.04 for the downward and upward loading directions, respectively. This specimen exhibited a bond slip failure in the upward loading direction while a joint shear failure in the downward loading direction. The failure modes in both directions are predicted accurately by the analysis. The average calculation error is 4.2% which is considerably less than the error one could expect to have when modeling shear and bond slip behaviors.

Model 2 also captured the experiment response reasonably well. The ratio of the predicted load (P_p) to the experimental load (P_{exp}) is 1.02 and 1.08 for the downward and upward loading directions, respectively. The average calculation error is 5.0%, which is also well acceptable. Model 2 was also able to capture the failure modes in both loading directions accurately.

The post-peak response of joints sustaining shear and bond-slip failures are more challenging to capture and typically requires more sophisticated modeling approaches, such as component or finite element models. This is also evident from the predicted post-

peak responses which show deviations from the experimental responses. The rotational spring models are most useful for the calculation of load and deformation responses up to the peak load on which the design or assessment should be based in forensic engineering studies.

To demonstrate the significance of modeling the shear and bond-slip behaviors in joints, the same specimen is modelled using a rigid joint model. This approach only uses rigid links in the joint core without any rotational or shear springs. This neglects the deformations in the joints and enforces the assumption that the beam and column members remain perpendicular even under significant deformations. Figure 2-21 shows the comparison of the predicted results. The ratio of the predicted load (P_p) to the experimental load (P_{exp}) is 1.15 and 2.34 for the downward and upward loading directions, respectively. The omission of the bond slip failure in the upward loading direction resulted in a major discrepancy with the experimental results. If this modeling approach was used for the analysis, a highly inaccurate and unsafe prediction would have been obtained. Table 2.1 summarizes the responses obtained for this specimen from three modeling approaches.

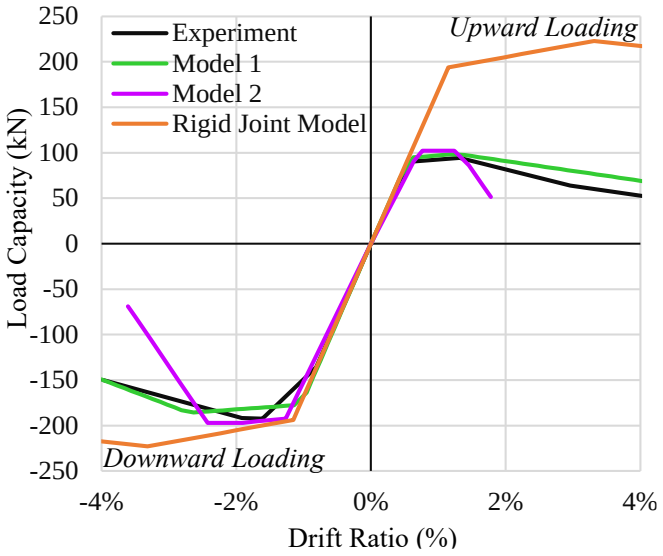

Figure 2-21: Comparison of the analysis results with the experimental result

Table 2.1: Comparison of predicted and experimental results

	Downward loading (kN)	P_p/P_{exp}	**Upward loading (kN)**	P_p/P_{exp}
Experiment	192.6	1.00	94.3	1.00
Model 1	185.6	0.96	98.1	1.04
Model 2	196.9	1.02	102.1	1.08
Rigid Joint Model	220.7	1.15	220.7	2.34

2.6 Conclusions

This study presented a beam-column joint modeling approach based on mathematical formulations available in the literature to aid practicing engineers in incorporating joint modeling into global frame analysis using 1D frame elements. The proposed approach integrates rotational spring models into lumped-plasticity-based frame analysis methods based on two distinct formulations. A spreadsheet tool is also developed to execute mathematical calculations. The modeling approach, and the spreadsheet, is verified by modeling of an exterior joint from literature through a global frame analysis.

The predicted responses are compared with the experimental results. The findings of the study support the following conclusions:

- Beam-column joints are susceptible to exhibiting shear and bond-slip failure modes. It is important to include both modes in global frame models for forensic studies. The rigid joint models omit both behaviors and may provide highly inaccurate and unsafe response predictions for joints exhibiting shear and/or bond slip behaviors.

- Rotational spring models provide a good balance between the simplicity and accuracy for the forensic analysis of frames. They are particularly useful for predicting the response up to the peak load capacity.

- The proposed modeling approach is numerically efficient and practical. It can be implemented into global frame analysis software when defining plastic hinges.

- The developed spreadsheet facilitates the derivation of the hinge curves and generates the data needed for inputting into global frame analysis software.

- The experimental validation study demonstrates that the proposed modeling approach captures both joint shear and bond slip failure models and predicts the beam-column joint capacity with a maximum error of 8.0% for the specimen investigated in this study.

- Model 1 is applicable to a wide range of joint types including interior and exterior joints with and without transverse reinforcement. The shear and bond slip behaviors are modelled with a single rotational spring. Joint Model 2 is limited to the exterior joints without transverse reinforcement. The shear and bond slip behaviors are

modelled with shear and rotational springs separately. This may provide advantages if discrete consideration of shear and bond slip behaviors is desired.

- The proposed modeling approach is not limited to joint Model 1 and Model 2. Any other validated rotational spring models may also be used.

2.7 Acknowledgments

The authors would like to thank Mr. Prajwol Hada, a graduate student in the Department of Civil and Environmental Engineering at the University of Toledo, for his help with sketching the figures and editing the references list.

Chapter 3

Journal Paper II – Plastic Hinge Modeling of Reinforced Concrete Beam-Column Joints using Artificial Neural Networks[2]

3.1 Abstract

Beam-column joints play a critical role in transferring forces between beam and column elements and maintaining structural integrity during severe loading. While the nonlinear behaviors of beams and columns are commonly modeled in global frame analyses through the use of plastic hinges, the behavior of joints is often omitted through the use of rigid end offsets. The objective of this study is to develop an artificial neural network and derive the plastic hinge curves required for modeling beam-column joints in global frame analyses. As the first step, a feed-forward artificial neural network (FFNN) is developed to predict the shear strengths of beam-column joints. A comprehensive dataset of 598 experimental joint specimens is compiled from 153 previously published research studies. The 555 data points which passed the exploratory data analysis, are used to train,

[2] Manuscript submitted to and under review in Engineering Structures, Nirmala Suwal & Serhan Guner, Plastic Hinge Modeling of Reinforced Concrete Beam-Column Joints using Artificial Neural Networks, © 2023, with permission from Elsevier. For the published version, please refer to https://www.utoledo.edu/engineering/faculty/serhan-guner/publications.html.

test, and validate the proposed network for applicability to a wide range of input variables and joint configurations. The accuracy and reliability of the proposed FFNN are evaluated using a comprehensive set of evaluation metrics in comparison with three existing networks from the literature. In the next step, the proposed FFNN is used to derive the shear stress-strain and moment-rotation curves required for defining joint hinges in global frame analyses. As the final step, a spreadsheet tool is developed to execute the network formulations, calculate the joint shear strength, and derive the joint hinge curves for the use of engineers and researchers.

3.2 Introduction

Reinforced concrete beam-column joints may undergo severe deformations leading to local damage, or, in extreme cases, failures affecting the integrity of an entire frame structure. The main phenomena affecting the behavior of joints are the shear and bond slip deformations in the joint core. In addition, joint deformations are a major contributor to lateral story drifts [1] which places another demand on the frame. While the nonlinear behaviors associated with beams and columns are commonly accounted for in global frame analyses, the behavior of joints is often neglected through the use of rigid end offsets or other techniques that suppress joint deformations.

The primary failure modes associated with joints include the joint shear and bond slip failures [2,3]. The joint shear failure occurs when the shear stress in the joint core exceeds its shear capacity, leading to diagonal cracking of the joint core as shown in Figure 3-1a. The bond slip failure occurs when a set of reinforcing bars embedded in or passing

through a joint core cannot develop the required bond strength with the surrounding concrete, leading to bar slippage and separation of the beam from the joint core as shown in Figure 3-1b. Joint failures may also take place in combination with the beam and column failure modes that may include flexural and shear failure modes as shown in Figure 3-1c.

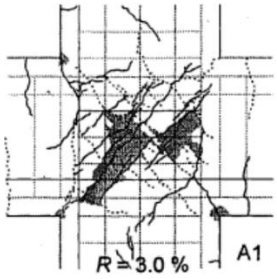

Shiohara and Kusuhara [4]

Sasmal et al. [5]

(a) Joint shear failure (S) **(b)** Bond slip failure (B)

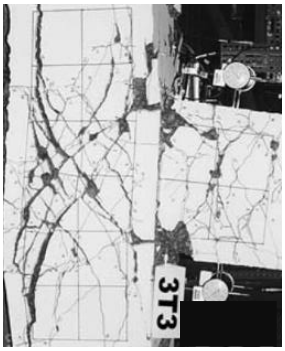

Hwang et al. [6]

(c) Combined joint shear-beam flexure failure (S-F)

Figure 3-1: Potential failure modes in beam-column joints

Reinforced concrete frames are commonly modeled using one-dimensional frame elements based on the plastic hinge approach. This approach requires defining a plastic hinge in the form of a spring with a pre-defined force-deformation behavior. This behavior is typically idealized with multi-linear curves having pre-defined points such as cracking, yielding, maximum, and failure. There are well-defined procedures for deriving the beam and column hinge curves to model the nonlinear behavior and failure modes of beams and

columns [7,8]. Many commonly used frame analysis tools employ these procedures to automatically derive the beam and column hinge curves. Modeling the behavior of beam-column joints, however, is more complex and there is no well-defined process or an automated joint hinge calculation in most common frame analysis tools.

Modeling techniques for beam-column joints range from simple rotational spring models [9-13] to more elaborate component models [14-17] and finite element models [18,19]. Implementation of rotational springs in the joints of a global frame model is simple; however, the derivation of spring curves, in the form of stress-strain or moment-rotation relations, are challenging. There are many studies and formulations that can be used to derive the spring properties, but each set of formulations are empirically derived based on the experimental testing of a handful of beam-column specimens. Consequently, each set of formulations is valid for the joint configurations included in the experimental tests used to derive the formulations. There are many different joint configurations due to the large number of parameters required for defining a joint – as an example, this study uses 13 parameters to define a beam-column joint. This creates a major challenge for finding formulations that are valid for the joint configurations being modeled, and, in many cases, valid joint formulations may not be found.

This study aims to develop an artificial neural network to predict the joint shear strength with high accuracy and for a wide range of joint configurations. The network is trained, tested, and validated with more than 500 experimental beam-column joint specimens representing a large range of parameters. The developed formulations are implemented into a spreadsheet tool to enable practicing engineers to easily derive the

shear stress-strain and moment-rotation curves for inputting into a global frame analysis model.

3.3 Review of Existing Literature

Artificial neural networks consist of interconnected cells called neurons. Neurons modify themselves based on the information flowing through them, mimicking the learning process of biological neurons in the human brain (Figure 3-2). Each neuron receives an input signal and plugs it into a mathematical function. This function is called an activation function. The role of this function is to convert the net input into the output of the neuron, also called 'output signal'. The output signals are modified by scalar values called 'weights' and 'biases' and then forwarded to the neurons in the subsequent layer. The neurons at the final layer output the ANN predictions.

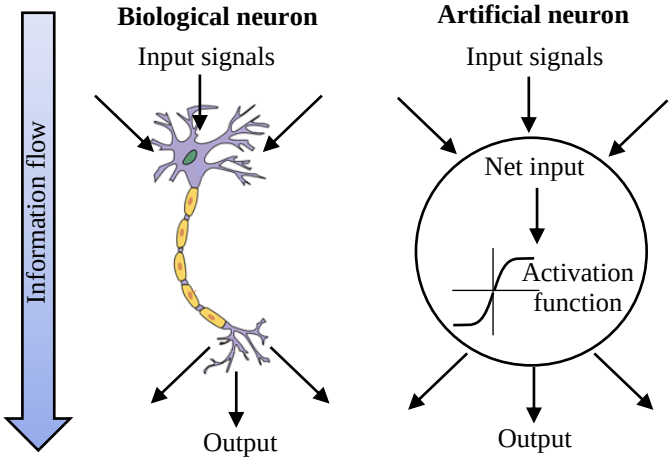

Figure 3-2: Biological and artificial neurons [20]

A typical ANN will initially have random weights and biases with small values (e.g., between 0 and 1), which will lead to inaccurate results. To increase its accuracy, the

ANN needs to be trained so that the weights and biases are adjusted to give more accurate results. Training of the ANN allows it to find approximate solutions to complex problems that would be challenging to solve with conventional techniques. The main types of ANNs are feed-forward, radial basis, Kohonen self-organizing, recurrent, convolutional, and modular. The feed-forward neural networks (FFNNs), which are used in this study, are one of the simplest types of ANNs. Conventional FFNNs consist of an input layer, one (and only one) hidden layer, and one output layer while deep FFNNs have multiple hidden layers. Their name comes from the information flow which always goes in one direction, from inputs to outputs (i.e., forward). More information on the types and formulations of ANNs can be found in Almeida and Guner [20].

A number of studies explored the use of ANNs for the prediction of beam-column joint shear strengths and failure modes. Kotsovou et al. [21] used an ANN to evaluate the shear capacity of exterior beam-column joints based on a database of 153 specimens. The ANN predictions achieved a mean of 0.99 and standard deviation of 6.4% for the predicted-to-experimental shear strengths which were shown to be significantly better than the values obtained from the design codes such as ACI 318 [7], EC2 [22], and EC8 [23]. Gao and Lin [24] explored various machine learning methods, including an ANN, to predict the failure modes of interior beam-column joints based on a database of 580 experimental specimens. They found that the ANN predicted the correct failure mode for 77% of the specimens. Alagundi and Palanisamy [25] proposed an ANN to predict the shear strength of exterior beam-column joints and compared its performance to the empirical equations from various design codes. This ANN was developed based on a limited experimental database of 75 specimens and provided a mean of 1.05 for the predicted-to-experimental shear strength

ratios; the standard deviation was not reported. To remedy the limitations of the aforementioned models, Haido [26] proposed an ANN to predict the shear strengths of both exterior and interior joints and compared its performance with empirical formulations and the values obtained from various design codes. This ANN was developed based on a database of 200 experimental specimens. Compared to the design code equations, this model demonstrated better accuracy with a mean of 0.97 and a standard deviation of 24.1% for the predicted-to-experimental shear strength ratios. Marie et al. [27] compared six machine learning methods, including ordinary least squares (OLS), support vector machine (SVM), k-nearest neighbor (KNN), multivariate adaptive regression splines (MARS), ANN, and kernel regression, to predict the shear strengths of both interior and exterior beam-column joints. The experimental database included 98 specimens with and without transverse reinforcement. This ANN predicted the joint shear strengths with a mean ratio of 0.96 for the predicted-to-experimental shear strength ratios; the standard deviation was not reported.

These studies demonstrate the successful applications of ANNs for predicting the beam-column joint shear strengths. This current study aims to develop an ANN with higher accuracy and more general applicability, including exterior and interior joints with or without transverse reinforcement. The end goal is to use this network to derive the joint spring curves that can be readily used in a global frame analysis model for capturing the behavior of the joint.

3.4 Proposed Feed-Forward Neural Network (FFNN)

A feed-forward neural network is developed to predict the shear stress that would cause the failure of the joint, termed as the shear strength. The main components of this network include the training algorithm, activation functions, prediction error, optimization function, learning rate, network configuration, and number of iterations. A feed-forward algorithm, with the supervised back-propagation technique, is used for the training.

The input values (x) in the input layer are modified by weights (w) and biases (b) associated with each neuron using Eq. (1). The resulting net input (u) is modified by the activation function, in Eq. (2), to produce the output (y). A sigmoid function is chosen as the activation function because it is smooth and differentiable over its entire length and has been used successfully in previous applications [20,28-30]. Once the output is predicted by the network, the mean squared error (MSE) is calculated for n data points, as defined in Eq. (3), between the predicted (τ_{pred}) and experimental (τ_{exp}) shear strengths. The back propagation is performed to minimize the MSE by propagating it from the output layer back through the network to the input layer.

$$u = \sum (wx + b) \tag{1}$$

$$y = \frac{1}{1 + e^{-u}} \tag{2}$$

$$\text{MSE} = \frac{1}{n} \sum (\tau_{pred} - \tau_{exp})^2 \tag{3}$$

Adaptive moment estimation (Adam) [31] is used as an optimization function to update the weights and biases according to Eqs. (4) and (5), respectively, with a learning rate (k) of 0.01. This allows the weights and biases to converge to optimum values with

less iterations (i.e., faster) while providing more accurate shear strength predictions. Adam uses the stochastic momentum for gradient descent [32] (V_d) along with the root mean square propagation ($\sqrt{Sd_b + \varepsilon}$) [33].

$$w = w - k\frac{Vdw}{\sqrt{Sd_w + \varepsilon}} \tag{4}$$

$$b = b - k\frac{Vd_b}{\sqrt{Sd_b + \varepsilon}} \tag{5}$$

The stochastic momentum gradient descent (V_d) accelerates the convergence speed of a stable FFNN by building up velocity in consistent gradient directions over time. This gradient is determined by the derivative of the MSE with respect to the weights or biases. For t number of iterations, V_d is expressed in Eq. (6) for weights and Eq. (7) for biases, where β is a constant taken as 0.9.

$$Vd_{wt} = \beta Vd_{w(t-1)} + (1-\beta)\frac{dMSE}{dw} \tag{6}$$

$$Vd_{bt} = \beta Vd_{b(t-1)} + (1-\beta)\frac{dMSE}{db} \tag{7}$$

The root mean square propagation ($\sqrt{Sd_b + \varepsilon}$) has the ability to adjust the learning rate based on the historical gradients and improve the convergence speed. For t number of iterations, the term (S_d) is expressed in Eq. (8) for weights and Eq. (9) for biases. The term ε is introduced to avoid the division-by-zero error. A small value in the range of 10^{-8} to 10^{-10} may be used for ε. In this study, the value of 10^{-8} is used.

$$Sd_{wt} = \beta Sd_{w(t-1)} + (1-\beta)(\frac{dMSE}{dw})^2 \tag{8}$$

$$Sd_{bt} = \beta Sd_{b(t-1)} + (1-\beta)\left(\frac{dMSE}{db}\right)^2 \quad (9)$$

With the goal of capturing the advantages of both stochastic momentum gradient descent and root mean square propagation, Adam is implemented in the proposed FFNN by using TensorFlow [34], which is an open-source machine learning platform in Python programming language [35].

A parametric study is conducted to determine the most efficient network configuration and the optimum number of iterations. The experimental database is split into training (80%), testing (10%), and validation (10%) datasets. The network with the components discussed above is trained, tested, and validated with these sets. The MSEs are computed for various network configurations and number of iterations. As shown in Figure 3-3a, the most efficient network configuration was found for a single hidden layer with 27 neurons. As shown in Figure 3-3b, 100 iterations were found to give the lowest MSEs for the training, testing, and validation, and thus used in the developed network.

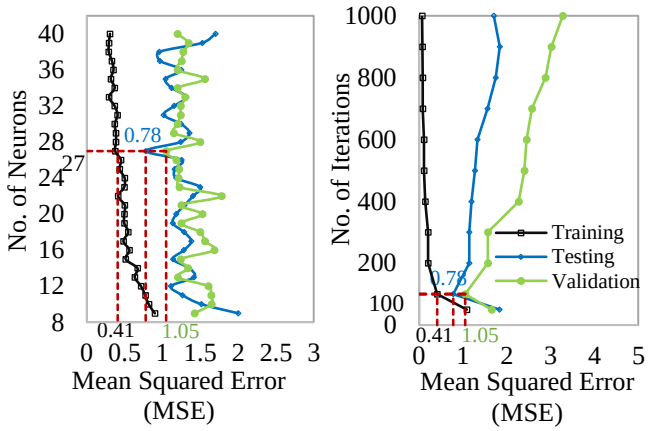

(a) Neurons **(b)** Iterations

Figure 3-3: MSEs computed for various network configurations and number of iterations.

The final configuration of the network is presented in Figure 3-4. The 13 input variables include the followings: f'_c is the concrete compressive strength; ρ_{jt} is the joint transverse reinforcement ratio; f_{yjt} is the joint transverse reinforcement yield strength; ρ_b is the beam longitudinal reinforcement ratio; f_{yb} is the beam longitudinal reinforcement yield strength; b_b is the beam width; h_b is the beam depth; ρ_c is the column longitudinal reinforcement ratio; f_{yc} is the column longitudinal reinforcement yield strength; b_c is the column width; h_c the column depth; ALF is the axial load factor which equals to $P/f'_c h_c b_c$ where P is the axial load applied to the column, and JT is the joint type. The output variable is the joint shear strength, τ_{pred}.

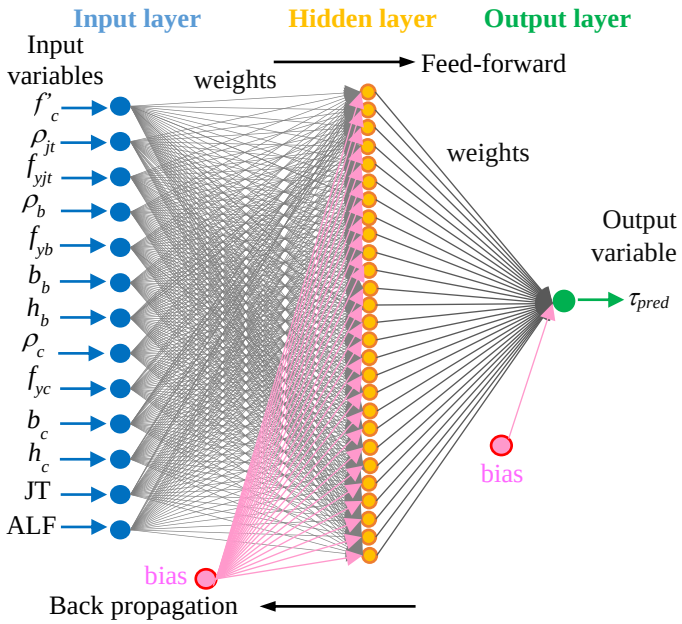

Figure 3-4: Proposed network configuration

3.4.1 Experimental Database

An experimental database of 598 beam-column joint specimens is compiled from 153 previously published research studies and presented in Appendix. The common

properties of the specimens include: *i)* the top beam reinforcing bars are hooked 90 degrees toward the joint core for exterior joints and continuous for interior joints; *ii)* the bottom beam reinforcing bars are either embedded straight or hooked towards the joint core for exterior joints and continuous for interior joints; *iii)* the vertical column reinforcing bars passing the joint core are straight; and *iv)* the specimens are planar without out-of-plane elements. Figure 3-5 illustrates the common reinforcing bar configuration of the specimens.

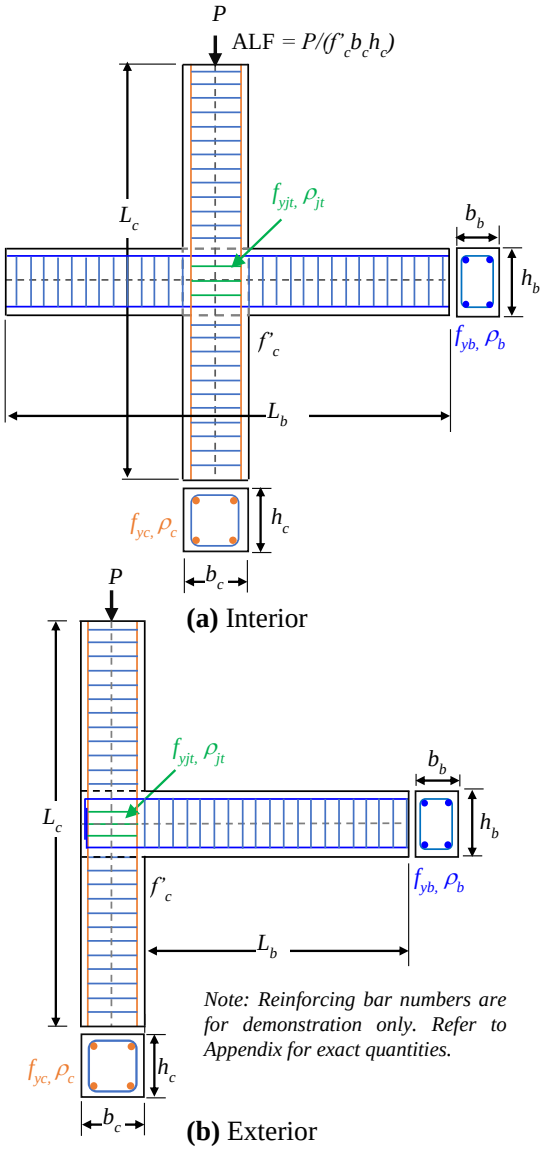

Figure 3-5: Common properties of experimental specimens

The experimental database includes 273 exterior joints with transverse reinforcement, 120 exterior joints without transverse reinforcement, 148 interior joints with transverse reinforcement, and 57 interior joints without transverse reinforcement. As presented in Table 3.1, the vast majority of specimens experienced joint shear failure (S) or a combined joint shear and interface flexure failure (S-F). Only a few specimens experienced a bond slip failure (B) which is a failure mode predominantly experienced by joints with sub-standard longitudinal reinforcement detailing. 97 specimens with missing or unreported failure modes are not included in Table 3.1. More details on the complete experimental database is provided in Appendix.

Table 3.1: Observed failure modes in the experimental database

Failure modes		**S**	**S-F**	**B**	**Total**
Exterior	w	116	93	2	211
	w/o	79	19	12	110
Interior	w	44	88	0	132
	w/o	23	25	0	47
Total		262	225	14	501

w/o: without and **w**: with transverse reinforcement

3.4.2 Exploratory Data Analysis (EDA)

An exploratory data analysis is performed to understand the characteristics of the database and detect and eliminate any outliers before using the database for the development of the identified network configuration in Figure 3-4. The data structure of variables is defined as either continuous or categorical. Out of 14 variables (13 input and

1 output), only JT is a categorical variable which is converted into numerical values: 0 for an interior joint, and 1 for an exterior joint.

The presence of outliers in the database can adversely affect any ANN, leading to overfitting or underfitting and reducing its accuracy. The Cook's distance method [36,37] is used to detect the outliers in the database. A data point is defined as an outlier if the computed Cook's distance (D_i), in Eq. (10), exceeds the threshold limit (I_t) in Eq. (11). In these equations, τ_{pred} is the predicted shear strength, $\tau_{pred(i)}$ is the predicted shear strength when a data point, say i^{th} point, is excluded from the database, p is the total number of weights and biases associated with a data point, MSE is the mean squared error as defined in Eq. (3), and n is the total number of data points in the database.

$$D_i = \frac{\sum_{i=1}^{n}\left(\tau_{pred} - \tau_{pred(i)}\right)^2}{p\text{MSE}} \tag{10}$$

$$I_t = \frac{4}{n} \tag{11}$$

The results of the EDA for the entire database are presented in Figure 3-6, where 43 data points are identified as outliers. These outliers are removed from the experimental database, leaving a resulting database with 555 data points.

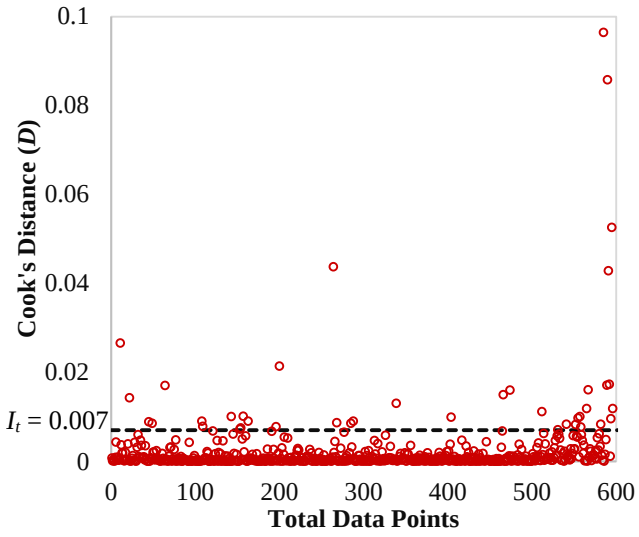

Figure 3-6: Outlier detection using Cook's distance method

Table 3.2 shows the ranges of parameter values for the resulting database, which covers a wide range to provide a general applicability for the developed network. It is important to note that neural networks are not appropriate for extrapolation of data. Therefore, they should only be used for the input inside the minimum and maximum data ranges of the parameters used in the training.

Table 3.2: Statistical description of the database after EDA

Variable	**Min**	**Max**	**Unit**
Concrete compressive strength (f'_c)	15.8	102.0	MPa
Beam-column joint transverse reinforcement ratio, (ρ_{jt})	0.0	2.6	%
Joint transverse reinforcement yield strength, (f_{yjt})	235	1374	MPa
Beam rebar ratio (ρ_b)	0.4	4.3	%
Beam rebar yield strength (f_{yb})	286	1091	MPa
Depth of beam (h_b)	150	750	mm
Width of beam (b_b)	100	610	mm
Column rebar ratio (ρ_c)	0.3	7.7	%
`Column rebar yield strength (f_{yc})	274	1092	MPa

Depth of column (h_c)	140	700	mm
Width of column (b_c)	100	900	mm
Axial load factor (ALF)	0.0	0.7	%
Joint type (JT)	0	1	
Shear Strength (τ)	1.3	17.4	MPa

A correlation coefficient analysis is performed to quantify the correlation between the input and output variables using Eq. (12) where R is the correlation coefficient, *n* is the number of data points, and *X* and *Y* are any two variables for which the correlation is being calculated.

$$R=\frac{n\sum_{i=1}^{n}XY-(\sum_{i=1}^{n}x)(\sum_{i=1}^{n}Y)}{[n\sum_{i=1}^{n}X-(\sum_{i=1}^{n}Y)^2][n\sum_{i=1}^{n}X-(\sum_{i=1}^{n}Y)^2]} \quad (12)$$

The results of the correlation coefficient analysis are presented in Figure 3-7 using a heatmap, which is a graphical representation of the correlation matrix. A correlation matrix may be used to summarize the data, as input for a more advanced investigation, or as a diagnostic tool for an advanced analysis [38,39]. The correlation coefficients range from +1 to -1, where +1 indicates the highest positive (direct) correlation and -1 indicates the highest negative (inverse) correlation. The shown heatmap uses a correlation color bar, from -0.2 to +0.8 as applicable to this study, where a darker color indicates a stronger correlation. For instance, the correlation coefficient between the input concrete compressive strength (f'_c) and output shear strength (τ_{exp}) is 0.57, indicating a strong positive correlation of 57%. The darker color cells in the final row indicate the strong correlations between input and output variables.

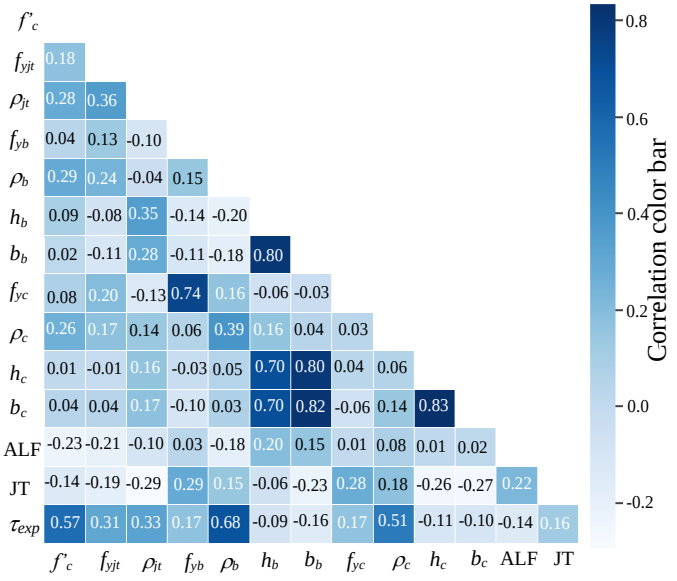

Figure 3-7: Correlation coefficient matrix

3.4.3 Training, Testing, and Validation

Using 555 data points which passed the EDA, and the final network configuration, the training, testing, and validation processes are repeated. A random sampling method is used to ensure all data has an equal chance of being selected [40] in a data split of 80%, 10%, and 10%, which is a common approach also used in other studies [25,41,42]. The distribution of specimen types is shown in Table 3.3.

Table 3.3: Data split for training, testing, and validation

Joint Type	**Interior**		**Exterior**		**Total**
	w/o	**w**	**w/o**	**w**	
Training (80%)	43	107	91	204	445
Testing (10%)	5	13	11	26	55
Validation (10%)	5	13	11	26	55
Total	53	133	113	256	555

w/o: without and **w**: with transverse reinforcement

The training of the network is carried out by performing 100 iterations, as found to give the lowest MSEs in Section 3.4, in which the forward and back propagations are applied to each input data point. The iterations are completed once all data points have been used. At the end of each iteration, the calculation either continues to the next iteration or stops if the maximum number of iterations is reached. This concludes the training process. Subsequent to the training stage, the testing of the network is carried out by performing the forward propagation and computing the error for each input data point. Unlike during training, the back propagation is not performed. Because of this, the weights and biases are not updated, and multiple iterations are not performed.

The accuracy and reliability of the proposed network are evaluated using six performance evaluation metrics. Table 3.4 shows these metrics and their formulations. R is the correlation coefficient which is described previously in Section 3.4.2. It is used here to evaluate the correlation between the predicted and experimental shear strength values, τ_{pred} and τ_{exp}. R ranges from 0 to 1 where 1 indicates the highest correlation. R^2 is the determination coefficient which indicates the extent to which the predicted value matches the experimental value regardless of their direction. R^2 ranges from 0 to 1 where 1 indicates the best fit. MAE is the mean absolute error which is the average error between the predicted and experimental values. MSE is the mean squared error which is the average squared differences between predicted and experimental values. RMSE is the root mean squared error which is the average magnitude of the errors between predicted and experimental values. CV is the coefficient of variation which is the ratio of the standard deviation to the mean. For the error metrics (MAE, MSE, and RMSE) and CV, smaller numbers indicate more accurate results.

Table 3.4: Performance evaluation metrics

Metrics	Formula	
R	$\frac{n\sum \tau_{exp}\tau_{pred} - (\sum \tau_{exp})(\sum \tau_{pred})}{[n\sum \tau_{exp}{}^2 - (\sum \tau_{exp})^2][n\sum \tau_{pred}{}^2 - (\sum \tau_{pred})^2]}$	(13)
R^2	$1 - \frac{\sum (\tau_{exp} - \tau_{pred})^2}{\sum (\tau_{exp} - \bar{\tau}_{exp})^2}$	(14)
MAE	$\frac{1}{n}\sum \lvert \tau_{exp} - \tau_{pred} \rvert$	(15)
MSE	$\frac{1}{n}\sum (\tau_{exp} - \tau_{pred})^2$	(16)
RMSE	$\sqrt{\frac{1}{n_s}\sum (\tau_{exp} - \tau_{pred})^2}$	(17)
CV	$\frac{RMSE}{\frac{1}{n}\sum \tau_{pred}} \times 100$	(18)

The scatterplots of the predicted-to-experimental shear strength ratios are shown in Figure 3-8 for the training, testing, and validation stages. In these plots, an ideal result, where the network predicts exactly the experimental results, would be a 45° line (y = x) with $R^2 = 1$, which is close to the graph obtained in the training stage (Figure 3-8a). The testing and validation were performed with the experimental data that was not used in the training (i.e., never seen by the network) as described above. As shown in Figures 3-8b and c, the accuracy in the testing and validation is similar to that in the training with a larger coefficient of variation and a slightly less inclined trendline (y = 0.95x versus y = 0.99x from training). This indicates that the network predictions are slightly on the conservative side in favor of safety. The average predicted-to-experimental shear strength ratio for the 110 testing and validation specimens is 0.99, with a coefficient of variation of

14.7%. These results show that the developed network is able to make accurate and reliable predictions of the joint shear strength for all four combinations of joint types.

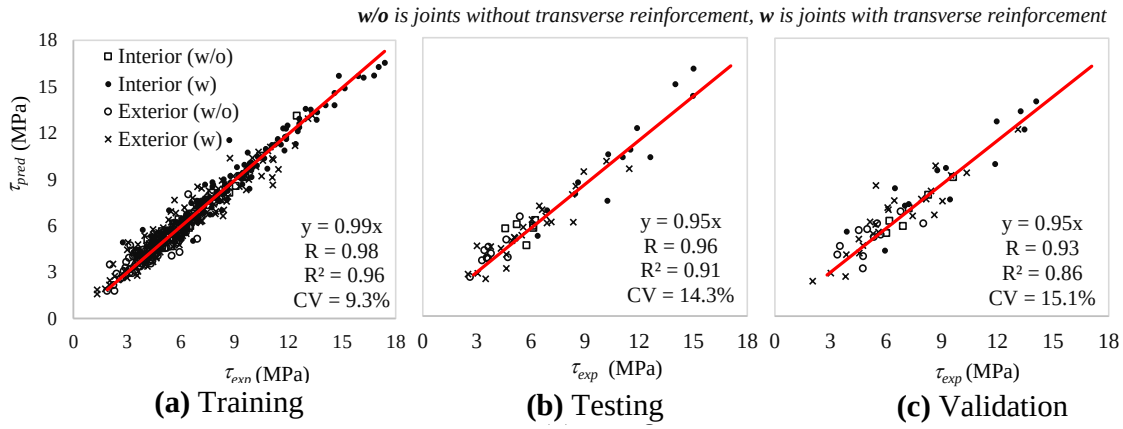

Figure 3-8: Scatterplots of the predicted-to-experimental shear strength ratios

3.5 Comparisons with Other Networks from the Literature

To further investigate the accuracy, the proposed network is compared with three existing networks from literature, developed by Alagundi and Palanisamy [25], Haido [26], and Kotsovou et al. [21]. The comparisons use the same experimental database of 555 specimens and include: *i)* global performance evaluation metrics based on all joint types; *ii)* local performance evaluation metrics based on specific joint types; and *iii)* variable evaluation metrics with respect to the input variables.

Figure 3-9 presents the global performance evaluation results for the training, testing, and validation datasets. In all three cases, the proposed network, denoted as FFNN, provides more accurate or same R and R^2 values. All four networks have diminished accuracies for the testing and validation datasets while the proposed FFNN still provides more accurate results. The accuracy obtained from the proposed FFNN is comparable to

the accuracy that could be obtained from sophisticated and time-consuming mechanics-based models [12,43,44].

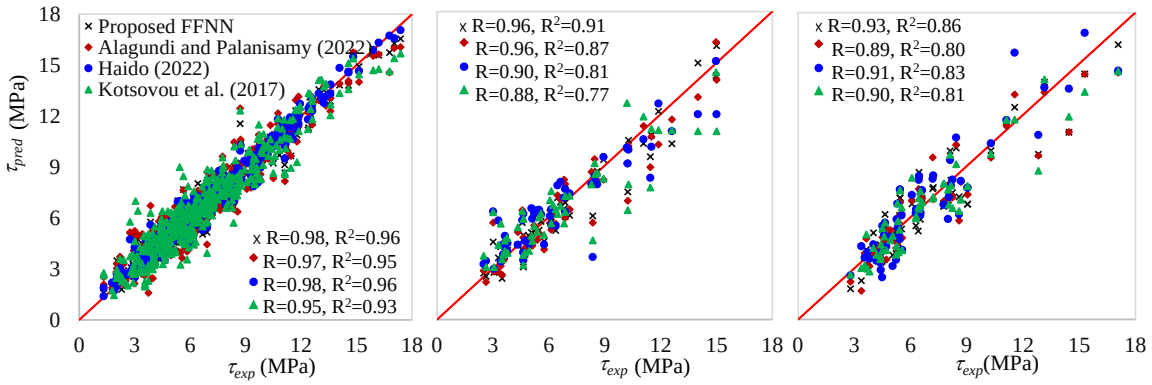

(a) Training **(b)** Testing **(c)** Validation

Figure 3-9: Global performance comparison of the proposed network with three existing networks

Table 3.5 presents the performance evaluation metrics in terms of the errors and coefficient of variations for the testing and validation including 110 data points. For all metrics, the proposed FFNN returns smaller errors and CV values indicating better accuracy and reliability.

Table 3.5: Error and coefficient of variation comparisons

Network	MAE	MSE	RMSE	CV (%)
Proposed FFNN	0.72	0.92	0.95	14.7%
Alagundi and Palanisamy (2022)	0.84	1.36	1.16	17.5%
Haido (2022)	0.91	1.47	1.21	17.8%
Kotsovou et al. (2017)	0.94	1.68	1.29	19.0%

Figure 3-10 presents the local performance evaluation metrics based on the joint types, including interior and exterior joints with or without transverse reinforcement, for the proposed network as compared to the three existing networks. The same testing and

validation datasets were used including 55 data points each. For all types of joints, the proposed network yields a higher value of R and R^2 and lower values of MAE, MSE, and RMSE indicating superior accuracy. For interior joints without transverse reinforcement (10 data points), the proposed network provides increased R and R^2 by an average of 9.4% and 19.7%, respectively, and reduced MAE, MSE, and RMSE by an average of 31.2%, 33.3%, and 18.7%, respectively as compared to the three other networks. For interior joints with transverse reinforcement (26 data points), R and R^2 are increased by 3.9%, and 7.8%, and MAE, MSE, and RMSE are lowered by an average of 21.1%, 35.9%, and 20.4%, respectively. For exterior joints without transverse reinforcement (22 data points), R and R^2 are increased by 9.2% and 16.7% while MAE, MSE, and RMSE are reduced by 31.9%, 67.6%, and 43.7%, respectively. For the exterior joints with transverse reinforcement (52 data points), R and R^2 are increased by 1.5%, and 3.8%, and MAE, MSE, and RMSE are reduced by 11.6%, 24.3%, and 13.1%, respectively. These results clearly show the accuracy and reliability of the proposed network for all joint types considered. The improved accuracy for the joints with no transverse reinforcement, which are traditionally more challenging to capture using mechanics-based models, is particularly notable.

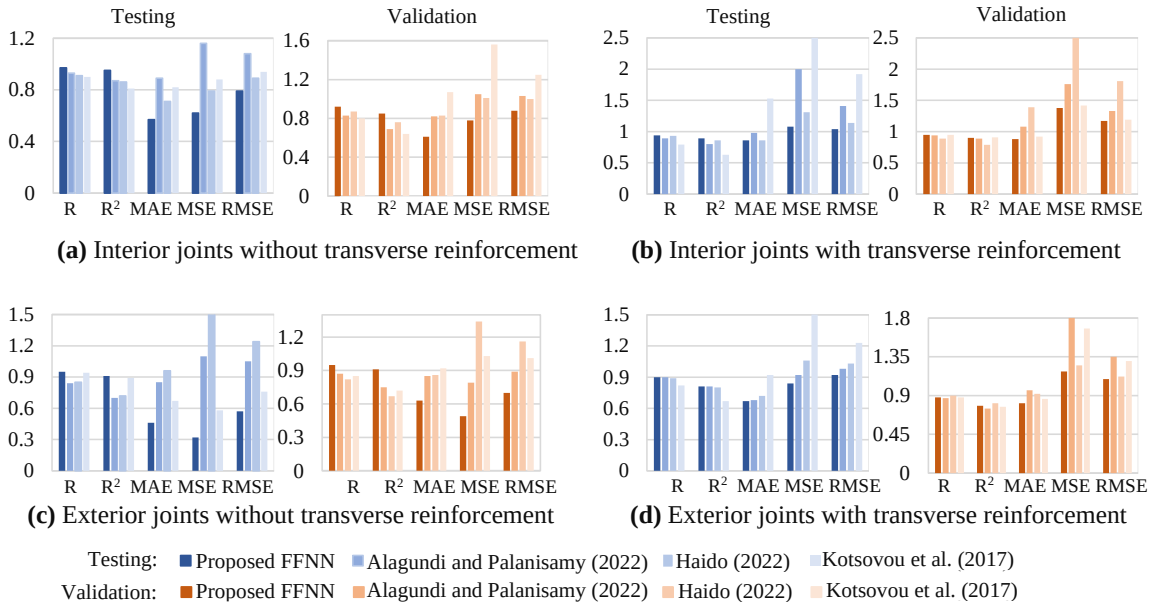

Figure 3-10: Local performance comparison of the proposed network with three existing networks

Table 3.6 compares the coefficient of variations obtained from the proposed network with other networks for the testing and validation including 110 data points. The results indicate that the proposed network provides less variation for the predicted-to-experimental shear strength ratios, and thus is more reliable.

Table 3.6: Coefficient of variation comparisons

CV (%)	**Interior**		**Exterior**	
	w/o	**w**	**w/o**	**w**
Proposed FFNN	11.9%	10.7%	14.8%	17.1%
Alagundi and Palanisamy (2022)	13.7%	12.5%	19.7%	20.5%
Haido (2022)	13.9%	14.6%	26.9%	17.5%
Kotsovou et al. (2017)	17.5%	13.2%	21.3%	21.2%

w/o: without and **w**: with transverse reinforcement

As the final assessment, the predictive capabilities of the proposed network are compared to the networks from the literature with respect to the input variables. Figure 3-11 presents the scatterplots of the predicted-to-experimental shear strength ratios across the

complete ranges of each input variable. Beam and column width and depth variables are combined into two plots using aspect ratios. In these plots, the ideal ratio, where the network predictions are exactly equal to the experimental values, is shown with a horizontal line at 1.0. For all 13 input variables, the predictions of the proposed network are closer to the 1.0 line with less scatter and without a visible bias as compared to the other networks. These results further demonstrate the accuracy and reliability of the proposed network.

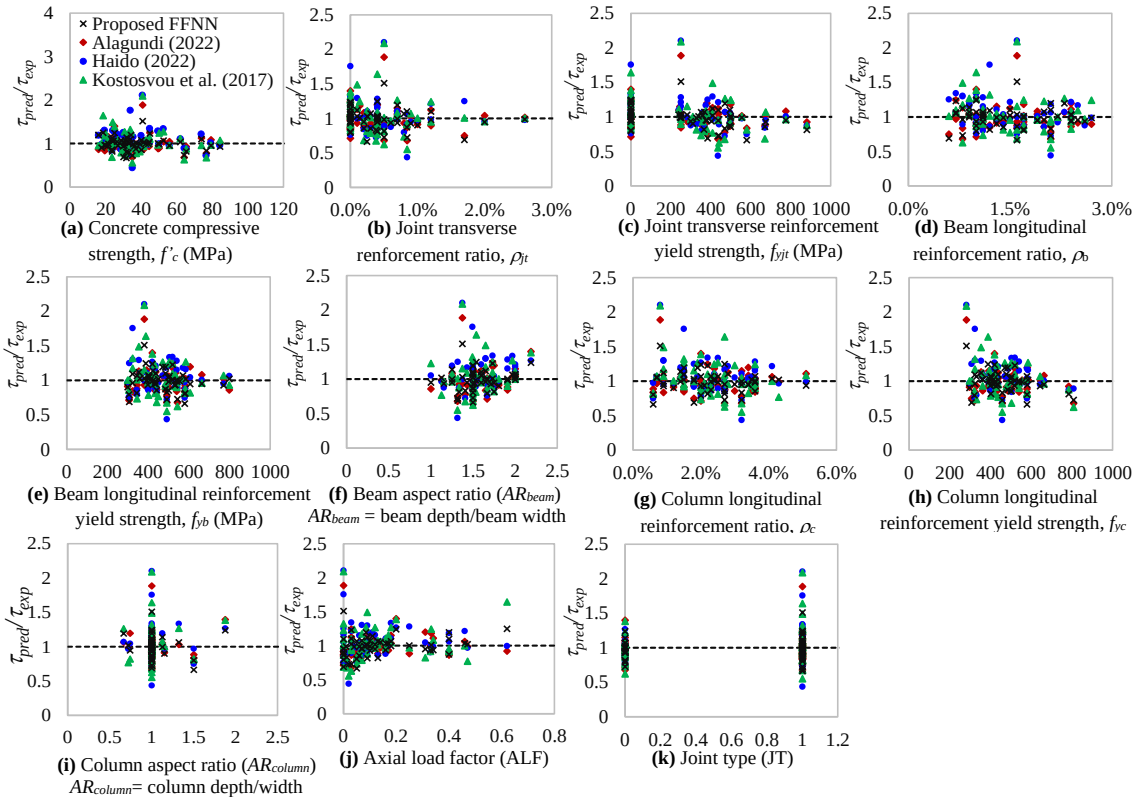

Figure 3-11: Input variable range comparison of the proposed network with three existing networks

3.6 Derivation of Joint Spring Curves

The lumped-plasticity approach is commonly used for the analysis of frames where plastic hinges are inserted at the critical locations of beams and columns with pre-defined hinge curves that represent the post-yield behavior in one or more degrees of freedom. In these analyses, a rotational spring can be inserted at the intersection of beams and columns as a plastic hinge to define the post-yield behavior of joints. The proposed network is used to derive the shear stress-strain and moment-rotation curves to define the behavior of joint springs.

The rotational spring curves are derived using the joint shear strength predicted by the proposed FFNN based on four points: (1) cracking, (2) yielding, (3) maximum, and (4) residual. The cracking strength is defined as $0.48\sqrt{f'_c}$ as recommended by Anderson et al. [45]. The yield and residual strengths are 95% and 20% of the shear strength (τ_{pred}), respectively, adopted by Jeon [12] based on an experimental test result of 154 specimens. The shear strain values (γ) corresponding to the cracking and yield strengths are adopted from Anderson et al. [45] based on the experimental test results of 11 specimens. The shear strains corresponding to the maximum and residual strengths are also based on the experimental test results of 154 specimens [12]. The resulting shear stress-strain curve is presented in Figure 3-12 with the shear strain (γ) values summarized in Table 3.7 for different types of joints.

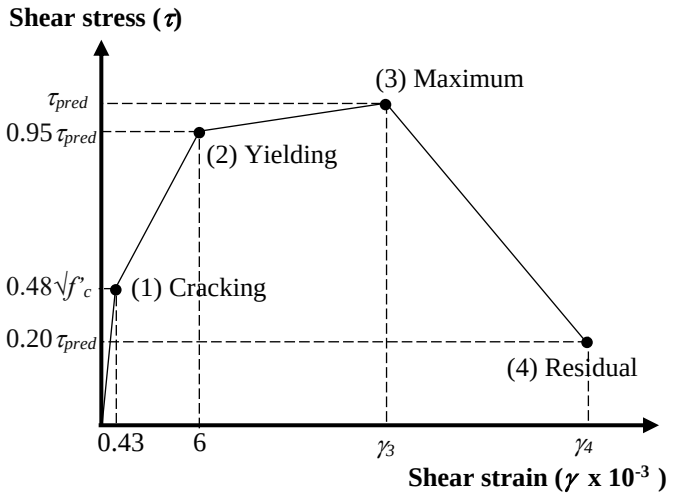

Figure 3-12: Shear stress-strain curve

Table 3.7: Shear strain and rotation values (x10^{-3}) for different types of joints

Joint type	**Interior**		**Exterior**	
	w/o	**w**	**w/o**	**w**
γ_1 and θ_1	0.43			
γ_2 and θ_2	6			
γ_3 and θ_3	19	20	16	20
γ_4 and θ_4	117	187	77	185

w/o: without and **w**: with transverse reinforcement

To define a rotational spring in a global frame analysis model, a moment-rotation curve is typically required. This curve is obtained by converting the shear stress-strain curve into an equivalent moment-rotation curve using Eqs. (19), (20), and (21) adopted from Celik and Ellingwood [46].

$$M_{\max} = \tau_{pred} A_j \frac{1}{\frac{1-h_c/L_b}{jh_b} - \frac{1}{L_c}} \tag{19}$$

$$M_{crack} = \left(0.48\sqrt{f'_c}\right) A_j \frac{1}{\frac{1-h_c/L_b}{jh_b} - \frac{1}{L_c}} \tag{20}$$

$$\theta = \gamma \tag{21}$$

M_{max} *is* the equivalent moment capacity; M_{crack} is the equivalent cracking moment; h_b is the beam depth; h_c is the column depth; A_j is the joint core area ($A_j = h_b \times h_c$); L_c is the length of the column between the points of contraflexure; L_b is the length of beam between the points of contraflexure; and j is a constant taken as 0.875. Since the joint rotation is the change in the angle between the two edges of the joint core, the rotation is equivalent to the shear strain as stated in Eq. (21). The resulting moment-rotation curve is presented in Figure 3-13 with the rotation values summarized in Table 3.7 for different types of joints. More details on this approach and application to various joint configurations, including the joints with straight reinforcing bar embedment, are provided in Suwal and Guner [13].

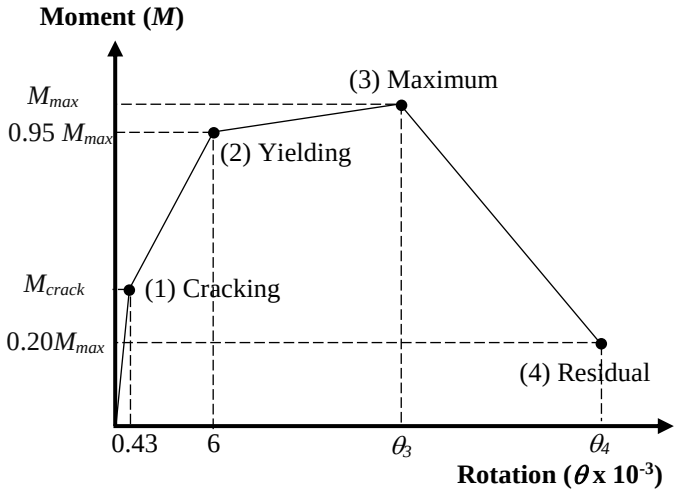

Figure 3-13: Moment-rotation curves for the definition of a rotational spring

To facilitate the calculation process, a spreadsheet tool [47] is created and shared as a freeware for the use of engineers and researchers. A user bulletin [48] is also prepared to demonstrate the application and experimental validation of the spreadsheet with four specimens. The spreadsheet executes the proposed FFNN calculations and provides the

shear strength (τ_{pred}) for a given beam-column joint configuration. The predicted strength is then converted to shear stress-strain and moment-rotation curves using the approach defined above. The abscissa and ordinate values calculated in the spreadsheet can readily be used for the definition of joint hinges in common global frame analysis software.

3.7 Summary and Conclusions

A feed-forward artificial neural network (FFNN) is developed to predict the shear strengths of reinforced concrete beam-column joints. A comprehensive database of 555 data points which passed the exploratory data analysis, are used to train, test, and validate the proposed network for applicability to a wide range of input variables and joint configurations. The accuracy and reliability of the proposed network are evaluated using a comprehensive set of evaluation metrics. In addition, the proposed network is compared with three existing networks from the literature based on global, local, and input variable performance evaluation metrics. As the final step, the proposed network is integrated into lumped-plasticity-based global frame analysis models by deriving the shear stress-strain and moment-rotation curves for defining joint hinges. The results of this study support the following conclusions:

- Feed-forward artificial neural networks can be developed to predict the shear strengths of reinforced concrete beam-column joints accurately, reliably and in very short amounts of time.
- The datasets used in the training and testing of a neural network play a critical role in identifying the optimum parameters and network layout. An exploratory data analysis

is recommended to understand the characteristics of the database and detect and eliminate any outliers before using the data for the development of a network.

- The exploratory data analysis detected and eliminated 43 outliers from a database of 598 experimental specimens in this study. The use of the remaining database for the development of the proposed FFNN helped improve its accuracy and reliability.
- The proposed FFNN is shown to predict the shear strengths of beam-column joints rapidly and accurately. The predicted-to-experimental shear strength ratios for the 110 testing and validation specimens provided a mean of 0.99 and a coefficient of variation of 14.7%.
- The proposed FFNN is shown to provide more accurate and reliable response simulations than three existing networks from the literature. It provided a 4.3% increase in the correlation coefficient and 8.7% increase in the determination coefficient while providing a 18.7% decrease in the coefficient of variation for the 110 experimental data points used in the testing and validation, as compared to the average values obtained from three existing networks.
- The approach presented for deriving the shear stress-strain and moment-rotation curves enables the application of the proposed network in plastic-hinge-based frame analyses. The developed spreadsheet executes the required calculations and facilitates defining joint hinges in global frame analysis models.

3.8 Data Availability

Some or all data, models, or code that support the findings of this study are available from the corresponding author upon reasonable request.

Chapter 4

Conclusions

In the first part of this study, a modeling approach is proposed for beam-column joints using rotational spring models. The results demonstrate that rotational spring models provide a good balance between simplicity and accuracy for the analysis of frames. Additionally, a spreadsheet tool is developed to facilitate the derivation of the hinge curves of rotational spring models and generate the data needed for inputting into global frame analysis software. Finally, an experimental validation study is conducted, which demonstrates that the proposed modeling approach captures both joint shear and bond slip failure models and predicts the beam-column joint capacity with a maximum error of 8.0% for the specimen investigated in this study.

In the second part, a feed-forward neural network (FFNN) is developed to predict the shear strengths of reinforced concrete beam-column joints. To improve the accuracy and reliability of the proposed FFNN, an exploratory data analysis is conducted to detect and eliminate outliers from the database. The proposed FFNN is shown to predict the shear strengths of beam-column joints rapidly and accurately. The predicted-to-experimental

shear strength ratios for the 110 testing and validation specimens provided a mean of 0.99 and a coefficient of variation of 14.7%. Furthermore, an approach is presented for deriving the shear stress-strain and moment-rotation curves of rotational spring models enabling the application of the proposed network in plastic-hinge-based frame analyses. A spreadsheet tool is developed to execute the required calculations and facilitate defining joint hinges in global frame analysis models.

References

Chapter 1

[1] Suwal N, Guner S. Nonlinear modeling of beam-column joints in forensic analysis of concrete buildings. Computers and Concrete 2023; 31(5):419-432. <https://www.utoledo.edu/engineering/faculty/serhanguner/docs/JP25_Suwal_Guner_Joints.pdf>

Chapter 2

[1] Vecchio FJ, Bentz EC, Collins MP. Tools for forensic analysis of concrete structures. Computers and Concrete 2004;1(1):1-14. <http://vectoranalysisgroup.com/journal_publications/jp48.pdf>

[2] Parisi F, Augenti N. Structural failure investigations through probabilistic nonlinear finite element analysis: Methodology and application. Engineering Failure Analysis 2017;80:386-402. <https://doi.org/10.1016/j.engfailanal.2017.07.004>

[3] Ghobarah A, Said A. Shear strengthening of beam-column joints. Engineering Structures 2002;24(7):881-888. <https://doi.org/10.1016/S0141-0296(02)00026-3>

[4] Shin M, Lafave JM. Modeling of cyclic joint shear deformation contributions in RC beam-column connections to overall frame behavior. Structural Engineering and Mechanics 2004;18(5):645–669. <https://doi.org/10.12989/sem.2004.18.5.645>

[5] Birely AC, Lowes LN, Lehman DE. A model for the practical nonlinear analysis of reinforced-concrete frames including joint flexibility. Engineering Structures 2012;34(1):455-465. <https://doi.org/10.1016/j.engstruct.2011.09.003>

[6] Gombosuren D, Maki T. Prediction of joint shear deformation index of RC beam-column joints. Buildings 2020;10(10):176. <https://doi.org/10.3390/buildings10100176>

[7] Pantelides CP, Hansen J, Nadauld J, Reaveley LD. Assessment of reinforced concrete building exterior joints with substandard details. PEER Report 2002/18. Pacific Earthquake Research Center, University of California, Berkeley, CA; 2002.

[8] Sharma A, Eligehausen R, Reddy GR. A new model to simulate joint shear behavior of poorly detailed beam-column connections in RC structures under seismic load, Part I: Exterior Joints. Engineering Structures 2011;33(3):1034-1051. <https://doi.org/10.1016/j.engstruct.2010.12.026>

[9] Alath S, Kunnath SK. Modeling inelastic shear deformations in RC beam-column joints. Engineering Mechanics: Proceedings of 10th Conference, The University of Colorado at Boulder 1995;(3):822-825.

[10] Biddah A, Ghobarah A. Modelling of shear deformation and bond slip in reinforced concrete joints. Structural Engineering and Mechanics 1999;7(4):413–32. <https://doi.org/10.12989/sem.1999.7.4.413>

[11] Park S. Experimental and analytical studies on old reinforced concrete buildings with seismically vulnerable beam-column joints. Ph.D. Dissertation, University of California, Berkeley; 2010.

[12] Jeon JS. Aftershock vulnerability assessment of damaged reinforced concrete buildings in California. Ph.D. Dissertation, Georgia Institute of Technology, Atlanta; 2013.

[13] De Risi MT, Ricci P, Verderame G. Modelling exterior unreinforced beam-column joints in seismic analysis of non-ductile RC frames. Earthquake Engineering and Structures Dynamics 2017;46(6):899-923. <https://doi.org/10.1002/eqe.2835>

[14] Grande E, Imbimbo M, Napoli A, Nitiffi R, Realfonzo R. A nonlinear macro-model for the analysis of monotonic and cyclic behavior of Exterior RC beam-column joints. Journal of Building Engineering 2021;39:16. <https://doi.org/10.1016/j.jobe.2021.102202>

[15] Vecchio FJ, Collins MP. Modified compression-field theory for reinforced concrete elements subjected to shear. Journal of the American Concrete Institute 1986;83(2):219–231. <http://vectoranalysisgroup.com/journal_publications/jp2.pdf>

[16] Anderson M, Lehman D, Stanton J. A cyclic shear stress-strain model for joints without transverse reinforcement. Engineering Structures 2008;30(4):941–954. <https://doi.org/10.1016/j.engstruct.2007.02.005>

[17] Hassan WM. Analytical and experimental assessment of the seismic vulnerability of beam-column joints without transverse reinforcement in concrete building. Ph.D. Dissertation, University of California, Berkeley, CA; 2011. <http://vectoranalysisgroup.com/journal_publications/jp72.pdf>

[18] Celik OC, Ellingwood BR. Modeling beam-column joints in fragility assessment of gravity load designed reinforced concrete frames. Journal of Earthquake Engineering 2008;12(3):357-381. <https://doi.org/10.1080/13632460701457215.>

[19] Youssef M, Ghobarah A. Modelling of RC beam-column joints and structural walls. Journal of Earthquake Engineering 2001;5(1):93–111. <https://doi.org/10.1080/13632460109350387>

[20] Lowes LN, Altoontash A. Modeling reinforced-concrete beam-column joints subjected to cyclic loading. Journal of Structural Engineering 2003;129(12):1686–97.

[21] Mitra N, Lowes LN. Evaluation, calibration, and verification of a reinforced concrete beam-column joint model. Journal of Structural Engineering 2007;133(1):105–120.

[22] Pan Z, Guner S, Vecchio FJ. Modeling of interior beam-column joints for nonlinear analysis of reinforced concrete frames. Engineering Structures 2017;142(4):182-191.

<https://www.utoledo.edu/engineering/faculty/serhanguner/docs/JP7_Pan_et_al_2017.pdf>

[23] Guner S, Vecchio FJ. User's manual of VecTor5, Department of Civil Engineering, University of Toronto, Toronto, Canada; 2008. <https://www.utoledo.edu/engineering/faculty/serhanguner/docs/M1-VT5Manual-V1-3.pdf>

[24] Eligehausen R, Ozbolt J, Genesio G, Hoehler MS, Pampanin S. Three-dimensional modeling of poorly detailed RC frame joints. In Proceedings of the Annual NZSEE Conference, New Zealand 2006;(23):1-10.

[25] Sharma A, Genesio G, Reddy GR, Eligehausen R. Nonlinear dynamic analysis using microplane model for concrete and bond slip model for prediction of behavior of non-seismically detailed RC beam-column joints. Journal of Structural Engineering 2009;36(4):250-257.

[26] Sagbas G, Vecchio FJ, Christopoulos C. Computational modeling of the seismic performance of beam-column subassemblies. Journal of Earthquake Engineering 2011;15(4):640-663.

[27] Wong PS, Vecchio FJ, Trommels H. VecTor2 and Formworks User's Manual. Technical Report, Department of Civil Engineering, University of Toronto, ON, Canada; 2013. <http://vectoranalysisgroup.com/user_manuals/manual1.pdf>

[28] Vecchio FJ. Distributed stress model for reinforced concrete: formulation. Journal of Structural Engineering 2000;126(8):1070-1077. <http://www.vectoranalysisgroup.com/journal_publications/jp35.pdf>

[29] Guner S, Vecchio FJ. Analysis of shear-critical reinforced concrete plane frame elements under cyclic loading. Journal of Structural Engineering 2011;137(8):834-843. <https://ascelibrary.org/doi/abs/10.1061/%28ASCE%29ST.1943541X.-0000346>

[30] Sasmal S, Nath D. Evaluation of performance of non-invasive upgrade strategy for beam-column sub-assemblages of poorly designed structures under seismic type loading. Earthquake Engineering & Structural Dynamics 2016;45(11):1817-1835. <https://doi.org/10.1002/eqe.2730>

[31] Abusafaqa FR, Samaaneh MA, Dwaikat MBM. Improving ductility behavior of sway-special exterior beam-column joint using ultra-high-performance fiber-reinforced concrete. Structures 2022;36(12):979-996. <https://doi.org/10.1016/j.istruc.2021.12.059>

[32] Thai FT. Machine learning for structural engineering: A state-of-the-art review. Structures 2022;38(4):448–491. <https://doi.org/10.1016/j.istruc.2022.02.003>

[33] Unal M, Burak B. Joint shear strength prediction of reinforced concrete beam-to-column connections. Structural Engineering and Mechanics 2012;41(3):421-440. <https://doi.org/10.12989sem.2012.41.3.421>

[34] Jeon JS, Lowes LN, DesRoches R. Numerical models for beam-column joints in reinforced concrete building frames.", ACI Special Publication 2014;6(3):297-323.

[35] Kotsovou GM, Cotsovos DM, Lagaros ND. Assessment of RC exterior beam-column joints based on artificial neural networks and other methods. Engineering Structures 2017;144:1-18. <https://doi.org/10.1016/j.engstruct.2017.04.048>

[36] Mangalathu S, Jeon JS. Classification of failure mode and prediction of shear strength for reinforced concrete beam-column joints using machine learning techniques. Engineering Structures 2018;160:85-94, <https://doi.org/10.1016/j.engstruct.2018.01.008>

[37] Tibshirani R. Regression shrinkage and selection via the lasso. Journal of the Royal Statistical Society. Series B (Methodological) 1996:58(1):267–288.

[38] Alwanas AAH, Al-Musawi AA, Salih SQ, Tao H, Ali M, Yaseen ZM. Load-carrying capacity and mode failure simulation of beam-column joint connection: Application of self-tuning machine leaning model. Engineering Structures 2019;194:220-229. <https://doi.org/10.1016/j.engstruct.2019.05.048>

[39] Huang GB, Zhu QY, Siew CK. Extreme learning machine: theory and applications. Neurocomputing 2006;70(1):489-501. <https://doi.org/10.1016/j.neucom.2005.12.126>

[40] Naderpour H, Mirrashid, M. Classification of failure modes in ductile and non-ductile concrete joints. Engineering Failure Analysis 2019;103:361-375. <https://doi.org/10.1016/j.engfailanal.2019.04.047>

[41] Wu X, Kumar V, Ross QJ, Ghosh J, Yang Q, Motoda H, McLachlan GJ, Ng A, Liu B, Yu P, Zhou ZH. Top 10 algorithms in data mining. Knowledge and Information Systems 2008;14(1):1-37.

[42] Gao X, Lin C. Prediction model of the failure mode of beam-column joints using machine learning methods. Engineering Failure Analysis 2021;120:105072. <https://doi.org/10.1016/j.engfailanal.2020.105072>

[43] Alagundi S, Palanisamy T. Neural network prediction of joint shear strength of exterior beam-column joint. Structures 2022;37:1002-1018. <https://doi.org/10.1016/j.istruc.2022.01.013>

[44] Haido JH. Prediction of the shear strength of RC beam-column joints using new ANN formulations. Structures 2022;38:1191-1209. <https://doi.org/10.1016/j.istruc.2022.02.046>

[45] Clyde C, Pantelides CP, Reavely LD. Performance-based evaluation of exterior reinforced concrete building joints for seismic excitation. PEER Report 2000. Pacific Earthquake Research Center, CA; 2000.

[46] Suwal N, Guner, S. Beam-column joint hinge generator for shear and bond slip behaviors", Excel spreadsheet, Department of Civil and Environmental Engineering, University of Toledo, OH, USA; 2023. <https://www.utoledo.edu/engineering/faculty/serhan-guner/docs/7S-JointHingeGenerator.xlsx>

[47] Suwal N, Guner S. User Bulletin 10: Joint hinge generator for shear and bond slip behaviors. Documentation 2023; 12pp. <https://www.utoledo.edu/engineering/faculty/serhanguner/docs/B10_JointHingeGenerator.pdf >

[48] Priestley MJN. Displacement based seismic assessment of reinforced concrete buildings. Journal of Earthquake Engineering 1997;1(1):157–92.

[49] Murty CVR, Rai D, Bajpai KK, Jain SK. Effectiveness of reinforcement details in exterior reinforced concrete beam–column joints for earthquake resistance. ACI Structural Journal 2003;100(2):149–56.

[50] CSI (Computers and Structures, Inc). SAP2000 - Integrated Software for Structural Analysis and Design. User's Manual, Version 19, Computers and Structures Inc., Berkeley, California; 2016. <https://docs.csiamerica.com/manuals/sap2000/CSiRefer.pdf>

[51] Guner S. Performance assessment of shear-critical reinforced concrete plane frames. Ph.D. Dissertation, University of Toronto; 2008. <https://www.utoledo.edu/engineering/faculty/serhanguner/docs/T1_Guner_PhD_2018.pdf>

[52] CSI (Computers and Structures, Inc). ETABS - Integrated Building Design Software. User's Guide, Computers and Structures, Inc., Berkeley, California; 2016. <https://ottegroup.com/wp-content/uploads/2021/02/ETABS2016-Users-Guide.pdf>

[53] RISA (RISA Tech, Inc). RISA-Rapid Interactive Structural Analysis" General Reference, Version 21, RISA Tech, Inc, Foothill Ranch, California; 2021. <https://risa.com/assets/documentation/General_Reference_3D.pdf>

[54] MIDAS (MIDASoft). MIDAS CIVIL - Analysis for Civil Structures. Analysis Reference, MIDASoft, Inc, New York; 2021. <https://www.midasoft.com/hubfs/Analysis_Reference.pdf>

[55] CSI (Computers and Structures, Inc). PERFORM-3D™ - Nonlinear Analysis and Performance Assessment for 3D Structures. User's Guide, Version 5, Computers and Structures, Inc., Berkeley, California; 2011. <https://usermanual.wiki/Document/Perform3DUserGuide.2744216353.pdf>

[56] Pantelides CP, Hansen J, Nadauld J, Reaveley LD. Seismic performance of reinforced concrete building exterior joints with substandard details. Journal of Structural Integrity and Maintenance 2017,2(1):1-11. <https://doi.org/10.1080/24705314.2017.1280589>

Chapter 3

[1] Hu B, Kundu T. Seismic performance of interior and exterior beam–column joints in recycled aggregate concrete frames. Journal of Structural Engineering 2019;145(3):16pp. <https://doi.org/10.1061/(ASCE)ST.1943-541X.0002261>

[2] Paulay T, Scarpas A. The Behavior of Exterior Beam-Column Joints. Bulletin of the New Zealand National Society for Earthquake Engineering 1981;14(3):131-144. <https://www.nzsee.org.nz/db/Bulletin/Archive/14(3)0131.pdf>

[3] Clyde C, Pantelides CP, Reavely LD. Performance-based evaluation of exterior reinforced concrete building joints for seismic excitation. PEER Report 2000. Pacific Earthquake Research Center, CA; 2000.

[4] Shiohara H, Kusuhara F. Benchmark test for validation of mathematical models for non-linear and cyclic behavior of R/C beam-column joints. Department of Architecture, Graduate School of Engineering, University of Tokyo; 2007.

[5] Sasmal S, Lakshmanan N, Ramanjaneyulu K, Iyer NR, Novak B, Srinivas et al. Development of upgradation schemes for gravity load designed beam-column sub assemblage under cyclic loading. Construction and Building Materials 2011;25(8):3625-3638. <https://doi.org/10.1016/j.conbuildmat.2011.03.058>

[6] Hwang SJ, Lee HJ, Liao TF, Wang KC, Tsai HH. Role of hoops on shear strength of reinforced concrete beam-column joints. ACI Structural Journal 2005;102(3):445-453. <https://doi.org/10.14359/14416>

[7] ACI (American Concrete Institute). Building code requirements for structural concrete and commentary. ACI 319-19, Farmington Hills, MI: ACI; 2019.

[8] ASCE (American Society of Civil Engineers). Minimum design loads and associated criteria for buildings and other structures. ASCE/SEI 7-16, Reston, VA: ASCE; 2017.

[9] Alath S, Kunnath SK. Modeling inelastic shear deformations in RC beam-column joints. Engineering Mechanics: Proceedings of 10th Conference, The University of Colorado at Boulder 1995;(3):822-825.

[10] Biddah A, Ghobarah A. Modelling of shear deformation and bond slip in reinforced concrete joints. Structural Engineering and Mechanics 1999;7(4):413–432. <https://doi.org/10.12989/sem.1999.7.4.413>

[11] Birely AC, Lowes, L.N. and Lehman DE. A model for the practical nonlinear analysis of reinforced-concrete frames including joint flexibility. Engineering Structures 2012;34(1):455-465. <https://doi.org/10.1016/j.engstruct.2011.09.003>

[12] Jeon JS. Aftershock vulnerability assessment of damaged reinforced concrete buildings in California. Ph.D. Dissertation, Georgia Institute of Technology, Atlanta; 2013.

[13 Suwal N, Guner S. Nonlinear modeling of beam-column joints in forensic analysis of concrete buildings. Computers and Concrete 2023;31(5):419-432. <https://doi.org/10.12989/cac.2023.31.5.419>

<https://www.utoledo.edu/engineering/faculty/serhan-guner/docs/Suwal_Guner_2023_Read_Proof.pdf >

[14] Youssef M, Ghobarah A. Modelling of RC beam-column joints and structural walls. Journal of Earthquake Engineering 2001;5(1):93–111. <https://doi.org/10.1080/13632460109350387>

[15] Lowes LN, Altoontash A. Modeling reinforced-concrete beam-column joints subjected to cyclic loading. Journal of Structural Engineering 2003;129(12):1686–1697. <https://doi.org/10.1061/(ASCE)0733-9445(2003)129:12(1686)>

[16] Shin M, Lafave JM. Modeling of cyclic joint shear deformation contributions in RC beam-column connections to overall frame behavior. Structural Engineering and Mechanics 2004;18(5):645–669. <https://doi.org/10.12989/sem.2004.18.5.645>

[17] Mitra N, Lowes LN. Evaluation, calibration, and verification of a reinforced concrete beam-column joint model. Journal of Structural Engineering 2007;133(1):105–120. <https://doi.org/10.1061/(ASCE)0733-9445(2007)133:1(105)>

[18] Eligehausen R, Ozbolt J, Genesio G, Hoehler MS, Pampanin S. Three-dimensional modeling of poorly detailed RC frame joints. In Proceedings of the Annual NZSEE Conference, New Zealand 2006;(23):10pp.

[19] Guner S, Vecchio FJ. Analysis of shear-critical reinforced concrete plane frame elements under cyclic loading. Journal of Structural Engineering 2011;137(8):834-843. <https://ascelibrary.org/doi/abs/10.1061/%28ASCE%29ST.1943-541X.0000346>

[20] Almeida SA, Guner S. Review of Artificial Neural Network and a new feed-forward network for anchorage analysis in cracked concrete. The Concrete Industry in the Era of Artificial Intelligence, ACI 2021;SP-350(5):54-68. <https://www.utoledo.edu/engineering/faculty/serhanguner/docs/JP23_Almeida_Guner_AI_Concrete_2021.pdf>

[21] Kotsovou GM, Costovos DM, Lagaros ND. Assessment of RC exterior beam-column joints based on artificial neural networks and other methods. Engineering Structures 2017;144:1-18. <https://doi.org/10.1016/j.engstruct.2017.04.048>

[22] EN 1992-1. Eurocode 2: Design of concrete structures – Part 1-1: general rules, and rules for buildings, London; 2004.

[23] EN 1998-1. Eurocode 8: Design of structures for earthquake resistance – Part 1-1: general rules, seismic actions, and rules for buildings, London; 2004.

[24] Gao X, Lin C. Prediction model of the failure mode of beam-column joints using machine learning methods. Engineering Failure Analysis 2021;120(1239):24pp. <https://doi.org/10.1016/j.engfailanal.2020.105072>

[25] Alagundi S, Palanisamy T. Neural network prediction of joint shear strength of exterior beam-column joint. Structures 2022;37:1002-1018. <https://doi.org/10.1016/j.istruc.2022.01.013>

[26] Haido JH. Prediction of the shear strength of RC beam-column joints using new ANN formulations. Structures 2022;38:1191-1209. <https://doi.org/10.1016/j.istruc.2022.02.046>

[27] Marie HS, El-Hassan KA, Almetwally EM, El-Mandouh MA. Joint shear strength prediction of beam-column connections using machine learning via experimental results. Case Study in Construction Materials 2022;17:17pp. <https://doi.org/10.1016/j.cscm.2022.e01463>

[28] Gesoglu M, Güneyisi E. Prediction of load-carrying capacity of adhesive anchors by soft computing techniques. Materials and Structures 2007;40:939-951. <https://doi.org/10.1617/s11527-007-9265-6>

[29] Ashour AF, Alquedra MA. Concrete breakout strength of single anchors in tension using neural networks. Advanced Engineering Software 2005;36:87-97. <https://doi.org/10.1016/j.advengsoft.2004.08.001>

[30] Almeida SA, Guner S. A hybrid methodology using finite elements and neural network for the analysis of adhesive anchors exposed to hurricanes and adverse environments. Engineering Structures 2020;212:9pp. <https://doi.org/10.1016/j.engstruct.2020.110505> <https://www.utoledo.edu/engineering/faculty/serhan-guner/docs/JP15_Almeida_Guner_2020.pdf>

[31] Qian N. On the momentum term in gradient descent learning algorithms. Neural Networks 1999;12(1):145-151. <https://doi.org/10.1016/S0893-6080(98)00116-6>

[32] Kingma DP, Ba JL. Adam: A method for stochastic optimization. The 3rd International Conference for Learning Representations, San Diego 2015;15pp. <https://arxiv.org/abs/1412.6980v9>

[33] Hinton G, Srivastava N, Swersky K. Neural networks for machine learning. Coursera, video lectures 2012; 264:41pp.

[34] Abadi M, Agarwal A, Barham P, Brevedo E, Chen Z, Citro C et al. Tensorflow (v2.10.0): Large-scale machine learning on heterogeneous systems software 2015. <https://www.tensorflow.org/>

[35] Rossum G, Drake Jr. FL. Python reference manual. Center for Mathematics and Computer Science, Amsterdam, Netherlands; 1995. <https://dl.acm.org/doi/10.5555/869369>

[36] Cook RD. Detection of influential observation in linear regression. Technometrics 1977;19(1):15-18. <https://doi.org/10.2307/1268249>

[37] Cook RD. Influential observations in linear regression. Journal of American Statistical Association 1979;74(365):169-174. <https://doi.org/10.1080/01621459.1979.10481634>

[38] Lazaridis PC, Kavvadias IE, Demertzis K, Iliadis L, Vasiliadis LK. Structural damage prediction of a reinforced concrete frame under single and multiple seismic events using machine learning algorithms. Applied Science 2022;12(8):22pp. <https://doi.org/10.3390/app12083845>

[39] Schober P, Boer C, Schwarte LA. Correlation Coefficients. Anesthesia Analgesia 2018;126(5):1763-1768. <https://doi.org/10.1213/ane.0000000000002864>

[40] Etikan I, Bala K. Sampling and sampling methods. Biometrics and Biostatistics International Journal 2017;5(6):3pp. <https://doi.org/10.15406/bbij.2017.05.00149>

[41] Mori M, Flores RG, Suzuki Y, Nukazawa K, Hiraoka T, Nonaka H. Prediction of microcystis occurrences and analysis using machine learning in high-dimension, low sample-size, and imbalanced water quality data. Harmful Algae 2022;117:14pp. <https://doi.org/10.1016/j.hal.2022.102273>

[42] Kumari K, Mrunalini M. Detecting denial of service attacks using machine learning algorithm. Journal of Big Data 2022; 9(56):17pp. <https://doi.org/10.1186/s40537-022-00616-0>

[43] Kim J, LaFave JM. Joint shear behavior of reinforced concrete beam-column connections subjected to seismic lateral loading. Newmark Structural Laboratory Report Series, Department of Civil and Environmental Engineering, University of Illinois at Urbana Champaign, USA; 2009. <https://hdl.handle.net/2142/14281>

[44] Park S. Experimental and analytical studies on old reinforced concrete buildings with seismically vulnerable beam-column joints. Ph.D. Dissertation, University of California, Berkeley; 2010.

[45] Anderson M, Lehman D, Santon J. A cyclic shear stress-strain model for joints without transverse reinforcement. Engineering Structures 2008;30(4):941-954. <https://doi.org/10.1016/j.engstruct.2007.02.005>

[46] Celik OC, Ellingwood BR. Modeling beam-column joints in fragility assessment of gravity load designed reinforced concrete frames. Journal of Earthquake Engineering 2008;12(3):357-381. <https://doi.org/10.1080/13632460701457215>

[47] Suwal N, Guner S. Beam-column joint hinge generator using an artificial neural network. Excel spreadsheet. Department of Civil and Environmental Engineering, University of Toledo, OH, USA; 2023.

<www.utoledo.edu/engineering/faculty/serhan-guner/docs/8S-ANNJointHingeGenerator.xlsx>

[48] Suwal N, Guner S. User Bulletin 11: Joint hinge generator spreadsheet using an artificial neural network. Documentation. Department of Civil and Environmental Engineering, University of Toledo, OH, USA 2023; 6pp. <https://www.utoledo.edu/engineering/faculty/serhan-guner/docs/B11_ANNJointHingeGenerator.pdf >

Appendix A

Experimental Database

The experimental database compiled for the development of the proposed FFNN is presented in Table A.1. It comprises 598 experimental specimens compiled from 153 research studies. The first row of Table A.1 presents the variables of the joint specimen where joint type is either interior or exterior; f'_c is the concrete compressive strength; ρ_{jt} is the joint transverse reinforcement ratio; f_{yjt} is the joint transverse reinforcement yield strength; ρ_b is the beam longitudinal reinforcement ratio; f_{yb} is the beam longitudinal reinforcement yield strength; b_b is the beam width; h_b is the beam depth; ρ_c is the column longitudinal reinforcement ratio; f_{yc} is the column longitudinal reinforcement yield strength; b_c is the column width; h_c the column depth; ALF is the axial load factor which equals to $P/(f'_c b_c h_c)$ where P is the axial load of the column; and τ_{exp} is the joint shear strength. Three types of failure modes are observed where 'S' denotes a joint shear failure, 'B' denotes a bond-slip failure; and 'S-F' denotes combination of joint shear and beam or column flexural failures at the joint interfaces. 97 specimens have missing or unreported failure modes which is denoted as 'unknown.'

Table A.1: Experimental database of beam-column joints

No. of studies	S.N	Research Studies	Specimen	Joint Type	f'_c (MPa)	ρ_{jt}	f_{yjt} (MPa)	ρ_b	f_{yb} (MPa)	h_b (mm)	b_b (mm)	ρ_c	f_{yc} (MPa)	h_c (mm)	b_c (mm)	ALF	τ_{exp} (MPa)	Failure Mode
1	1	Adachi et al. (1995)	A0	Exterior	73.9	0.5%	939	3.7%	969	250	160	3.1%	969	220	220	0.06	10.3	S
2	2	Alire (2002)	PEER0995	Interior	60.4	0.0%	0	2.2%	504	508	406	1.2%	505	457	406	0.11	7.2	S-F
	3	Alire (2002)	PEER1595	Interior	61.5	0.0%	0	1.9%	841	508	406	3.5%	538	457	406	0.11	10.5	S-F
	4	Alire (2002)	PEER4150	Interior	33	0.0%	0	4.1%	545	508	406	3.5%	545	457	406	0.1	11.3	S-F
3	5	Almusallam and Al-Salloum (2007)	IC1	Interior	30	0.0%	0	2.1%	420	350	160	1.6%	420	300	160	0.2	6.4	S-F
	6	Almusallam and Al-Salloum (2007)	IC2	Interior	25	0.0%	0	2.1%	420	350	160	1.6%	420	300	160	0.2	4.6	S-F
4	7	Al-Salloum et al. (2011)	ECON1	Exterior	33.4	0.0%	0	2.1%	510	350	160	1.6%	510	300	160	0.2	4.6	S
5	8	Alva et al. (2007)	LVP2	Exterior	44.2	0.3%	602	2.7%	594	400	200	3.3%	594	300	200	0.15	7.3	S
	9	Alva et al. (2007)	LVP4	Exterior	24.6	0.3%	602	2.7%	594	400	200	3.3%	594	300	200	0.15	5.5	S
	10	Alva et al. (2007)	LVP3	Exterior	23.9	0.6%	602	2.7%	594	400	200	3.3%	594	300	200	0.15	6.1	S
	11	Alva et al. (2007)	LVP5	Exterior	25.9	0.6%	602	2.7%	594	400	200	3.3%	594	300	200	0.15	6.4	S
6	12	Antonopoulos and Triantafillou (2003)	C1	Exterior	19.4	0.0%	0	1.6%	585	300	200	1.5%	585	200	200	0.06	2.8	S
	13	Antonopoulos and Triantafillou (2003)	C2	Exterior	23.7	0.0%	0	1.6%	585	300	200	1.5%	585	200	200	0.05	3.1	S
	14	Antonopoulos and Triantafillou (2003)	S-C	Exterior	30.6	0.0%	0	1.6%	585	300	200	1.5%	585	200	200	0.12	3.6	S
7	15	Aoyama et al. (1993)	H2	Interior	45.6	0.5%	441	1.8%	544	300	200	2.7%	544	300	300	0.04	7.0	S-F
	16	Aoyama et al. (1993)	H4	Interior	64.2	0.5%	441	1.8%	544	300	200	2.7%	809	300	300	0.03	10.2	S-F
8	17	Atta et al. (2003)	G2-B	Exterior	60	0.0%	0	1.1%	360	400	200	2.4%	360	200	200	0.17	5.8	S
	18	Atta et al. (2003)	G3-B	Exterior	62	0.3%	240	1.1%	360	400	200	2.4%	360	200	200	0.16	5.6	S-F
	19	Atta et al. (2003)	G1-A	Exterior	67	0.5%	240	1.1%	360	400	200	2.4%	360	200	200	0.15	5.6	J
	20	Atta et al. (2003)	G1-B	Exterior	36	0.5%	240	1.1%	360	400	200	2.4%	360	200	200	0.28	5.8	J
	21	Atta et al. (2003)	G1-C	Exterior	33	0.5%	240	1.1%	360	400	200	2.4%	360	200	200	0.3	5.7	J
	22	Atta et al. (2003)	G3-C	Exterior	68	0.5%	240	1.1%	360	400	200	2.4%	360	200	200	0.15	5.6	S-F
	23	Atta et al. (2003)	G3-E	Exterior	68	0.5%	240	1.1%	360	400	200	2.4%	360	200	200	0.15	5.5	S-F
	24	Atta et al. (2003)	G3-F	Exterior	62	0.5%	240	1.1%	360	400	200	2.4%	360	200	200	0.16	5.3	Unknown
	25	Atta et al. (2003)	G2-C	Exterior	65	0.8%	240	1.1%	360	400	200	2.4%	360	200	200	0.15	5.6	S-F

	26	Atta et al. (2003)	G3-D	Exterior	64	1.3%	240	1.1%	360	400	200	2.4%	360	200	200	0.16	5.7	S-F
9	27	Beres et al. (1991)	E01	Exterior	26.1	0.0%	0	1.8%	490	610	356	2.0%	517	406	406	0.13	2.9	B
	28	Beres et al. (1991)	E05	Exterior	31.5	0.0%	0	1.8%	490	610	356	2.0%	519	406	406	0.24	3.3	B
	29	Beres et al. (1991)	E07	Exterior	29.3	0.0%	0	1.8%	490	610	356	2.0%	519	406	406	0.12	2.8	B
	30	Beres et al. (1991)	E-10	Exterior	20.5	0.0%	0	1.8%	490	610	356	2.0%	517	406	406	0.59	2.9	B
	31	Beres et al. (1991)	E-12	Exterior	18.9	0.0%	0	1.8%	474	610	356	0.9%	499	406	406	0.14	2.2	B
	32	Beres et al. (1991)	E-13	Exterior	17	0.0%	0	1.8%	474	610	356	0.9%	499	406	406	0.18	2.3	B
	33	Beres et al. (1991)	E04	Exterior	24.5	0.2%	483	1.8%	490	610	356	2.0%	501	406	406	0.09	3.4	B
	34	Beres et al. (1991)	I-11	Interior	29.9	0.0%	0	1.8%	459	610	356	2.0%	487	406	406	0.09	4.1	Unknown
	35	Beres et al. (1991)	I-13	Interior	25	0.0%	0	1.8%	341	610	356	2.0%	550	406	406	0.1	4.4	Unknown
	36	Beres et al. (1991)	I-15	Interior	23.4	0.0%	0	1.8%	461	610	356	2.0%	497	406	406	0.58	4.3	Unknown
	37	Beres et al. (1991)	I-17	Interior	21.2	0.0%	0	1.8%	472	610	356	0.9%	472	406	406	0.17	3.5	Unknown
	38	Beres et al. (1991)	I-20	Interior	20	0.0%	0	1.8%	461	610	356	0.9%	478	406	406	0.53	4.1	Unknown
10	39	Biddah (1997)	J4	Exterior	24	0.0%	0	0.8%	440	610	610	0.7%	440	510	610	0.07	1.9	B
11	40	Chalioris (2008)	Jca-0	Exterior	20.6	0.0%	0	1.2%	470	300	200	1.2%	470	300	200	0.1	1.7	S
	41	Chalioris (2008)	JA-0	Exterior	34	0.0%	0	1.7%	580	300	200	1.7%	580	300	200	0.05	4.4	S
	42	Chalioris (2008)	Jcb-0	Exterior	23	0.0%	0	1.7%	470	300	200	1.2%	470	300	200	0.1	2.0	S
	43	Chalioris (2008)	JB-0	Exterior	31.6	0.0%	0	1.7%	580	300	200	0.6%	580	300	200	0.05	4.7	S
	44	Chalioris (2008)	Jca-s1	Exterior	21	0.2%	470	1.2%	470	300	200	1.2%	470	300	200	0.1	1.3	S-F
	45	Chalioris (2008)	Jcb-s1	Exterior	23	0.2%	470	1.7%	470	300	200	1.2%	470	300	200	0.1	2.0	S-F
	46	Chalioris (2008)	Jca-s2	Exterior	21	0.3%	470	1.2%	470	300	200	1.2%	470	300	200	0.1	1.3	S
	47	Chalioris (2008)	Jca-s2	Exterior	23	0.3%	470	1.7%	470	300	200	1.2%	470	300	200	0.1	2.0	S
	48	Chalioris (2008)	JB-s1	Exterior	32	0.2%	580	1.7%	580	300	200	1.7%	580	300	200	0.05	4.6	Unknown
	49	Chalioris (2008)	JA-s5	Exterior	34	0.8%	580	1.7%	580	300	200	1.7%	580	300	200	0.05	4.5	Unknown
12	50	Chang et al. (1997)	BCB1	Interior	54.7	0.0%	0	2.6%	354	400	300	2.3%	354	500	300	0.18	6.4	S-F
	51	Chang et al. (1997)	BCS1	Interior	54.7	0.0%	0	2.6%	354	400	300	2.3%	354	500	300	0.18	7.4	S-F
	52	Chang et al. (1997)	BCS2	Interior	54.7	0.5%	352	2.8%	354	400	300	2.3%	354	500	300	0.18	8.2	Unknown
13	53	Chen (2006)	TDP2	Exterior	23.8	0.1%	408	1.2%	333	330	200	0.9%	333	230	230	0.08	1.7	S
	54	Chen (2006)	TDP1	Exterior	22.9	0.1%	408	1.2%	348	330	200	0.9%	348	230	230	0.09	1.8	S-F
	55	Chen (2006)	TDD2	Exterior	24	0.1%	408	1.7%	354	330	200	0.9%	354	230	230	0.09	2.5	S
14	56	Chen and Chen (1999)	JC	Exterior	20	0.6%	397	3.2%	439	500	300	1.6%	457	500	500	0	5.2	S-F

	57	Chen and Chen (1999)	JE	Exterior	19.9	0.6%	397	3.2%	439	500	300	1.6%	457	500	500	0	5.6	S-F
15	58	Chutarat and Aboutaha (2003)	Specimen1	Exterior	27.6	1.2%	365	2.8%	483	500	356	2.8%	483	406	406	0	5.6	S-F
	59	Chutarat and Aboutaha (2003)	SpecimenA	Exterior	33.1	1.2%	365	2.8%	483	500	356	2.8%	483	406	406	0	5.2	Unknown
16	60	Clyde et al. (2000)	Unit 2	Exterior	46.2	0.0%	0	4.2%	746	406	305	2.2%	742	457	305	0.1	7.5	S
	61	Clyde et al. (2000)	Unit 4	Exterior	41	0.0%	0	4.2%	746	406	305	2.2%	742	457	305	0.25	7.1	S
	62	Clyde et al. (2000)	Unit 5	Exterior	37	0.0%	0	4.2%	746	406	305	2.2%	742	457	305	0.25	6.8	S
	63	Clyde et al. (2000)	Unit 6	Exterior	40.1	0.0%	0	4.2%	746	406	305	2.2%	742	457	305	0.1	7.3	S
17	64	Dehkordi (2019)	NS-70	Exterior	30	0.8%	420	1.5%	420	300	250	2.0%	420	250	250	0.08	4.8	Unknown
	65	Dehkordi (2019)	RHS-70	Exterior	70	0.8%	420	1.5%	600	300	250	1.4%	600	250	250	0.04	4.8	Unknown
	66	Dehkordi (2019)	CNS-70	Exterior	30	0.8%	420	1.8%	600	300	250	1.4%	420	250	250	0.08	7.4	Unknown
18	67	Dhakal et al. (2005)	C1PD	Interior	31.6	0.0%	0	3.8%	538	550	300	2.2%	538	500	350	0.11	7.8	S
	68	Dhakal et al. (2005)	C1ND	Interior	31.6	0.0%	0	3.8%	538	550	300	2.2%	538	500	350	0.11	8.9	S
	69	Dhakal et al. (2005)	C4ND	Interior	32.7	0.0%	0	4.9%	538	550	300	2.5%	538	400	400	0.11	9.6	S
	70	Dhakal et al. (2005)	C1HD	Interior	31.6	0.0%	0	3.8%	538	550	300	2.2%	538	500	350	0.11	8.7	S
	71	Dhakal et al. (2005)	C4HD	Interior	32.7	0.0%	0	4.9%	538	550	300	2.5%	538	400	400	0.11	9.3	S
19	72	Durrani and Wight (1985)	X1	Interior	34.3	0.8%	352	2.3%	345	419	279	3.1%	414	362	362	0.05	7.2	S-F
	73	Durrani and Wight (1985)	X2	Interior	33.6	1.2%	352	2.3%	345	419	279	3.1%	414	362	362	0.06	7.3	S-F
	74	Durrani and Wight (1985)	X3	Interior	31	0.8%	352	1.7%	345	419	279	2.0%	331	362	362	0.05	5.4	S-F
20	75	Ehsani and Alameddine (1991)	LL8	Exterior	55.8	1.2%	437	2.5%	437	508	318	2.8%	437	356	356	0.04	7.8	S-F
	76	Ehsani and Alameddine (1991)	LL14	Exterior	93.8	1.2%	437	2.5%	437	508	318	2.8%	437	356	356	0.02	7.8	S-F
	77	Ehsani and Alameddine (1991)	LL11	Exterior	73.8	1.2%	437	2.5%	437	508	318	2.8%	437	356	356	0.03	7.8	S
	78	Ehsani and Alameddine (1991)	HL8	Exterior	55.8	1.2%	437	3.2%	437	508	318	3.2%	437	356	356	0.07	10.0	S
	79	Ehsani and Alameddine (1991)	HL11	Exterior	73.8	1.2%	437	3.2%	437	508	318	3.2%	437	356	356	0.06	9.9	S
	80	Ehsani and Alameddine (1991)	HL14	Exterior	93.8	1.2%	437	3.2%	437	508	318	3.2%	437	356	356	0.04	9.9	S
	81	Ehsani and Alameddine (1991)	LH11	Exterior	73.8	2.0%	437	2.5%	437	508	318	2.8%	437	356	356	0.03	7.8	S-F
	82	Ehsani and Alameddine (1991)	LH14	Exterior	93.8	2.0%	437	2.5%	437	508	318	2.8%	437	356	356	0.02	7.8	S-F
	83	Ehsani and Alameddine (1991)	LH8	Exterior	55.8	2.0%	437	2.5%	437	508	318	2.8%	437	356	356	0.04	7.8	S-F
	84	Ehsani and Alameddine (1991)	HH8	Exterior	55.8	2.0%	437	3.2%	437	508	318	3.2%	437	356	356	0.07	10.0	S-F
	85	Ehsani and Alameddine (1991)	HH11	Exterior	73.8	2.0%	437	3.2%	437	508	318	3.2%	437	356	356	0.06	9.9	S-F
	86	Ehsani and Alameddine (1991)	HH14	Exterior	93.8	2.0%	437	3.2%	437	508	318	3.2%	437	356	356	0.04	8.6	S-F
21	87	Ehsani et al. (1987)	4	Exterior	67.3	1.5%	437	2.7 %	448	439	259	4.0%	448	300	300	0.05	8.7	S-F

	88	Ehsani et al. (1987)	5	Exterior	44.6	1.5%	437	3.6%	448	439	259	2.5%	448	300	300	0.06	6.9	S-F
	89	Ehsani et al. (1987)	1	Exterior	64.7	1.9%	437	1.6%	448	480	300	3.2%	448	300	300	0.02	5.0	S-F
	90	Ehsani et al. (1987)	2	Exterior	67.3	1.9%	437	2.0%	448	480	300	3.2%	448	300	300	0.06	6.1	S-F
	91	Ehsani et al. (1987)	3	Exterior	64.7	1.9%	437	2.2%	448	439	259	3.2%	448	300	300	0.07	7.0	S-F
22	92	El-Amoury (2004)	T-S1	Exterior	30.8	0.0%	0	2.4%	477	400	250	1.3%	477	400	250	0.19	5.5	S-F
	93	El-Amoury (2004)	T-SB3	Exterior	30.6	0.0%	0	2.4%	477	400	250	1.3%	477	400	250	0.2	4.0	B
23	94	Endoh et al. (1991)	LA1	Interior	34.8	0.7%	286	3.7%	801	300	200	3.5%	550	300	300	0.06	9.8	S
	95	Endoh et al. (1991)	HLC	Interior	40.6	0.4%	290	3.1%	368	300	200	2.7%	360	300	300	0.05	8.4	S-F
	96	Endoh et al. (1991)	A1	Interior	30.6	0.6%	320	3.7%	780	300	200	3.5%	539	300	300	0.06	9.2	S
24	97	Eshani and Wight (1985)	6B	Exterior	38.4	1.0%	437	2.4%	331	480	300	2.0%	490	340	340	0.07	4.6	S-F
	98	Eshani and Wight (1985)	5B	Exterior	24.3	1.2%	437	3.2%	331	480	300	4.4%	414	340	340	0.13	6.2	S
	99	Eshani and Wight (1985)	1B	Exterior	33.6	1.3%	437	3.3%	331	480	259	2.5%	490	300	300	0.06	6.4	S
	100	Eshani and Wight (1985)	2B	Exterior	35	1.5%	437	3.5%	331	439	259	3.2%	490	300	300	0.07	7.0	S
	101	Eshani and Wight (1985)	3B	Exterior	40.9	1.7%	437	3.3%	331	480	259	2.5%	490	300	300	0.06	6.8	S
	102	Eshani and Wight (1985)	4B	Exterior	44.6	1.7%	437	3.5%	331	439	259	3.2%	490	300	300	0.06	6.8	S-F
25	103	Faleschini et al. (2018)	1	Exterior	39	2.6%	555	1.7%	555	500	300	2.3%	555	300	300	0.11	8.2	Unknown
	104	Faleschini et al. (2018)	2	Exterior	48.5	2.6%	555	1.7%	555	500	300	2.3%	555	300	300	0.1	8.7	Unknown
	105	Faleschini et al. (2018)	3	Exterior	44	2.6%	555	1.7%	555	500	300	2.3%	555	300	300	0.1	8.5	Unknown
26	106	Filiatrault et al. (1994)	Sp-1	Exterior	34	0.0%	0	1.5%	475	450	350	2.3%	475	350	350	0.08	5.8	B
27	107	Fuji and Morita (1991)	B2	Exterior	30	0.5%	291	5.7%	409	250	160	3.1%	387	220	220	0.07	5.1	S
	108	Fuji and Morita (1991)	B1	Exterior	30	0.5%	291	5.7%	1069	250	160	3.1%	387	220	220	0.07	5.9	S
	109	Fuji and Morita (1991)	B3	Exterior	30	0.5%	291	5.7%	1069	250	160	3.1%	387	220	220	0.24	6.6	S
	110	Fuji and Morita (1991)	B4	Exterior	30	1.5%	291	5.7%	1069	250	160	3.1%	387	220	220	0.24	6.9	S
28	111	Fujii and Morita (1987)	OBO	Interior	43.5	0.4%	367	1.8%	369	250	160	3.1%	369	220	220	0.05	7.0	S-F
	112	Fujii and Morita (1991)	A1	Interior	40.2	0.5%	291	3.2%	1069	250	160	4.2%	643	220	220	0.08	9.9	S
	113	Fujii and Morita (1991)	A2	Interior	40.2	0.5%	291	2.6%	409	250	160	4.2%	387	220	220	0.08	9.1	S
	114	Fujii and Morita (1991)	A3	Interior	40.2	0.5%	291	3.2%	1069	250	160	4.2%	643	220	220	0.23	9.9	S
	115	Fujii and Morita (1991)	A4	Interior	40.2	1.5%	291	3.2%	1069	250	160	4.2%	643	220	220	0.23	10.1	S
29	116	Ghobarah and Said (2002)	T1	Exterior	30.8	0.0%	0	2.4%	425	400	250	2.2%	425	400	250	0.19	5.6	S-F
30	117	Goto and Joh (1996)	J-OH	Interior	31.5	0.0%	0	4.2%	538	350	200	3.8%	578	300	300	0.28	9.6	S
	118	Goto and Joh (1996)	BJ-PL	Interior	29.7	0.4%	326	2.7%	395	350	200	3.1%	640	300	300	0.17	6.5	S-F

	119	Goto and Joh (1996)	BJ-PH	Interior	30.5	0.9%	326	2.7%	395	350	200	3.1%	640	300	300	0.17	6.9	S-F
	120	Goto and Joh (1996)	J-LO	Interior	24	0.3%	355	3.5%	697	350	200	2.0%	388	300	450	0.17	8.4	S
	121	Goto and Joh (1996)	C5-LO	Interior	32.7	0.0%	360	4.2%	426	350	200	3.8%	578	200	450	0.27	10.4	Unknown
	122	Goto and Joh (1996)	J-HH	Interior	32.8	1.6%	381	4.2%	426	350	200	3.8%	578	300	300	0.27	9.6	S
	123	Goto and Joh (1996)	J-HO	Interior	31.4	1.6%	381	4.2%	426	350	200	3.8%	578	300	300	0.28	9.3	S
	124	Goto and Joh (1996)	J-MM	Interior	32.4	0.8%	381	4.2%	426	350	200	3.8%	578	300	300	0.27	9.7	S
	125	Goto and Joh (1996)	J-MO	Interior	32.7	0.8%	381	4.2%	426	350	200	3.8%	578	300	300	0.27	10.0	S
31	126	Ha (1992)	1	Exterior	41.2	0.2%	387	2.9%	414	200	150	2.9%	414	200	200	0.03	5.6	S-F
	127	Ha (1992)	4	Exterior	68.6	0.2%	387	2.9%	414	200	150	2.9%	414	200	200	0.02	5.4	S-F
32	128	Hakuto et al. (2000)	O4	Interior	52.9	0.0%	0	2.4%	308	500	300	1.7%	321	460	460	0	5.5	S-F
	129	Hakuto et al. (2000)	O5	Interior	32.8	0.0%	0	2.1%	306	500	300	1.7%	321	460	460	0	5.8	S-F
33	130	Hamil (2000)	C7LN0	Exterior	38.4	0.0%	0	2.5%	500	300	110	3.6%	500	150	150	0.05	5.9	S
	131	Hamil (2000)	C9LN0	Exterior	40.8	0.0%	0	2.5%	500	300	110	3.6%	500	150	150	0.05	5.5	S
	132	Hamil (2000)	C4ALN0	Exterior	42.4	0.0%	0	3.8%	500	210	110	3.6%	500	150	150	0.05	7.3	S
	133	Hamil (2000)	C6ALH0	Exterior	100.8	0.0%	0	3.8%	500	210	110	3.6%	500	150	150	0.04	9.5	S
	134	Hamil (2000)	C6LN0	Exterior	51.2	0.0%	0	3.8%	500	210	110	3.6%	500	150	150	0.04	6.4	S
	135	Hamil (2000)	C6LN1A	Exterior	48.8	0.0%	0	3.8%	500	210	110	3.6%	500	150	150	0.05	7.5	S
	136	Hamil (2000)	C6LN1AE	Exterior	44	0.0%	0	3.8%	500	210	110	3.6%	500	150	150	0.06	8.0	S
	137	Hamil (2000)	C7LN1	Exterior	37.6	0.3%	500	2.5%	500	300	110	3.6%	500	150	150	0.06	6.6	S
	138	Hamil (2000)	C7LN3	Exterior	40	0.3%	500	2.5%	500	300	110	3.6%	500	150	150	0.06	7.1	S
	139	Hamil (2000)	C9LN1	Exterior	38.4	0.3%	500	2.5%	500	300	110	3.6%	500	150	150	0.06	5.5	S
	140	Hamil (2000)	C9LN3	Exterior	36.8	0.3%	500	2.5%	500	300	110	3.6%	500	150	150	0.06	6.3	S
	141	Hamil (2000)	C6LN1R	Exterior	48.8	0.4%	500	3.8%	500	210	110	3.6%	500	150	150	0.06	7.6	S
	142	Hamil (2000)	C4ALN1	Exterior	45.6	0.4%	500	7.4%	500	210	110	3.6%	500	150	150	0.05	9.4	Unknown
	143	Hamil (2000)	C4ALN3	Exterior	52	0.6%	500	7.4%	500	210	110	3.6%	500	150	150	0.04	11.2	Unknown
	144	Hamil (2000)	C4ALN5	Exterior	63	1.2%	500	7.4%	500	210	110	3.6%	500	150	150	0.04	12.4	Unknown
	145	Hamil (2000)	C6LN3	Exterior	61	0.6%	500	7.4%	500	210	110	3.6%	500	150	150	0.04	8.7	Unknown
	146	Hamil (2000)	C6LN5	Exterior	46	1.2%	500	7.4%	500	210	110	3.6%	500	150	150	0.05	11.0	Unknown
	147	Hamil (2000)	C6ALH3	Exterior	121	0.6%	500	7.4%	500	210	110	3.6%	500	150	150	0.04	12.2	Unknown
	148	Hamil (2000)	C7LN5	Exterior	50	1.2%	500	4.1%	500	300	110	3.6%	500	150	150	0.04	10.2	Unknown
	149	Hamil (2000)	C9LN5	Exterior	44	1.2%	500	4.1%	500	300	110	3.6%	500	150	150	0.05	8.7	Unknown

34	150	Hanson and Connor (1967)	V	Exterior	22.8	0.0%	0	2.8%	352	508	305	5.5%	447	381	381	0.52	4.7	S
35	151	Hayashi et al. (1993)	NO47	Interior	54.2	0.7%	347	3.2%	382	400	300	2.2%	645	400	400	0.2	7.6	S-F
	152	Hayashi et al. (1993)	NO48	Interior	54.2	0.7%	347	1.8%	645	400	300	2.2%	645	400	400	0.2	8.5	S-F
	153	Hayashi et al. (1993)	NO49	Interior	54.2	0.7%	347	3.5%	599	400	300	2.2%	645	400	400	0.2	11.9	S-F
	154	Hayashi et al. (1993)	NO50	Interior	54.2	0.7%	347	1.4%	858	400	300	2.2%	645	400	400	0.2	8.4	S-F
36	155	Hiramatsu et al. (1995)	S1	Interior	52.2	0.3%	876	5.2%	836	300	210	2.3%	836	300	300	0.2	11.7	S
37	156	Ho and Cho (2008)	NJC	Exterior	29.6	2.1%	455	2.9%	455	200	150	2.8%	403	200	200	0.15	5.2	Unknown
	157	Ho and Cho (2008)	HJC	Exterior	49.5	2.1%	455	2.9%	455	200	150	2.8%	403	200	200	0.15	5.0	Unknown
38	158	Hoffschild et al. (1995)	RCBC1	Exterior	26.3	0.0%	0	1.9%	566	200	165	1.3%	566	190	190	0.1	4.5	S
39	159	Hwang (2004)	28-0 T0	Exterior	33	0.0%	0	2.1%	491	500	380	3.2%	458	550	550	0.02	7.3	Unknown
	160	Hwang (2004)	28-3 T4	Exterior	35	0.8%	436	2.1%	491	500	380	3.2%	458	550	550	0.02	8.4	Unknown
	161	Hwang (2004)	70-3T44	Exterior	75.2	1.1%	436	2.8%	491	450	320	3.2%	458	450	450	0.01	10.9	Unknown
	162	Hwang (2004)	70-1T55	Exterior	69.7	0.3%	469	2.8%	491	450	320	3.2%	458	450	450	0.01	11.1	Unknown
	163	Hwang (2004)	70-2T5	Exterior	76.6	0.4%	469	2.8%	491	450	320	3.2%	458	450	450	0.01	11.5	Unknown
	164	Hwang (2004)	70-3T44	Exterior	76.8	1.1%	498	2.8%	491	450	320	3.6%	458	420	420	0.01	10.5	Unknown
40	165	Hwang et al. (2005)	3T3	Exterior	69	0.9%	0	2.8%	430	450	320	3.7%	421	420	420	0.02	7.2	S-F
	166	Hwang et al. (2005)	2T4	Exterior	71	0.9%	0	2.8%	430	450	320	3.7%	421	420	420	0.02	6.9	S-F
	167	Hwang et al. (2005)	1T44	Exterior	72.8	0.9%	0	2.8%	430	450	320	3.7%	421	420	420	0.02	5.1	S-F
	168	Hwang et al. (2005)	3T44	Exterior	76.8	0.9%	0	2.8%	430	450	320	3.7%	421	420	420	0.01	5.0	Unknown
	169	Hwang et al. (2005)	0T0	Exterior	67.3	0.0%	0	2.8%	430	450	320	3.7%	421	420	420	0.02	6.4	S-F
	170	Hwang et al. (2005)	1B8	Exterior	61.8	0.0%	0	2.8%	435	450	320	3.7%	430	420	420	0.02	8.0	S-F
	171	Hwang et al. (2005)	3T4	Exterior	75.2	0.8%	436	2.8%	430	450	320	3.2%	458	450	450	0.01	5.1	Unknown
	172	Hwang et al. (2005)	2T5	Exterior	76.6	0.8%	469	2.8%	491	450	320	3.2%	458	450	450	0.01	5.1	Unknown
	173	Hwang et al. (2005)	1T55	Exterior	69.7	0.8%	469	2.8%	491	450	320	3.2%	458	450	450	0.01	5.1	Unknown
	174	Hwang et al. (2005)	1T44	Exterior	72.8	0.4%	498	2.8%	430	450	320	3.7%	421	420	420	0.02	6.7	Unknown
41	175	Ilki et al. (2011)	JOP	Exterior	8.3	0.0%	0	1.3%	333	500	250	1.3%	333	500	250	0.13	1.2	S
42	176	Inoue et al. (1990)	SP2	Interior	43.3	0.3%	1253	3.2%	473	417	301	1.8%	473	440	440	0.28	10.3	S-F
	177	Ishida et al. (1996)	No. 1	Interior	25.8	0.8%	354	2.2%	383	550	300	1.2%	378	500	500	0.11	6.3	S-F
43	178	Ishida et al. (2001)	CN	Interior	33.4	0.2%	365	2.2%	462	750	450	1.6%	464	700	800	0.09	6.9	S-F
44	179	Ishida et al. (2004)	HS-HS	Interior	70	0.4%	1116	1.8%	707	300	200	1.8%	707	300	300	0.1	12.6	S-F
	180	Ishida et al. (2005)	A-0	Exterior	27	0.5%	271	2.4%	700	250	160	3.1%	700	220	220	0.15	5.4	S

	181	Ishida et al. (2005)	A-0-F	Exterior	27	0.5%	271	2.4%	467	250	160	3.1%	467	220	220	0.15	5.2	S-F
45	182	Ishikawa and Kamimura (1990)	No. 3	Interior	23.3	1.0%	330	2.8%	373	250	180	3.2%	373	250	250	0.18	7.3	Unknown
46	183	Iwaoka et al. (2005)	J15-3	Exterior	180	0.2%	935	3.6%	682	400	260	2.7%	690	380	330	0.05	14.9	Unknown
	184	Iwaoka et al. (2005)	J10-1	Exterior	115	0.2%	935	3.6%	682	400	260	2.7%	690	380	330	0.05	13.6	S
	185	Iwaoka et al. (2005)	J15-1	Interior	182	0.2%	935	3.7%	682	400	220	3.0%	690	380	300	0.25	24.5	Unknown
47	186	Jinno et al. (1985)	NO05	Exterior	32	0.0%	0	1.3%	392	380	260	3.8%	371	300	300	0	4.1	S
	187	Jinno et al. (1985)	NO06	Exterior	28.9	0.4%	304	1.3%	392	380	260	3.8%	371	300	300	0	4.2	S-F
	188	Jinno et al. (1985)	NO07	Exterior	28.9	0.4%	304	1.3%	392	380	260	3.8%	371	300	300	0	4.2	S-F
	189	Jinno et al. (1985)	NO08	Exterior	28.9	0.8%	304	1.3%	392	380	260	3.8%	371	300	300	0	4.3	S-F
	190	Jinno et al. (1985)	NO09	Exterior	28.9	0.8%	304	1.3%	392	380	260	3.8%	371	300	300	0	4.3	S-F
	191	Jinno et al. (1985)	NO10	Exterior	28.9	0.8%	304	1.3%	392	380	260	3.8%	371	300	300	0	4.6	S-F
48	192	Jinno et al. (1991)	NO1	Interior	28.3	0.3%	686	1.7%	405	400	300	2.9%	405	400	400	0.17	7.8	S-F
	193	Jinno et al. (1991)	NO2	Interior	28.3	0.3%	686	1.7%	913	400	300	2.9%	913	400	400	0.17	9.4	S
	194	Jinno et al. (1991)	NO3	Interior	80.2	0.3%	686	1.7%	593	400	300	2.9%	593	400	400	0.17	13.1	S-F
	195	Jinno et al. (1991)	NO4	Interior	80.2	0.3%	686	1.7%	593	400	300	2.9%	593	400	400	0.17	14.6	S-F
	196	Jinno et al. (1991)	NO5	Interior	80.2	0.3%	686	1.7%	913	400	300	2.9%	913	400	400	0.17	17.5	S-F
	197	Jinno et al. (1991)	NO6	Interior	101.9	0.3%	686	1.7%	726	400	300	2.9%	726	400	400	0.17	15.9	S-F
	198	Jinno et al. (1991)	NO7	Interior	101.9	0.3%	686	1.7%	913	400	300	2.9%	913	400	400	0.17	17.4	S-F
	199	Jinno et al. (1991)	NO8	Interior	101.9	0.3%	686	2.3%	913	400	300	2.9%	913	400	400	0.17	20.1	S-F
49	200	Joh and Goto (2000)	PL-13	Interior	26.4	0.4%	366	1.9%	363	350	200	2.2%	402	300	300	0.09	6.0	S-F
	201	Joh and Goto (2000)	PH-16	Interior	23.6	0.5%	366	2.3%	344	350	200	2.7%	402	300	300	0.13	6.4	S-F
	202	Joh and Goto (2000)	PH-13	Interior	26.3	0.5%	366	2.7%	363	350	200	2.7%	402	300	300	0.13	7.3	S-F
	203	Joh and Goto (2000)	PH-10	Interior	25.6	0.5%	366	2.3%	372	350	200	2.7%	402	300	300	0.11	7.0	S-F
50	204	Joh et al. (1988)	X0-1	Interior	21.3	0.2%	363	2.9%	363	350	150	1.1%	363	300	300	0.16	4.2	Unknown
51	205	Joh et al. (1989)	LO-NO	Exterior	27.9	0.1%	380	4.2%	606	350	200	2.5%	581	260	350	0.02	4.8	S
	206	Joh et al. (1989)	HO-NO	Exterior	29.6	0.4%	380	4.2%	606	350	200	2.5%	581	260	350	0.02	6.3	S
	207	Joh et al. (1989)	MM-NO	Exterior	27.8	0.4%	380	4.2%	606	350	200	2.8%	581	260	350	0.02	6.1	S
	208	Joh et al. (1989)	HH-NO	Exterior	29.3	0.4%	380	4.2%	606	350	200	2.5%	581	260	350	0.02	7.2	S
	209	Joh et al. (1989)	H'O-NO	Exterior	31.5	0.4%	380	4.2%	606	350	200	2.5%	581	260	350	0.02	5.9	S
	210	Joh et al. (1989)	LO-N96	Exterior	31.5	0.2%	380	4.2%	606	350	200	3.4%	581	260	350	0.3	5.8	S
	211	Joh et al. (1989)	HH-N96	Exterior	30.5	0.4%	380	4.2%	606	350	200	3.4%	581	260	350	0.31	6.8	S

52	212	Joh et al. (1990)	NRC-J1	Exterior	51.5	0.6%	815	3.2%	1091	250	200	2.4%	1091	250	250	0.02	11.4	S
	213	Joh et al. (1990)	NRc-J2	Exterior	81.8	0.6%	815	3.2%	1091	250	200	2.4%	1091	250	250	0.02	13.1	S
	214	Joh et al. (1990)	NRC-J4	Exterior	88.9	0.6%	815	3.2%	1091	250	200	2.4%	1091	250	250	0.3	14.5	S
	215	Joh et al. (1990)	NRC-J3	Exterior	86.9	0.3%	840	3.2%	1091	250	200	2.4%	1091	250	250	0.02	13.3	S
53	216	Joh et al. (1991	JXO-B1	Interior	21.3	0.2%	307	1.5%	371	350	150	1.1%	371	300	300	0.16	4.3	Unknown
54	217	Joh et al. (1991b)	JX0-B8LH	Interior	26.9	0.2%	377	1.1%	404	350	200	2.0%	404	300	300	0.15	3.7	Unknown
	218	Joh et al. (1991b)	JX0-B8MH	Interior	28.1	0.4%	377	1.1%	404	350	200	2.0%	404	300	300	0.14	4.1	Unknown
55	219	Joh et al. (1992)	NRC-J8	Exterior	53.7	0.2%	717	4.9%	675	250	200	2.8%	675	250	250	0.02	7.1	S
	220	Joh et al. (1992)	NRC-J12	Exterior	83.7	0.2%	717	4.9%	698	250	200	2.4%	698	250	250	0.02	12.8	S
	221	Joh et al. (1992)	NRC-J14	Exterior	64.9	0.2%	717	4.9%	547	250	200	2.4%	698	250	250	0.02	7.8	S-F
	222	Joh et al. (1992)	NRC-J10	Exterior	65.7	0.2%	760	3.3%	675	250	200	2.0%	675	250	250	0.02	6.4	S-F
	223	Joh et al. (1992)	NRC-J11	Exterior	78.7	0.2%	760	2.1%	675	250	200	2.0%	675	250	250	0.02	5.9	S-F
	224	Joh et al. (1992)	NRC-J5	Exterior	58.1	0.6%	762	4.6%	753	250	200	2.4%	1092	250	250	0.02	10.9	S-F
	225	Joh et al. (1992)	NRC-J6	Exterior	32.2	0.6%	762	4.6%	753	250	200	2.4%	1092	250	250	0.02	7.2	S-F
	226	Joh et al. (1992)	NRC-J7	Exterior	57.7	0.6%	762	3.1%	753	350	200	2.4%	1092	250	250	0.02	10.0	S-F
	227	Joh et al. (1992)	NRC-J9	Exterior	49.3	0.6%	770	3.3%	675	250	200	2.0%	675	250	250	0.02	9.3	S
	228	Joh et al. (1992)	NRC-J13	Exterior	79.4	0.6%	770	4.9%	698	250	200	2.4%	698	250	250	0.02	11.1	S-F
56	229	Kaku and Asakusa (1991)	1	Exterior	31.1	0.5%	250	3.2%	381	220	160	1.6%	360	220	220	0.17	6.2	S-F
	230	Kaku and Asakusa (1991)	2	Exterior	41.7	0.5%	250	3.2%	381	220	160	1.6%	360	220	220	0.1	6.2	S-F
	231	Kaku and Asakusa (1991)	3	Exterior	41.7	0.5%	250	3.2%	381	220	160	1.6%	360	220	220	0	5.3	S-F
	232	Kaku and Asakusa (1991)	7	Exterior	32.2	0.5%	250	3.2%	381	220	160	1.8%	395	220	220	0.12	6.3	S-F
	233	Kaku and Asakusa (1991)	8	Exterior	41.2	0.5%	250	3.2%	381	220	160	1.8%	395	220	220	0.08	6.1	S-F
	234	Kaku and Asakusa (1991)	9	Exterior	40.6	0.5%	250	3.2%	381	220	160	1.8%	395	220	220	0	6.0	S-F
	235	Kaku and Asakusa (1991)	16	Exterior	37.4	0.5%	250	3.2%	381	220	160	3.2%	381	220	220	0	6.1	S-F
	236	Kaku and Asakusa (1991)	17	Exterior	39.7	0.5%	250	3.2%	381	220	160	1.1%	395	220	220	0	4.4	S-F
	237	Kaku and Asakusa (1991)	18	Exterior	40.7	0.5%	250	3.2%	381	220	160	0.8%	282	220	220	0	3.0	S-F
	238	Kaku and Asakusa (1991)	4	Exterior	44.7	0.1%	281	3.2%	381	220	160	1.6%	360	220	220	0.17	6.0	S-F
	239	Kaku and Asakusa (1991)	5	Exterior	36.7	0.1%	281	3.2%	381	220	160	1.6%	360	220	220	0.09	5.2	S-F
	240	Kaku and Asakusa (1991)	6	Exterior	40.4	0.1%	281	3.2%	381	220	160	1.6%	360	220	220	0	5.1	S-F
	241	Kaku and Asakusa (1991)	10	Exterior	44.4	0.1%	281	3.2%	381	220	160	1.8%	395	220	220	0.17	6.1	S-F
	242	Kaku and Asakusa (1991)	11	Exterior	41.9	0.1%	281	3.2%	381	220	160	1.8%	395	220	220	0.08	6.0	S-F

	243	Kaku and Asakusa (1991)	12	Exterior	35.1	0.1%	281	3.2%	381	220	160	1.8%	395	220	220	0	5.0	S-F
	244	Kaku and Asakusa (1991)	14	Exterior	41	0.1%	281	3.2%	381	220	160	1.6%	381	220	220	0.08	5.9	S-F
	245	Kaku and Asakusa (1991)	15	Exterior	39.7	0.1%	281	3.2%	381	220	160	1.6%	381	220	220	0.08	6.0	S-F
57	246	Kaku et al. (1993)	J11A	Interior	57.6	0.5%	893	2.2%	371	350	260	3.3%	371	400	300	0.24	9.7	S-F
	247	Kaku et al. (1993)	J12A	Interior	56.6	0.5%	893	3.0%	371	350	260	3.3%	371	400	300	0.25	12.5	S-F
	248	Kaku et al. (1993)	J31A	Interior	55.2	0.5%	893	2.5%	363	350	260	3.3%	371	400	300	0.25	11.6	S-F
	249	Kaku et al. (1993)	J32A	Interior	55.2	0.6%	893	3.2%	363	350	260	3.3%	371	400	300	0.25	12.0	S-F
58	250	Kamimura et al. (2004)	NN.1	Interior	36.2	0.4%	344	2.9%	345	250	180	1.8%	380	250	350	0.03	6.5	S-F
59	251	Kanada et al. (1984)	U40L	Exterior	24.3	0.0%	0	3.4%	387	380	260	2.6%	385	300	300	0	3.7	S
	252	Kanada et al. (1984)	U20L	Exterior	26.7	0.0%	0	1.8%	387	380	260	1.3%	387	300	300	0	3.4	B
	253	Kanada et al. (1984)	U41L	Exterior	26.7	0.4%	387	3.4%	387	380	260	2.6%	385	300	300	0	4.0	S-F
	254	Kanada et al. (1984)	U42L	Exterior	30.1	0.8%	387	3.4%	387	380	260	2.6%	385	300	300	0	4.0	S-F
60	255	Karayannis and Sirkelis (2005)	AJ1s	Exterior	32.8	0.2%	580	1.1%	580	300	200	0.7%	580	200	200	0.05	3.0	Unknown
61	256	Karayannis et al. (1998)	Jo0	Exterior	20.8	0.0%	0	1.1%	580	200	100	1.6%	580	200	100	0.1	3.7	S
62	257	Karayannis et al. (2008)	A0	Exterior	31.6	0.0%	0	0.5%	580	300	200	0.5%	580	200	200	0.05	2.6	S
	258	Karayannis et al. (2008)	C0	Exterior	31.6	0.0%	0	1.5%	580	300	200	1.3%	580	300	200	0.05	3.6	S
	259	Karayannis et al. (2008)	B0	Exterior	31.6	0.0%	0	1.6%	580	300	200	0.5%	580	300	200	0.05	4.2	S
	260	Karayannis et al. (2008)	A1	Exterior	31.6	0.2%	580	0.5%	580	300	200	0.9%	580	200	200	0.05	2.3	Unknown
	261	Karayannis et al. (2008)	A2	Exterior	31.6	0.2%	580	0.5%	580	300	200	0.9%	580	200	200	0.05	2.3	Unknown
	262	Karayannis et al. (2008)	A3	Exterior	31.6	0.2%	580	0.5%	580	300	200	0.9%	580	200	200	0.05	2.3	Unknown
	263	Karayannis et al. (2008)	C2	Exterior	31.6	0.2%	580	1.5%	580	300	200	1.7%	580	300	200	0.05	4.4	Unknown
	264	Karayannis et al. (2008)	B1	Exterior	31.6	0.2%	580	1.6%	580	300	200	0.6%	580	300	200	0.05	4.6	Unknown
	265	Karayannis et al. (2008)	C2	Exterior	31.6	0.4%	580	1.5%	580	300	200	1.7%	580	300	200	0.05	4.4	Unknown
	266	Karayannis et al. (2008)	C2	Exterior	31.6	0.4%	580	1.5%	580	300	200	1.7%	580	300	200	0.05	4.4	Unknown
63	267	Kashiwazaki et al. (1992)	MKJ-1	Interior	84.3	0.9%	675	1.1%	771	300	200	0.9%	644	300	300	0.1	11.1	S-F
	268	Kashiwazaki et al. (1992)	MKJ-2	Interior	84.3	0.9%	675	1.7%	771	300	200	2.7%	718	300	300	0.07	13.0	S-F
	269	Kashiwazaki et al. (1992)	MKJ-3	Interior	98.5	0.9%	675	1.5%	742	300	200	1.7%	794	300	300	0.07	13.0	S-F
	270	Kashiwazaki et al. (1992)	MKJ-4	Interior	98.5	0.9%	675	2.2%	742	300	200	3.8%	771	300	300	0.07	14.6	S-F
64	271	Kawai et al. (1997)	O8V	Exterior	88.1	0.3%	928	2.4%	522	450	325	2.7%	522	475	475	0.67	10.6	S-F
	272	Kawai et al. (1997)	I8C	Interior	85.5	0.3%	928	2.7%	522	450	325	2.7%	522	475	475	0.2	12.4	S-F
65	273	Khan et al. (2018)	TC	Exterior	30	0.0%	0	5.5%	605	250	200	3.8%	605	250	200	0.03	5.6	Unknown

66	274	Kitayama et al. (1991)	B3	Interior	24.5	0.9%	235	3.4%	311	300	200	2.3%	371	300	300	0.08	6.9	S-F
	275	Kitayama et al. (1991)	A1	Interior	30.6	0.6%	320	3.0%	780	300	200	3.5%	539	300	300	0.06	9.2	S-F
	276	Kitayama et al. (1991)	A4	Interior	30.6	0.6%	320	2.5%	780	300	200	3.5%	539	300	300	0.06	9.9	S-F
	277	Kitayama et al. (1991)	J1	Interior	25.7	0.3%	368	2.8%	401	300	200	2.3%	401	300	300	0.08	7.3	S-F
67	278	Kitayama et al. (1992)	I5	Interior	85.4	0.4%	250	2.3%	769	300	200	3.5%	534	300	300	0.02	10.7	S-F
	279	Kitayama et al. (1992)	I6	Interior	85.4	0.4%	250	2.8%	772	300	200	3.5%	534	300	300	0.02	13.5	S-F
	280	Kitayama et al. (1992)	I1	Interior	98.8	0.4%	360	6.7%	799	300	200	5.1%	747	300	300	0.04	24.7	S-F
	281	Kitayama et al. (1992)	I3	Interior	41.4	0.4%	360	4.0%	799	300	200	3.5%	361	300	300	0.03	11.9	S-F
68	282	Kitayama et al. (2000)	PB-1	Interior	21	0.7%	404	2.4%	534	380	250	5.1%	517	350	350	0.34	8.4	S-F
	283	Kitayama et al. (2000)	PNB-2	Interior	21	0.7%	404	2.4%	534	380	250	5.1%	517	350	350	0.34	8.2	S-F
	284	Kitayama et al. (2000)	PNB-3	Interior	21.9	0.7%	404	2.4%	534	380	250	5.1%	517	350	350	0.33	7.8	S-F
69	285	Kordina (1984)	RE4	Exterior	32	0.3%	250	1.1%	420	300	200	2.0%	420	200	200	0.04	4.2	S
70	286	Kotsovou (2011)	S5	Exterior	35	0.9%	571	1.9%	587	450	300	4.1%	560	300	300	0	7.9	Unknown
	287	Kotsovou (2011)	S2’	Exterior	35	1.2%	571	1.9%	587	450	300	3.9%	560	300	300	0	8.0	Unknown
71	288	Kotsovou (2012)	S10	Exterior	35	0.4%	571	1.0%	563	450	300	3.2%	563	400	400	0	2.2	Unknown
	289	Kotsovou (2012)	S6	Exterior	35	0.4%	571	1.9%	563	450	300	1.9%	570	400	400	0	4.5	Unknown
	290	Kotsovou (2012)	S9	Exterior	35	0.5%	571	1.9%	563	450	300	1.9%	563	400	400	0	4.5	Unknown
72	291	Kuang and Wong (2006)	BS-LL	Exterior	42.1	0.0%	0	1.6%	520	450	260	2.2%	520	300	300	0.14	5.0	Unknown
	292	Kuang and Wong (2006)	BS-L-LS	Exterior	31.6	0.0%	0	1.6%	520	450	260	2.2%	520	300	300	0.14	4.3	Unknown
	293	Kuang and Wong (2006)	BS-U	Exterior	31	0.0%	0	1.6%	520	450	260	2.2%	520	300	300	0.14	4.3	Unknown
73	294	Kulkarni and Li (2007)	JA	Interior	33.7	0.0%	0	1.1%	484	500	250	1.6%	484	400	400	0.3	8.3	Unknown
	295	Kulkarni and Li (2007)	JB	Interior	34.8	0.0%	0	1.1%	484	500	250	1.6%	484	400	400	0.3	8.3	Unknown
74	296	Kurose et al. (1991)	J1	Interior	24.1	0.7%	550	1.7%	463	508	406	2.4%	463	508	508	0	8.6	Unknown
75	297	Kurusu (1988)	NO4	Interior	34.1	0.1%	354	1.2%	388	300	200	2.3%	388	300	300	0.06	6.2	Unknown
76	298	Kusuhara et al. (2004)	JE-0	Interior	27	0.3%	364	2.9%	387	300	180	2.3%	345	280	320	0	6.9	Unknown
77	299	Lee and Ko (2007)	S0	Exterior	32.6	0.7%	471	2.3%	471	450	300	1.9%	471	400	600	0.09	3.9	Unknown
	300	Lee and Ko (2007)	S50	Exterior	34.2	0.7%	471	2.3%	471	450	300	1.9%	471	400	600	0.09	3.8	Unknown
	301	Lee and Ko (2007)	W0	Exterior	28.9	1.0%	471	2.3%	471	450	300	1.9%	471	600	400	0.1	4.8	Unknown
	302	Lee and Ko (2007)	W75	Exterior	30.4	1.0%	471	2.3%	471	450	300	1.9%	471	600	400	0.1	4.9	Unknown
	303	Lee and Ko (2007)	W150	Exterior	29.1	1.0%	471	2.3%	471	450	300	1.9%	471	600	400	0.1	4.9	Unknown
78	304	Lee and Lee (2000)	EJ+0.0	Exterior	19	0.3%	673	2.9%	451	300	200	2.7%	451	300	300	0	3.5	S

79	305	Lee and Lee (2000)	EJ+0.1	Exterior	19	0.3%	673	2.9%	451	300	200	2.7%	451	300	300	0.1	3.7	S
80	306	Lee and Lee (2001)	HJ2-0.0	Exterior	38	0.2%	671	2.2%	540	300	200	2.7%	504	300	300	0	6.3	S
	307	Lee and Lee (2001)	HJ2-0.15	Exterior	38	0.2%	671	2.2%	540	300	200	2.7%	504	300	300	0.15	6.4	S
	308	Lee and Lee (2001)	HJ2-0.3	Exterior	38	0.2%	671	2.2%	540	300	200	2.7%	504	300	300	0.3	5.9	S
	309	Lee and Lee (2001)	HJ5-0.0	Exterior	38	0.6%	671	2.2%	540	300	200	2.7%	504	300	300	0	7.0	S
	310	Lee and Lee (2001)	HJ5-0.15	Exterior	38	0.6%	671	2.2%	540	300	200	2.7%	504	300	300	0.15	6.1	S
	311	Lee and Lee (2001)	HJ5-0.3	Exterior	38	0.6%	671	2.2%	540	300	200	2.7%	504	300	300	0.3	5.6	S
	312	Lee and Lee (2001)	NJ2-0.0	Exterior	23.5	0.2%	671	1.6%	442	300	200	2.7%	504	300	300	0	4.6	S
	313	Lee and Lee (2001)	NJ2-0.15	Exterior	23.5	0.2%	671	1.6%	442	300	200	2.7%	504	300	300	0.15	4.4	S
	314	Lee and Lee (2001)	NJ2-0.3	Exterior	23.5	0.2%	671	1.6%	442	300	200	2.7%	504	300	300	0.3	4.4	S
	315	Lee and Lee (2001)	NJ5-0.0	Exterior	23.5	0.6%	671	1.6%	442	300	200	2.7%	504	300	300	0	4.8	S
	316	Lee and Lee (2001)	NJ5-0.15	Exterior	23.5	0.6%	671	1.6%	442	300	200	2.7%	504	300	300	0.15	4.5	S
	317	Lee and Lee (2001)	NJ5-0.3	Exterior	23.5	0.6%	671	1.6%	442	300	200	2.7%	504	300	300	0.3	4.5	S
81	318	Lee et al. (2009)	J1	Interior	40	0.5%	510	3.4%	510	400	300	6.3%	514	350	350	0	10.9	S
	319	Lee et al. (2009)	BJ3	Interior	40	0.5%	510	1.3%	510	400	300	6.3%	514	350	350	0	9.4	S-F
82	320	Lee et al. (2010)	JI0	Interior	27	0.0%	0	2.3%	456	600	300	2.5%	456	400	400	0.19	6.2	S
	321	Lee et al. (2010)	A1	Interior	32.3	0.0%	0	1.2%	503	600	300	2.5%	460	300	900	0	4.7	S
	322	Lee et al. (2010)	M1	Interior	32	0.1%	499	1.2%	503	600	300	2.5%	460	300	900	0	4.7	S-F
83	323	Leon (1990)	BCJ2	Interior	27.6	0.5%	414	1.3%	414	305	203	2.8%	414	254	254	0	2.8	S-F
	324	Leon (1990)	BCJ3	Interior	27.6	0.4%	414	1.3%	414	305	203	2.3%	414	254	305	0	6.7	S-F
84	325	Le-Trung et al. (2010)	SD	Exterior	36.5	0.3%	324	1.8%	324	200	134	1.5%	324	167	167	0	4.1	Unknown
	326	Le-Trung et al. (2010)	NS	Exterior	33.8	0.0%	0	1.8%	324	200	134	1.5%	324	167	167	0	3.3	S
85	327	Liu (2006)	RC-1	Exterior	19.4	0.0%	0	1.4%	324	330	200	0.9%	324	230	230	0.07	2.6	S-F
	328	Liu (2006)	RC-6	Exterior	25.9	0.1%	384	1.1%	307	330	250	1.8%	307	250	250	0.06	2.8	S-F
	329	Liu (2006)	NZ-7	Exterior	30	1.7%	384	1.1%	307	330	250	1.8%	307	250	250	0	3.5	Unknown
86	330	Li et al. (2009)	AL2	Interior	32.1	0.0%	0	2.2%	473	400	200	3.1%	473	400	200	0	6.3	S-F
87	331	Matsumoto et al. (2010)	B-0	Interior	54.6	0.5%	1276	3.4%	522	400	250	2.2%	746	400	450	0.2	11.9	Unknown
	332	Matsumoto et al. (2010)	J-0	Interior	54.6	0.5%	1276	3.4%	710	400	250	2.2%	746	400	450	0.2	13.6	Unknown
88	333	Megget (1971)	Unit 1	Exterior	28.3	0.6%	317	2.2%	286	460	255	1.2%	305	380	330	0	3.9	S-F
89	334	Megget (1974)	Unit A	Exterior	22.1	1.6%	317	2.5%	374	460	255	2.5%	365	380	330	0.07	5.4	S-F
90	335	Meinheit and Jirsa (1981)	1	Interior	26.2	0.5%	409	3.1%	449	457	279	2.1%	457	457	330	0.4	7.8	S

	336	Meinheit and Jirsa (1981)	2	Interior	41.8	0.5%	409	3.1%	449	457	279	4.3%	449	457	330	0.25	11.4	S
	337	Meinheit and Jirsa (1981)	3	Interior	26.6	0.5%	409	3.1%	449	457	279	6.7%	402	457	330	0.39	8.7	S
	338	Meinheit and Jirsa (1981)	4	Interior	36.1	0.4%	409	2.1%	449	457	406	4.3%	438	330	457	0.3	10.2	S
	339	Meinheit and Jirsa (1981)	5	Interior	35.9	0.5%	409	3.1%	449	457	279	4.3%	449	457	330	0.04	10.9	S
	340	Meinheit and Jirsa (1981)	6	Interior	36.7	0.5%	409	3.1%	449	457	279	4.3%	449	457	330	0.48	11.8	S-F
	341	Meinheit and Jirsa (1981)	7	Interior	37.2	0.4%	409	2.1%	449	457	406	4.3%	438	330	457	0.47	10.3	S
	342	Meinheit and Jirsa (1981)	13	Interior	41.3	1.5%	409	3.1%	449	457	279	4.3%	449	457	330	0.25	11.1	S
	343	Meinheit and Jirsa (1981)	14	Interior	33.2	1.1%	409	2.1%	449	457	406	4.3%	438	330	457	0.32	10.6	S
	344	Meinheit and Jirsa (1981)	12	Interior	35.2	2.4%	423	3.1%	449	457	279	4.3%	449	457	330	0.3	14.0	S-F
91	345	Melo et al. (2012)	TPA-1	Exterior	24.4	0.0%	0	0.7%	405	400	250	0.7%	405	250	250	0.13	3.6	S
	346	Melo et al. (2012)	TPA-2	Exterior	25.8	0.0%	0	0.7%	405	400	250	0.7%	405	250	250	0.12	3.6	S
	347	Melo et al. (2012)	TP-B1	Exterior	15.8	0.0%	0	0.7%	405	400	250	0.7%	405	250	250	0.2	3.6	S
	348	Melo et al. (2012)	TPB-2	Exterior	27.3	0.0%	0	0.7%	405	400	250	0.7%	405	250	250	0.12	3.6	S
	349	Melo et al. (2012)	TPC	Exterior	23.8	0.0%	0	0.7%	405	400	250	0.7%	405	250	250	0.14	3.6	S
	350	Melo et al. (2012)	TD	Exterior	20.8	0.0%	0	0.7%	465	400	250	0.7%	465	250	250	0.15	3.7	S
92	351	Morita et al. (2004)	M1	Interior	17.1	0.3%	344	3.43%	520	400	300	5.9%	520	350	300	0	6.3	S
	352	Morita et al. (2004)	M2	Interior	18.2	0.3%	344	3.43%	520	400	300	5.9%	520	350	300	0	6.9	S
	353	Morita et al. (2004)	M3	Interior	18.8	0.3%	344	3.43%	520	400	300	5.9%	520	350	300	0	6.3	S
	354	Morita et al. (2004)	M6	Interior	19.4	0.3%	344	2.4%	520	400	300	5.9%	520	350	300	0	6.6	S
	355	Morita et al. (2004)	M4	Interior	20.6	2.1%	429	3.43%	520	400	300	5.9%	520	350	300	0	7.6	S
93	356	Murty et al. (2003)	Q1	Exterior	25.6	0.0%	0	1.6%	382	400	200	2.4%	382	250	200	0	6.3	S
	357	Murty et al. (2003)	P1	Exterior	27.3	0.0%	0	1.6%	382	400	200	2.4%	382	250	200	0	6.9	S
	358	Murty et al. (2003)	R1	Exterior	30.2	0.0%	0	1.6%	382	400	200	2.4%	382	250	200	0	7.0	S
	359	Murty et al. (2003)	S1	Exterior	27.8	0.0%	0	1.6%	382	400	200	2.4%	382	250	200	0	6.6	S
	360	Murty et al. (2003)	P2	Exterior	26.3	2.3%	382	1.6%	382	400	200	2.4%	382	250	200	0	8.2	S
	361	Murty et al. (2003)	P3	Exterior	27	2.3%	382	1.6%	382	400	200	2.4%	382	250	200	0	7.3	S
	362	Murty et al. (2003)	Q2	Exterior	27.2	2.3%	382	1.6%	382	400	200	2.4%	382	250	200	0	8.9	S
	363	Murty et al. (2003)	Q3	Exterior	26.9	2.3%	382	1.6%	382	400	200	2.4%	382	250	200	0	8.6	S
	364	Murty et al. (2003)	R2	Exterior	27.3	2.3%	382	1.6%	382	400	200	2.4%	382	250	200	0	9.3	S
	365	Murty et al. (2003)	R3	Exterior	27.1	2.3%	382	1.6%	382	400	200	2.4%	382	250	200	0	8.8	S
	366	Murty et al. (2003)	S2	Exterior	26.8	2.3%	382	1.6%	382	400	200	2.4%	382	250	200	0	8.8	S

	367	Murty et al. (2003)	S3	Exterior	30.1	2.3%	382	1.6%	382	400	200	2.4%	382	200	250	0	8.0	S
94	368	Nakamura et al. (1991)	No.5	Interior	64.1	1.2%	873	1.7%	785	400	300	2.2%	785	400	400	0.1	16.3	S-F
	369	Nakamura et al. (1991)	No.6	Interior	63.1	1.2%	873	1.7%	785	400	300	2.2%	785	400	400	0.1	17.3	S-F
	370	Nakamura et al. (1991)	No.7	Interior	76	1.2%	873	1.7%	785	400	300	2.2%	785	400	400	0.08	16.8	S-F
	371	Nakamura et al. (1991)	No.1	Interior	65.3	0.4%	880	1.7%	582	400	300	2.2%	785	400	400	0.09	12.6	S-F
	372	Nakamura et al. (1991)	No.2	Interior	68.4	0.4%	880	1.7%	785	400	300	2.2%	785	400	400	0.09	15.3	S
	373	Nakamura et al. (1991)	No.4	Interior	91.9	0.4%	880	1.7%	785	400	300	2.2%	785	400	400	0.07	17.1	S-F
95	374	Nishi et al. (1992)	JO-2	Interior	24.9	0.4%	448	1.6%	366	150	120	2.3%	366	150	150	0.7	6.3	Unknown
96	375	Nishiyama et al. (1989)	RC2	Exterior	29.8	0.8%	335	2.5%	425	300	200	3.2%	425	300	300	0.04	6.3	S-F
97	376	Noguchi and Kurusu (1988)	NO2	Interior	34.1	0.1%	354	2.6%	325	300	200	2.3%	388	300	300	0.06	5.5	Unknown
98	377	Noguchi and Kashiwazaki (1992)	OKJ-1	Interior	70	0.9%	955	3.5%	718	300	200	2.8%	718	300	300	0.12	14.4	S-F
	378	Noguchi and Kashiwazaki (1992)	OKJ-4	Interior	70	0.9%	955	3.5%	718	300	200	2.8%	718	300	300	0.12	15.1	S-F
	379	Noguchi and Kashiwazaki (1992)	OKJ-5	Interior	70	0.9%	955	4.4%	718	300	200	3.4%	718	300	300	0.12	14.8	S
	380	Noguchi and Kashiwazaki (1992)	OKJ-6	Interior	53.5	0.9%	955	3.3%	718	300	200	2.8%	718	300	300	0.12	13.2	S
99	381	Ogawa et al. (2003)	BUCS	Exterior	18.6	0.4%	402	1.0%	388	400	260	2.7%	388	300	300	0.2	4.0	S
	382	Ogawa et al. (2003)	BUVS	Exterior	18.6	0.4%	402	1.0%	389	400	260	2.7%	388	300	300	0.62	3.4	S
100	383	Oh et al. (1992)	EJS-200-0	Exterior	26.8	0.0%	0	2.5%	434	200	140	2.7%	417	200	200	0	4.9	S
	384	Oh et al. (1992)	EJS-400-0	Exterior	41.7	0.0%	0	2.5%	434	200	140	2.7%	417	200	200	0	6.3	S
	385	Oh et al. (1992)	EJS-200-0.3N	Exterior	26.8	0.4%	375	2.5%	434	200	140	2.7%	417	200	200	0	5.5	Unknown
	386	Oh et al. (1992)	EJS-200-2-0.6N'	Exterior	24	0.7%	375	2.5%	434	200	140	2.7%	417	200	200	0	5.7	Unknown
	387	Oh et al. (1992)	EJS-200-2-0.6N	Exterior	24	0.4%	375	2.5%	434	200	140	3.1%	417	200	200	0	5.6	Unknown
	388	Oh et al. (1992)	EJS-400-0.3N	Exterior	41.7	0.4%	375	2.5%	434	200	140	2.7%	417	200	200	0	6.8	Unknown
	389	Oh et al. (1992)	EJS-400-0.6N'	Exterior	44.6	0.7%	375	2.5%	434	200	140	2.7%	417	200	200	0	7.0	Unknown
	390	Oh et al. (1992)	EJS-400-0.6N	Exterior	44.6	0.4%	375	2.5%	434	200	140	3.1%	417	200	200	0	7.0	Unknown
	391	Oh et al. (1992)	EJS-400-0.6H	Exterior	43.1	0.9%	765	3.6%	417	200	140	2.7%	417	200	200	0	8.4	Unknown
	392	Oh et al. (1992)	EJS-400-1.2H	Exterior	43.1	1.8%	765	3.6%	417	200	140	2.7%	417	200	200	0	9.1	Unknown
101	393	Ohwada (1970)	No. 1	Interior	21.5	0.0%	0	1.3%	392	300	150	3.2%	392	200	200	0.18	6.1	Unknown
102	394	Ohwada (1970)	No. 3	Interior	21.5	0.7%	245	1.3%	392	300	150	3.2%	392	200	200	0.18	6.9	S
	395	Ohwada (1970)	No. 2	Interior	21.5	0.3%	245	1.3%	392	300	150	3.2%	392	200	200	0.18	7.6	S

103	396	Ohwada (1973)	P-1	Interior	11.6	0.0%	0	1.5%	400	300	150	4.0%	400	200	200	0.34	3.7	S
	397	Ohwada (1973)	P-2	Interior	13.3	0.0%	0	1.3%	385	300	150	3.2%	385	200	200	0.29	4.2	S
	398	Ohwada (1973)	P-3	Interior	12.8	0.0%	0	1.0%	385	300	150	3.2%	385	200	200	0.31	4.3	S
	399	Ohwada (1973)	P-4	Interior	13.4	0.7%	245	1.3%	385	300	150	3.2%	385	200	200	0.29	4.3	S-F
104	400	Ohwada (1976)	JO-0	Interior	20.1	0.0%	0	3.9%	402	150	100	3.4%	402	150	100	0	7.6	S
105	401	Ohwada (1977)	JO-1	Interior	20	0.0%	0	2.0%	432	150	150	3.4%	432	150	150	0	6.1	S
	402	Ohwada (1977)	JO-2	Interior	20	0.4%	450	2.0%	432	150	150	3.4%	432	150	150	0	7.3	S
106	403	Ohwada (1980)	JO-3	Interior	20.6	0.0%	0	2.0%	394	150	150	3.4%	394	150	150	0	6.9	S
	404	Ohwada (1980)	JO-4	Interior	14	0.0%	0	2.0%	360	150	150	6.8%	360	150	150	0	6.2	S
	405	Ohwada (1980)	LJO-1	Interior	20	0.0%	0	2.0%	372	150	150	6.8%	372	150	150	0	6.6	S
	406	Ohwada (1980)	LJO-3	Interior	20	0.0%	0	2.0%	372	150	150	4.5%	372	150	150	0	6.1	S
	407	Ohwada (1980)	LJO-2	Interior	20	0.3%	407	2.0%	372	150	150	6.8%	372	150	150	0	6.5	S
107	408	Ohwada (1981)	LJO-4	Interior	17.1	0.0%	0	1.8%	368	200	120	2.3%	368	150	150	0.16	5.0	S
	409	Ohwada (1981)	LJO-5	Interior	17.1	0.0%	0	1.8%	368	200	120	2.3%	368	150	150	0.41	5.3	S-F
108	410	Oka and Shiohara (1992)	J-11	Interior	39.2	0.4%	401	6.3%	365	300	240	7.7%	365	300	300	0.12	12.6	S
	411	Oka and Shiohara (1992)	J-10	Interior	39.2	0.4%	598	2.9%	687	300	240	3.4%	687	300	300	0.12	10.8	S
	412	Oka and Shiohara (1992)	J-6	Interior	79.2	0.2%	775	2.9%	663	300	240	3.4%	663	300	300	0.12	15.0	S-F
	413	Oka and Shiohara (1992)	J-8	Interior	79.2	0.4%	775	6.3%	364	300	240	7.7%	364	300	300	0.12	17.0	S
	414	Oka and Shiohara (1992)	J-1	Interior	81.2	0.4%	1374	2.9%	627	300	240	3.4%	627	300	300	0.11	14.1	S-F
	415	Oka and Shiohara (1992)	J-2	Interior	81.2	0.4%	1374	2.9%	1429	300	240	3.4%	627	300	300	0.11	15.3	S
	416	Oka and Shiohara (1992)	J-4	Interior	72.8	0.4%	1374	3.7%	506	300	240	5.3%	492	300	300	0.13	14.6	S-F
	417	Oka and Shiohara (1992)	J-5	Interior	72.8	0.4%	1374	2.9%	824	300	240	3.4%	824	300	300	0.13	16.2	S
109	418	Onish et al. (1990)	No.1	Exterior	25.9	0.0%	0	0.7%	389	250	250	1.2%	389	250	250	0	3.8	S-F
	419	Onish et al. (1990)	No.4	Exterior	25.2	0.0%	0	1.2%	389	250	250	1.2%	389	250	250	0	3.7	S-F
	420	Onish et al. (1990)	No.2	Exterior	28.1	0.2%	314	0.7%	389	250	250	1.2%	389	250	250	0	4.1	S-F
	421	Onish et al. (1990)	NO.5	Exterior	28.1	0.5%	314	1.2%	389	250	250	1.2%	389	250	250	0	4.7	S-F
110	422	Oskouei (2010)	Specimen-1	Exterior	24.3	0.5%	282	1.5%	417	400	350	2.5%	417	350	350	0	4.0	S
	423	Oskouei (2010)	Specimen-2	Exterior	19.6	0.5%	282	1.5%	417	400	350	2.5%	417	350	350	0	4.3	S
111	424	Ota et al. (2004)	RC	Interior	74.2	0.2%	944	2.2%	538	400	280	2.5%	538	400	400	0.08	12.5	S-F
112	425	Otani et al. (1984)	J1	Interior	25.7	0.3%	368	2.0%	401	300	200	2.3%	401	300	300	0.08	7.3	S-F
	426	Otani et al. (1984)	J2	Interior	24	0.6%	368	2.0%	401	300	200	2.3%	401	300	300	0.08	7.5	S-F

	427	Otani et al. (1984)	J3	Interior	24	1.7%	368	2.0%	401	300	200	2.3%	401	300	300	0.08	8.0	S-F
	428	Otani et al. (1984)	J4	Interior	25.7	0.3%	368	2.0%	401	300	200	2.3%	401	300	300	0.3	7.1	S-F
	429	Otani et al. (1984)	J5	Interior	28.7	0.3%	368	2.0%	401	300	200	2.3%	401	300	300	0.07	7.2	S-F
113	430	Owada (1984)	LJO-6	Interior	28.9	0.0%	0	1.8%	357	200	120	2.3%	357	150	150	0.23	8.1	Unknown
114	431	Owada (1992)	J0C-1	Interior	31.2	0.4%	447	2.6%	340	150	120	2.3%	343	150	150	0.13	5.3	S-F
	432	Owada (1992)	J0R-1	Interior	31.2	0.4%	447	2.6%	340	150	120	2.3%	343	150	150	0.13	8.3	S-F
115	433	Owada (2000)	JO-5	Interior	37.6	0.0%	0	3.3%	349	200	120	2.3%	349	150	150	0.17	9.1	S
116	434	Ozaki et al. (2010)	1	Interior	32.8	0.4%	338	2.2%	410	300	180	1.8%	410	300	300	0.09	8.6	S-F
117	435	Pantelides et al. (2002)	Unit 1	Exterior	33.1	0.0%	0	3.1%	459	406	406	2.5%	470	406	406	0.1	5.2	B
	436	Pantelides et al. (2002)	Unit 2	Exterior	33.1	0.0%	0	3.1%	459	406	406	2.5%	470	406	406	0.25	4.9	B
	437	Pantelides et al. (2002)	Unit 3	Exterior	34	0.0%	0	3.1%	459	406	406	2.5%	470	406	406	0.1	5.0	S
	438	Pantelides et al. (2002)	Unit 4	Exterior	34	0.0%	0	3.1%	459	406	406	2.5%	470	406	406	0.25	5.7	S
	439	Pantelides et al. (2002)	Unit 5	Exterior	31.7	0.0%	0	3.1%	459	406	406	2.5%	470	406	406	0.1	5.2	S
	440	Pantelides et al. (2002)	Unit 6	Exterior	31.7	0.0%	0	3.1%	459	406	406	2.5%	470	406	406	0.25	5.3	S
118	441	Park and Bullman (1997)	4b	Exterior	39.2	0.0%	0	0.9%	570	500	250	0.9%	550	300	300	0.09	4.0	S
	442	Park and Bullman (1997)	4c	Exterior	36.8	0.0%	0	0.9%	570	500	250	0.9%	550	300	300	0.17	4.0	S
	443	Park and Bullman (1997)	4d	Exterior	39.2	0.0%	0	0.9%	570	500	250	3.6%	580	300	300	0	2.9	S
	444	Park and Bullman (1997)	4e	Exterior	40	0.0%	0	0.9%	570	500	250	3.6%	580	300	300	0.1	3.8	S
	445	Park and Bullman (1997)	4f	Exterior	37.6	0.0%	0	0.9%	570	500	250	3.6%	580	300	300	0.18	4.3	S
	446	Park and Bullman (1997)	5b	Exterior	43.2	0.5%	480	0.9%	485	500	250	2.2%	485	300	300	0.08	5.5	S
119	447	Pessiki et al. (1990)	I-01	Interior	32.7	0.0%	0	1.3%	483	610	356	2.0%	456	406	406	0.25	6.3	S-F
	448	Pessiki et al. (1990)	I-02	Interior	32.5	0.0%	0	1.3%	483	610	356	2.0%	456	406	406	0.24	6.2	S-F
	449	Pessiki et al. (1990)	I-03	Interior	30.4	0.0%	0	1.3%	483	610	356	1.8%	486	406	406	0.31	6.0	S-F
	450	Pessiki et al. (1990)	I-04	Interior	31.9	0.0%	0	1.3%	483	610	356	1.9%	518	406	406	0.3	5.9	S-F
	451	Pessiki et al. (1990)	I-07	Interior	26	0.0%	0	0.8%	481	610	356	2.0%	461	406	406	0.43	4.7	S-F
	452	Pessiki et al. (1990)	I-08	Interior	25.4	0.0%	0	0.8%	481	610	356	2.0%	461	406	406	0.43	4.6	S-F
	453	Pessiki et al. (1990)	I-09	Interior	29.1	0.0%	0	0.8%	425	610	356	2.0%	461	406	406	0.1	4.6	S-F
	454	Pessiki et al. (1990)	I-05	Interior	29.8	0.2%	427	1.3%	531	610	356	1.9%	427	406	406	0.33	6.1	S-F
120	455	Pimanmas and Chaimahawan (2010)	J0	Interior	27.3	0.0%	0	2.2%	480	300	175	2.9%	480	350	200	0.17	5.9	Unknown
121	456	Rajagopal and Prabavathy (2013)	A2-II	Exterior	23	0.7%	410	1.3%	410	300	200	0.8%	410	200	300	0	4.6	Unknown
122	457	Realfonzo (2018)	Type 1	Exterior	16	0.0%	0	1.6%	540	400	300	0.7%	540	300	300	0.21	3.5	Unknown

	458	Realfonzo (2018)	Type 2	Exterior	16	0.0%	0	2.1%	540	400	300	2.8%	540	300	300	0.21	3.6	Unknown
123	459	Reys de Ortiz (1993)	BC1	Exterior	33.8	0.0%	0	1.1%	720	400	200	1.5%	461	300	200	0	5.4	S
	460	Reys de Ortiz (1993)	BC3	Exterior	33	0.0%	0	1.1%	720	400	200	2.1%	461	300	200	0	5.7	S
	461	Reys de Ortiz (1993)	BC5	Exterior	37.9	0.0%	0	1.1%	720	400	200	2.4%	461	300	200	0.13	5.5	S
	462	Reys de Ortiz (1993)	BC6	Exterior	35	0.0%	0	1.1%	720	400	200	2.4%	461	300	200	0.14	5.5	S
	463	Reys de Ortiz (1993)	BC2	Exterior	37.8	0.3%	461	1.1%	720	400	200	1.5%	461	300	200	0	6.0	S
124	464	Sagbas (2007)	ED1	Exterior	31.1	0.0%	0	2.1%	349	508	305	2.8%	335	381	381	0.09	4.5	S-F
125	465	Sanada and Li (2014)	J2	Exterior	20.2	0.0%	0	1.4%	373	450	300	2.5%	373	300	300	0	3.9	Unknown
126	466	Sarsam and Phipps (1985)	EX2	Exterior	52.5	0.0%	0	1.7%	504	305	152	2.5%	504	205	155	0.18	4.6	S
127	469	Scott (2007)	C7	Exterior	35.2	0.3%	250	1.4%	540	300	110	3.6%	540	150	150	0.35	5.0	S
	470	Scott (2007)	C9	Exterior	35.9	0.3%	250	1.4%	540	300	110	3.6%	540	150	150	0.34	4.4	S
	471	Scott (2007)	C1AL	Exterior	33.4	0.4%	250	1.1%	540	210	110	3.6%	540	150	150	0.07	5.2	S
	472	Scott (2007)	C2	Exterior	49.4	0.4%	250	1.1%	540	210	110	3.6%	540	150	150	0.25	5.1	S
	473	Scott (2007)	C3L	Exterior	35.5	0.4%	250	1.1%	540	210	110	3.6%	540	150	150	0.06	5.1	S
	474	Scott (2007)	C4	Exterior	41.4	0.4%	250	2.1%	540	210	110	3.6%	540	150	150	0.29	7.8	S
	475	Scott (2007)	C4A	Exterior	44.3	0.4%	250	2.1%	540	210	110	3.6%	540	150	150	0.28	8.4	S
	476	Scott (2007)	C4AL	Exterior	35.8	0.4%	250	2.1%	540	210	110	3.6%	540	150	150	0.06	7.5	S
	477	Scott (2007)	C6	Exterior	39.8	0.4%	250	2.1%	540	210	110	3.6%	540	150	150	0.31	5.7	S
	478	Scott (2007)	C6L	Exterior	45.8	0.4%	250	2.1%	540	210	110	3.6%	540	150	150	0.05	6.9	S
128	479	Shin et al. (1992)	HJC0-R0	Exterior	78.5	0.0%	0	2.4%	392	200	120	2.5%	392	150	150	0.01	10.3	S-F
	480	Shin et al. (1992)	HJC1-R0	Exterior	78.5	0.4%	235	2.4%	392	200	120	2.5%	392	150	150	0.01	11.1	S-F
129	481	Shinjo et al. (2009)	B-1	Interior	111	0.4%	1452	2.8%	549	400	300	2.2%	528	400	400	0.1	20.2	S-F
	482	Shinjo et al. (2009)	J-1	Interior	110	0.4%	1452	3.2%	716	400	300	2.2%	528	400	400	0.1	24.7	S
	483	Shinjo et al. (2009)	BJ-1	Interior	110	0.4%	1452	3.2%	549	400	300	2.2%	528	400	400	0.1	22.4	S
	484	Shrestha et al. (2009)	UC-1	Exterior	25.8	0.0%	0	2.7%	532	450	300	2.0%	532	300	300	0.08	2.4	0
130	485	Smith (1972)	Unit 5	Exterior	20.1	0.5%	310	3.1%	301	460	255	1.2%	274	380	330	0	3.0	S-F
	486	Smith (1972)	Unit 6	Exterior	17.7	1.0%	310	3.1%	299	460	255	1.2%	297	380	330	0	3.1	S-F
	487	Smith (1972)	Unit 4	Exterior	20.5	1.1%	310	3.1%	296	460	255	1.2%	274	380	330	0	2.9	S-F
131	488	Supaviriyakit and Pimanmas (2008)	J1	Interior	26.3	0.0%	0	2.2%	480	300	175	2.9%	480	350	200	0.13	6.2	S
132	489	Suzuki et al. (2002)	E00	Interior	24	0.4%	358	1.8%	384	500	230	1.4%	384	500	400	0.25	6.6	S
133	490	Takeuchi et al. (2003)	O-5	Exterior	42	0.4%	327	1.1%	445	450	350	2.9%	553	400	400	0.1	3.7	S

134	491	Taylor (1974)	C3/41/13Y	Exterior	22.4	0.4%	250	1.3%	500	200	100	4.1%	500	140	140	0.55	4.9	S
	492	Taylor (1974)	P1/41/24	Exterior	26.4	0.4%	250	2.4%	500	200	100	4.1%	500	140	140	0.46	6.6	S
	493	Taylor (1974)	P2/41/24	Exterior	29	0.4%	250	2.4%	500	200	100	4.1%	500	140	140	0.42	8.0	S
	494	Taylor (1974)	P2/41/24A	Exterior	37.6	0.4%	250	2.4%	500	200	100	4.1%	500	140	140	0.33	9.0	S
	495	Taylor (1974)	A3/41/24	Exterior	21.6	0.4%	250	2.4%	500	200	100	4.1%	500	140	140	0.57	7.2	S
	496	Taylor (1974)	B3/41/24	Exterior	17.6	0.4%	250	2.4%	500	200	100	4.1%	500	140	140	0.7	6.4	S
	497	Taylor (1974)	C3/41/24X	Exterior	40	0.4%	250	2.4%	500	200	100	4.1%	500	140	140	0.31	6.2	S
	498	Taylor (1974)	C3/41/24Y	Exterior	48	0.4%	250	2.4%	500	200	100	4.1%	500	140	140	0.26	8.3	S
	499	Taylor (1974)	D3/41/24	Exterior	42.2	0.4%	250	2.4%	500	200	100	4.1%	500	140	140	0.07	9.6	S
	500	Taylor (1974)	C3/41/24BY	Exterior	25.6	0.7%	250	2.4%	500	200	100	4.1%	500	140	140	0.48	5.5	S
135	501	Teroaka (1997)	NO4	Exterior	39.1	0.5%	328	1.4%	434	560	365	2.5%	421	540	540	0.01	4.9	S-F
	502	Teroaka (1997)	NO10	Exterior	34.8	0.6%	328	1.1%	421	560	365	2.5%	421	540	540	0.01	4.1	S-F
	503	Teroaka (1997)	NO3	Exterior	38.9	0.6%	328	1.4%	434	560	365	2.5%	421	540	540	0.01	4.7	S-F
	504	Teroaka (1997)	NO26	Interior	35.6	0.6%	300	1.9%	399	300	260	2.1%	399	340	340	0.17	9.4	S-F
	505	Teroaka (1997)	NO28	Interior	36.2	0.6%	300	2.6%	399	300	260	2.1%	399	340	340	0.16	11.5	S
	506	Teroaka (1997)	NO29	Interior	44	0.6%	300	1.9%	399	300	260	2.1%	399	340	340	0.23	9.5	S-F
136	507	Tsonos (1993)	S1	Exterior	37	0.8%	495	1.1%	485	300	200	2.3%	485	200	200	0.4	6.9	S-F
	508	Tsonos (1993)	S2	Exterior	26	0.8%	495	1.1%	507	300	200	0.8%	497	200	200	0.4	8.6	S-F
	509	Tsonos (1993)	S3	Exterior	19	0.8%	495	1.3%	497	300	200	0.8%	507	200	200	0.4	9.5	S-F
	510	Tsonos (1993)	S4	Exterior	21	0.8%	495	1.8%	497	300	200	1.2%	485	200	200	0.4	10.2	S
	511	Tsonos (1993)	S5	Exterior	25	0.8%	495	2.1%	507	300	200	1.9%	466	200	200	0.4	10.9	S
	512	Tsonos (1993)	S6	Exterior	33	0.8%	495	2.1%	485	300	200	1.5%	466	200	200	0.4	9.8	S
	513	Tsonos (1993)	P1	Exterior	16	0.8%	495	2.1%	485	300	200	3.1%	466	200	200	0.4	9.5	S
	514	Tsonos (1993)	Y1	Exterior	23	0.8%	495	2.1%	485	300	200	1.5%	478	200	200	0.4	8.9	S
	515	Tsonos (1993)	F1	Exterior	17	0.8%	495	2.1%	485	300	200	1.5%	485	200	200	0.4	13.1	S
	516	Tsonos (1993)	O1	Exterior	20	0.8%	495	2.1%	485	300	200	1.5%	485	200	200	0.4	9.8	S
	517	Tsonos (1993)	F2	Exterior	24	0.8%	495	2.1%	485	300	200	1.5%	485	200	200	0.4	9.6	S
	518	Tsonos (1996)	MS4	Exterior	33.6	1.2%	495	1.2%	466	300	200	3.1%	485	200	200	0.29	5.3	S-F
137	519	Tsonos (2002)	O1	Exterior	16	0.0%	0	2.1%	485	300	200	1.5%	485	200	200	0.4	5.4	S
138	520	Tsonos (2007)	S1	Exterior	37	0.7%	495	1.2%	485	300	200	2.3%	485	200	200	0.18	3.6	S-F
	521	Tsonos (2007)	S2	Exterior	26	0.7%	495	1.2%	465	300	200	0.8%	465	200	200	0.18	3.7	S-F

	522	Tsonos (2007)	S3	Exterior	19	0.7%	495	1.2%	465	300	200	0.8%	465	200	200	0.18	3.6	S-F
	523	Tsonos (2007)	S4	Exterior	21	0.7%	495	2.0%	485	300	200	1.2%	465	200	200	0.18	3.9	S
	524	Tsonos (2007)	S5	Exterior	25	0.7%	495	2.2%	485	300	200	1.9%	465	200	200	0.18	4.5	S
	525	Tsonos (2007)	S6	Exterior	33	0.7%	495	2.2%	485	300	200	1.5%	485	200	200	0.18	4.6	S
	526	Tsonos (2007)	S6'	Exterior	29	0.7%	495	2.2%	485	300	200	3.1%	485	200	200	0.18	5.3	S-F
	527	Tsonos (2007)	O1	Exterior	20	1.1%	495	2.2%	485	300	200	3.1%	485	200	200	0.18	3.6	S
	528	Tsonos (2007)	F2	Exterior	24	1.1%	495	2.2%	485	300	200	3.1%	485	200	200	0.18	4.6	S
	529	Tsonos (2007)	G1	Exterior	22	1.3%	500	1.8%	495	300	200	3.1%	495	200	200	0.23	4.4	S-F
	530	Tsonos (2007)	A1	Exterior	35	1.0%	540	1.2%	500	300	200	1.2%	500	200	200	0.14	4.4	S-F
	531	Tsonos (2007)	E2	Exterior	35	1.0%	540	1.2%	495	300	200	3.1%	495	200	200	0.14	4.2	S-F
	532	Tsonos (2007)	E1	Exterior	22	1.0%	540	1.8%	495	300	200	3.1%	495	200	200	0.23	5.9	S
	533	Tsonos and Papanikolau (2003)	F2	Exterior	31	0.0%	0	1.3%	530	300	300	0.8%	535	200	200	0.29	3.3	S
139	534	Tsonos and Papanikolau (2003)	F1	Exterior	20	0.0%	0	1.5%	520	300	300	2.3%	520	200	200	0.39	3.7	S-F
	535	Tsonos and Papanikolau (2003)	L1	Exterior	34	0.0%	0	2.1%	520	300	300	0.8%	535	200	200	0.26	5.0	S
	536	Tsonos et al. (1992)	P1	Exterior	16	0.0%	0	2.2%	485	300	200	3.1%	485	200	200	0.18	3.1	S
140	537	Tsonos et al. (1992)	V1	Exterior	23	0.0%	0	2.2%	485	300	200	3.1%	485	200	200	0.18	3.5	S
	538	Tsonos et al. (1992)	F1	Exterior	17	0.0%	0	2.2%	485	300	200	3.1%	485	200	200	0.18	4.4	S
	539	Uzumeri (1977)	1	Exterior	30.8	0.0%	0	2.1%	332	508	305	2.8%	331	381	381	0.41	5.0	S-F
	540	Uzumeri (1977)	5	Exterior	32	0.0%	0	1.7%	336	508	381	2.8%	336	381	381	0.4	4.8	S-F
	541	Uzumeri (1977)	2	Exterior	31.1	0.0%	0	2.1%	349	508	305	2.8%	335	381	381	0.41	4.6	S-F
	542	Uzumeri (1977)	6	Exterior	36.2	1.5%	357	1.7%	352	508	381	2.8%	340	381	381	0.42	4.9	S-F
141	543	Uzumeri (1977)	7	Exterior	30.8	0.9%	365	1.7%	352	508	381	2.8%	340	381	381	0.52	4.8	S-F
	544	Uzumeri (1977)	8	Exterior	26.3	1.5%	365	2.3%	352	508	381	2.8%	390	381	381	0.61	5.7	S-F
	545	Uzumeri (1977)	4	Exterior	31	0.9%	380	2.1%	349	508	305	2.8%	333	381	381	0.42	5.1	S-F
	546	Uzumeri (1977)	3	Exterior	27	0.4%	428	2.1%	350	508	305	2.8%	337	381	381	0.42	4.5	S-F
	547	Walker (2001)	PEER14	Interior	31.8	0.0%	0	1.9%	423	508	406	1.4%	423	457	406	0.11	5.2	S-F
	548	Walker (2001)	CD1514	Interior	29.8	0.0%	0	1.9%	423	508	406	1.4%	423	457	406	0.12	5.4	S-F
	549	Walker (2001)	CD3014	Interior	42.5	0.0%	0	1.9%	423	508	406	1.4%	423	457	406	0.08	6.2	S-F
142	550	Walker (2001)	PADH14	Interior	42.9	0.0%	0	1.9%	423	508	406	1.4%	423	457	406	0.08	6.5	S-F
	551	Walker (2001)	PEER22	Interior	38.4	0.0%	0	2.6%	527	508	406	2.8%	538	457	406	0.09	7.4	S-F
	552	Walker (2001)	CD3022	Interior	38.1	0.0%	0	2.6%	516	508	406	2.8%	510	457	406	0.09	7.9	S-F

	553	Walker (2001)	PADH22	Interior	36.3	0.0%	0	2.6%	527	508	406	2.8%	538	457	406	0.1	7.9	S-F
143	554	Wang and Hsu (2009)	Ko-JI1	Interior	31.7	0.0%	0	2.6%	533	500	300	3.4%	533	300	300	0.14	8.5	S
	555	Wang and Hsu (2009)	Ho-JI1	Interior	26.2	0.0%	0	1.9%	541	400	300	0.3%	541	400	400	0	6.3	S
144	556	Wang and Lee (2004)	JE1	Exterior	20	0.0%	0	2.0%	520	400	300	2.5%	461	400	400	0	2.9	S
145	557	Watanabe et al. (1998)	WJ-1	Interior	29	1.3%	364	1.6%	326	300	200	2.6%	358	300	300	0.07	6.9	S-F
	558	Watanabe et al. (1998)	WJ-3	Interior	29	1.3%	364	1.6%	364	300	200	2.6%	373	300	300	0.07	8.0	S-F
	559	Watanabe et al. (1998)	WJ-6	Interior	29	1.3%	364	2.2%	358	300	200	4.0%	373	300	300	0.07	9.8	S-F
146	560	Wong (2005)	BS-L-600	Exterior	36.4	0.0%	0	1.2%	520	600	260	2.2%	520	300	300	0.15	3.5	S
	561	Wong (2005)	JA-NN03	Exterior	44.8	0.0%	0	1.4%	520	450	260	2.2%	520	300	300	0.03	3.6	S-F
	562	Wong (2005)	JA-NN15	Exterior	46	0.0%	0	1.4%	520	450	260	2.2%	520	300	300	0.15	3.9	S-F
	563	Wong (2005)	BS-L	Exterior	30.9	0.0%	0	1.6%	520	450	260	2.2%	520	300	300	0.15	3.8	S
	564	Wong (2005)	BS-LL	Exterior	42.1	0.0%	0	1.6%	520	450	260	2.2%	520	300	300	0.15	4.8	S
	565	Wong (2005)	BS-L-LS	Exterior	31.6	0.0%	0	1.6%	520	450	260	2.2%	520	300	300	0.15	4.1	S
	566	Wong (2005)	BS-L-V2T10	Exterior	32.6	0.0%	0	1.6%	520	450	260	2.2%	520	300	300	0.15	4.7	S
	567	Wong (2005)	BS-L-V4T10	Exterior	28.3	0.0%	0	1.6%	520	450	260	2.2%	520	300	300	0.15	4.8	S
	568	Wong (2005)	BS-U	Exterior	31	0.0%	0	1.6%	520	450	260	2.2%	520	300	300	0.15	4.1	S
	569	Wong (2005)	JB-NN03	Exterior	47.4	0.0%	0	2.1%	520	300	260	2.2%	520	300	300	0.03	4.4	S
	570	Wong (2005)	BS-L-300	Exterior	34.1	0.0%	0	2.4%	520	300	260	2.2%	520	300	300	0.15	5.9	S
	571	Wong (2005)	BS-L-H1T10	Exterior	33.3	0.3%	500	1.6%	520	450	260	2.2%	520	300	300	0.15	4.6	S
	572	Wong (2005)	BS-L-H2T10	Exterior	42.1	0.4%	500	1.6%	520	450	260	2.2%	520	300	300	0.15	5.7	S
	573	Wong (2005)	JA-NY03	Exterior	34.9	0.5%	500	1.5%	520	400	260	2.2%	520	300	300	0.03	3.6	S-F
	574	Wong (2005)	JA-NY15	Exterior	38.5	0.5%	500	1.5%	520	400	260	2.2%	520	300	300	0.15	3.9	S-F
147	575	Wong and Kuang (2008)	BS-L-600	Exterior	36.4	0.0%	0	1.2%	520	600	260	2.4%	520	300	300	0.31	3.1	S
	576	Wong and Kuang (2008)	BS-L-450	Exterior	30.9	0.0%	0	1.7%	520	450	260	2.4%	520	300	300	0.36	3.5	S
	577	Wong and Kuang (2008)	BS-L-V2	Exterior	32.6	0.0%	0	1.7%	520	450	260	3.1%	520	300	300	0.34	4.5	S
	578	Wong and Kuang (2008)	BS-L-V4	Exterior	28.3	0.0%	0	1.7%	520	450	260	3.7%	520	300	300	0.39	4.5	S
	579	Wong and Kuang (2008)	BS-L-300	Exterior	34.1	0.0%	0	2.4%	520	300	260	2.4%	520	300	300	0.33	5.6	S
	580	Wong and Kuang (2008)	BS-L-H1	Exterior	33.3	0.1%	500	1.7%	520	450	260	2.4%	520	300	300	0.33	4.3	S
	581	Wong and Kuang (2008)	BS-L-H2	Exterior	42.1	0.1%	500	1.7%	520	450	260	2.4%	520	300	300	0.26	5.3	S
148	582	Wong and Kuang (2011)	BS-600	Exterior	36.4	0.0%	0	1.3%	520	600	260	2.4%	520	300	300	0.31	3.1	S
	583	Wong and Kuang (2011)	BS-450	Exterior	30.9	0.0%	0	1.7%	520	450	260	2.4%	520	300	300	0.36	3.5	S

	584	Wong and Kuang (2011)	BS-600-H2T8	Exterior	41.8	0.1%	500	1.3%	520	600	260	2.4%	520	300	300	0.27	4.0	S
	585	Wong and Kuang (2011)	BS-450-H1T10	Exterior	33.3	0.1%	500	1.7%	520	450	260	2.4%	520	300	300	0.33	4.3	S
	586	Wong and Kuang (2011)	BS-600-H4T8	Exterior	29.7	0.3%	500	1.3%	520	600	260	2.4%	520	300	300	0.37	3.8	S
	587	Wong and Kuang (2011)	BS-450-H2T10	Exterior	42.1	0.3%	500	1.7%	520	450	260	2.4%	520	300	300	0.26	5.3	S
	588	Yashita et al. (1996)	No. 1	Interior	43.1	0.4%	823	3.9%	409	395	300	2.0%	409	415	415	0.1	8.1	S-F
149	589	Yashita et al. (1996)	No. 3	Interior	54.3	0.4%	823	3.2%	405	395	300	2.0%	405	415	415	0.1	9.4	S-F
	590	Yashita et al. (1996)	No. 4	Interior	53.8	0.4%	823	3.2%	702	395	300	2.0%	702	415	415	0.1	11.6	S
	591	Yoshino et al. (1997)	No. 1	Interior	28.6	0.5%	420	1.3%	382	250	180	2.5%	379	250	250	0.16	7.2	S-F
150	592	Yoshino et al. (1997)	No. 3	Interior	28.6	0.5%	420	1.6%	379	250	180	2.5%	379	250	250	0.16	7.7	S-F
	593	Yoshino et al. (1997)	No. 4	Interior	28.6	0.5%	420	1.1%	379	250	180	2.5%	379	250	250	0.16	6.3	S-F
151	594	Yoshiya et al. (1991)	No. 2	Interior	39.2	0.4%	364	2.5%	388	450	300	2.1%	365	500	375	0.24	10.8	S-F
152	595	Zaid et al. (1999)	S3	Interior	28	0.5%	390	1.9%	470	300	200	3.8%	450	300	300	0.04	8.8	S-F
	596	Zhang and Li (2020)	EJ-0	Exterior	47.9	0.0%	0	2.1%	535	250	150	1.7%	535	250	250	0.14	3.2	S-F
153	597	Zhang and Li (2020)	EJ-2	Exterior	47.9	1.0%	300	2.1%	535	250	150	1.7%	535	250	250	0.14	3.1	S-F
	598	Zhang and Li (2020)	EJ-4	Exterior	47.9	1.6%	300	2.1%	535	250	150	1.7%	535	250	250	0.14	3.0	S-F